THE APPLICATION OF THE ATTAINABLE REGION ANALYSIS IN COMMINUTION

Ngangezwe Khumalo

A thesis submitted to the Faculty of Engineering and the Built Environment, University of the Witwatersrand, Johannesburg, in fulfilment of the requirements for the degree of Doctor of Philosophy.

Johannesburg, 2007

DECLARATION

I declare that this thesis is my own, unaided work (except for the referenced portions). It is being submitted for the Degree of Doctor of Philosophy in the University of the Witwatersrand, Johannesburg. It has not been submitted before for any degree or examination in any other university.

…………………………………………………………..

Ngangezwe Khumalo

08 September 2007

ABSTRACT

This work applies the concepts of the attainable region for process synthesis in comminution. The attainable region analysis has been successfully applied for process synthesis of reactor networks. The Attainable Region is defined as the set of all possible output states for a constrained or unconstrained system of fundamental processes (Horn, 1964). A basic procedure for constructing the attainable region for the fundamental processes of reaction and mixing has been postulated in reaction engineering (Glasser et al., 1987). This procedure has been followed in this work to construct the candidate attainable region for size reduction processes as found in a size reduction environment.

A population balance model has been used to characterise the evolution of particle size distributions from a comminution event. Herbst and Fuerstenau (1973) postulated the dependency of grinding on the specific energy. A specific energy dependent population balance model was used for the theoretical simulations and for the fitting of experimental data.

A new method of presenting particle size distributions as points in the Euclidian space was postulated in place of the traditional cumulative distribution. This allows successive product particle size distributions to be connected forming a trajectory over which the objective function can be evaluated. The curve connects products from successive batch grinding stages forming a pseudo-continuous process.

Breakage, mixing and classification were identified as the fundamental processes of interest for comminution. Agglomeration was not considered in any of the examples. Mathematical models were used to describe each fundamental process, i.e. breakage, mixing and classification, and an

algorithm developed that could calculate the evolution of product particle size distributions. A convex candidate attainable region was found from which process synthesis and optimisation solutions could be drawn in two dimensional Euclidian space. As required from Attainable Region Theory, the interior of the bounded region is filled by trajectories of higher energy requirements or mixing between two boundary optimal points.

Experimental validation of the proposed application of the attainable region analysis results in comminution was performed. Mono-sized feed particles were broken in a laboratory ball mill and the products were successfully fitted using a population balance model. It was shown that the breakage process trajectories were convex and they follow first order grinding kinetics at long grind times. The candidate attainable region was determined for an objective function to maximise the mass fraction in the median size class 2. It was proved that the same specific energy input produces identical products. The kinematic and loading conditions are supposed to be chosen as a subsequent event after the required specific energy is identified.

Finally the fundamental process of classification was added to the system of breakage and mixing. The attainable regions analysis affords the opportunity to quantify exactly the reduction in energy consumption due to classification in a comminution circuit, thus giving optimal targets. Classification showed the potential to extend the candidate attainable region for a fixed specific energy input. The boundary of the attainable region is interpreted as pieces of equipment and optimum process conditions. This solves both the original process synthesis and successive optimisation problems.

I dedicate this thesis to all my future offspring, my pride and joy.

ACKNOWLEDGEMENTS

First I would like to acknowledge my supervisors Professor Diane Hildebrandt and Professor David Glasser for this opportunity to research in this field. Their ideas and patience has seen this work mature to a point where it is ready to be presented as a doctoral thesis.

Secondly I would like to thank everyone at COMPS. Your support both academically and socially has sustained me to this point, without losing my mind due to the academic pressures.

I extend my gratitude to someone special in my life who was my best friend when this work was started and is now my wife, the future mother of my kids.

Above all, my Christian faith has been my shield and strength. I thank God the father of my Lord Jesus Christ.

I would like to acknowledge C.O.M.P.S., the Postgraduate Merit Award, and the Mellon Mentorship Scheme for the financial support.

CONTENTS   PAGE

LIST OF FIGURES

LIST OF TABLES

CHAPTER 1

1 INTRODUCTION

Comminution is the term used for size reduction of particles in a wide range of modern industries including pharmaceutical, cement, minerals and pigment production. It represents a global market worth of US$ 400 billion for the minerals processing industry (CRU International, 2001). It contributes to health, transport, electricity generation, jewellery and construction aspects of modern life, just to name a few.

1.1 ENERGY INTENSIVE PROCESS

There are two objective functions which the comminution community is optimising in order to reduce overall operational costs. These are optimal product particle size distributions to downstream processes and optimal energy consumption. Comminution processes, especially grinding, have been shown to consume as much as 50% of the total energy requirements in a minerals processing plant. According to Schonert (1988), the grinding process energy efficiency is in the range 4-8%, assessed on the basis of surface area produced. The energy calculated from production of new surface area by breakage of bonds should be the upper limit if we accept that particles break along cracks according to Griffiths crack theory. If we were, for arguments sake, to assume the process energy efficiency as 10%, this means that of the order of 40% of the total energy utilised is wasted. Opportunities to reduce this large inefficiency of approximately 40% should be investigated.

The word comminution is derived from the Latin 'comminuere', meaning 'to make small'. Comminution is the breaking of large pieces of rock to smaller

ones by the application of force. The comminution process is currently an energy inefficient process (Austin et al., 1984), e.g.

a) ball mill grinding of quartz has 15%,
b) tube mill grinding of coal has 6%,

of the total energy input available for actual size reduction, with most of the input energy being absorbed by the machine and lost as heat and sound. Theories relating energy input and the particle size produced from a given feed size are currently being established. The work of Tavares (1998) on breakage probability stands out in successfully addressing the understanding of single particle breakage fundamentals, with the results being described statistically.

The attainable region (AR) is the set of all possible outcomes that can be achieved by a set of fundamental processes operating on a given system and complying with the constraints of that system (Glasser et al., 1987). Once all the possible outcomes have been determined for a system, it is possible to optimize or design the process in terms of any defined objective function e.g. cost or particle size distribution and/or energy. The theory was originally developed for use on systems governed by reactions (Horn, 1964). It has been used to develop feasible regions of achievable states exceeding those limitations that arise from considering only traditional unit types. An example of this lies in the development of the DSSR, DCR and DCSR structures – these are idealized differential structures that are approximated by well accepted industrial units such as cold shot cooling reactors.

The attainable region approach has been successfully applied in chemical reaction engineering for simultaneous process synthesis and optimisation. The same approach will be applied in comminution to solve the highlighted

process synthesis and optimisation problems. The purpose of this work is to optimise comminution systems using attainable regions theory which, as described, is a method for process synthesis. It is in the interest of this work to use these theories to develop a new comminution method which is economically competitive, more energy efficient and reproducible.

1.2 OBJECTIVES OF THIS THESIS

We aim to advance the understanding of the application of fundamentals of breakage in practical ways and in relation to industrial requirements. In comminution we define the fundamental processes as breakage, classification and mixing. We will apply the attainable regions concept to see how the resultant process vectors move in the nominated Euclidian space when constructing the boundary of possible opportunities. The boundaries of these spaces will then be assessed based on a defined objective function.

The breakage process is made complex by the varied breakage mechanisms which have to be taken into account in order to produce representative information. This difficulty has been surmounted by the use of the research into the physical phenomenon underlying breakage which is energy (force) input. An assessment of the applied specific energy determines the breakage mechanism at play. Another complexity of the description of the comminution process is that single particles break into distributions of particles which can only be described statistically through collation into discreet size intervals.

From the previous work in the area, it has been shown that in comminution the classification process is vital in extending the attainable region of achievable mass fraction distributions. This work has been done for three geometric size classes with the chosen process regimes of breakage and classification as fundamental processes. Following from this work we

investigate these theoretical findings experimentally on laboratory scale grinding equipment. The additional process of classification plays an important role in making the system more selective, thus avoiding over grinding, and robust since it can be used to extend the process trajectories. This also has the desirable side effect of reducing the amount of unwanted fines generation. Classification also increases the net production rates of the overall process.

We also apply the fundamental process of mixing to the system of breakage and see how it affects the variables of interest which could be particle size distribution, time and energy. So far it has been shown that the combination of processes allows other regions of possible distributions to be achieved. The boundary is interpreted as comminution structures and thereby provides a solution to the problem of which type of equipment to use to achieve an optimal value of a certain objective function.

The envisaged contribution of this work to knowledge will be a methodology to answer questions such as:

a) how to better represent particle size distributions dynamically?
b) is the use of specific energy as a variable sufficient for modelling grinding product particle size distributions?
c) where and how to introduce and separate the feed and product streams in the comminution circuit?
d) what is the energy that is required to optimise a defined objective function?
e) what is the most economic balance between the energy input and the time span for grinding?
f) how do we best develop a conceptual design and optimization approach that can be adopted for comminution circuits?

1.3 THESIS OUTLINE

Chapter 2

This chapter is a review of the comminution background with the aim of providing a context for the research to follow. Three fundamental processes of breakage, mixing and classification are defined as taking place during comminution. These processes are discussed in detail in order to understand how they are individually modelled because the application of our analysis tool requires this information. Many models have been postulated in comminution literature describing how particle sizes change with energy input. These laws do hold to some extent for static breakage systems like the drop weight test but for continuous systems, the sub-processes are better described by the population balance model. Perfect classification is not possible practically; therefore Tromp curves have been developed to measure the selectivity of the classifier feed to course and fine streams. The concept of linear mixing is explored for comminution products under the assumption of constant density.

Chapter 3

The background of the attainable regions approach as a process synthesis tool is presented. It will be shown that this is fundamentally a geometrical tool which develops a convex candidate attainable region using fundamental processes. A simple system with reaction and mixing will be presented as a demonstration of the success this approach enjoys in chemical reaction engineering.

Chapter 4

This chapter presents a new method of presenting particle size distributions as points in a geometric space instead of the traditional cumulative plots. This allows for connectivity of these points and their trajectory describes a process path in time resulting in dynamic information. The candidate attainable region is constructed for the two fundamental processes of breakage and mixing for process synthesis and optimisation. Different scenarios of parallel and series unit configurations are investigated.

Chapter 5

The literature survey revealed that the grinding model depends on the specific energy provided to the particles. The theoretical work done in Chapter 4 was based on the fact that the extent of breakage is a function of specific energy input. This chapter describes the experiments which were carried out in a laboratory ball mill to verify this postulate of breakage's specific energy dependency. The mill rotational speed and the mill loading were variables of interest which according to literature determine the specific energy input.

Chapter 6

This chapter presents the product profiles of a system of breakage and classification as fundamental processes with the aim of extending the boundary of the candidate attainable region. The extent to which classification produces sharp product particle size distributions and reduces the energy consumption is investigated.

Chapter 7

Finally this chapter concludes the work of applying the attainable regions approach to comminution. It shows that the objectives set out at the beginning of this work have been successfully accomplished. This chapter sums up the application of the attainable region approach to comminution processes.

Chapter 8

This chapter lays the foundation of the further applications of the attainable regions approach for process synthesis in comminution. The concept of attainable regions can be extended to the maximisation of the final product as the objective function. This chapter addresses the possibilities for the inclusion of downstream processes such as leaching, flotation and smelting in future work.

CHAPTER 2

LITERATURE REVIEW: COMMINUTION

2.1 INTRODUCTION

Comminution is the term given to processes that reduce particle sizes in a wide range of applications including the pharmaceutical, minerals, cement and chemical industries. In this chapter we review the comminution literature that is relevant for the application of the attainable regions approach. The attainable regions approach requires models that describe the fundamental processes operating in a system. Many advances have been made over the last century to aid in the understanding of the comminution processes. Size reduction models have developed a maturity as they have grown from being purely empirical to now encompass fundamental concepts of the processes taking place. This has led to the development of mathematical formulations which can be used in simulations and optimisation packages.

The size reduction process can be described as being analogous to a chemical reaction, in that the rate at which particles break or reactants react determines how fast either processes takes place. However, the difference is that the breakage of particles produces a range of particle size distributions. This requires the introduction of the concept of the primary breakage distribution function, which is a measure of the appearance of the progeny particles in the various smaller size intervals. Particles in a size interval can be regarded as a species just like reacting species in chemical reactions.

Chemical reaction rates are strong functions of the temperature and pressure under which the reaction takes place. Changing the grinding mill kinematic and loading conditions determines the extent and rate of grinding in a similar

manner. It is also possible to use the residence time in both unit operations to determine the extent of grinding and reaction.

2.2 GRINDING THEORY

Fundamentally, breakage is a result of energy input to a particle. This energy input can be in the form of kinetic, compression, microwaves and /or chemical energy. A lot of effort has been expended to try and develop models which describe breakage products as a function of the energy input. The first theory of comminution was proposed by Rittinger (1867). He postulated that the required energy input to a particle is proportional to the new surface area produced according to Equation 2.1.

$$E_R = K_R \text{ [new surface area – old surface area]} \tag{2.1}$$

Where K_R is the grinding rate constant and E_R is the specific energy input (energy input per unit feed mass). This theory gives a basis for the minimum specific energy required to break the bonds that existed between the two new surfaces. However, Rose (1967) proved experimentally that the required energy for new surface generation is less than 1% of the energy input into a mill. He proposed that the rest of the energy was lost as heat, noise and elastic energy. The consequence of this is that the specific energy predicted from Equation 2.1 can not be taken as the control variable for designing commercial installations because it is a small and almost negligible percent. Rittinger's theory neglects the fact that particles absorb energy elastically before they reach their yield point.

Kick (1885) postulated a second theory of comminution stating that specific energy is proportional to the reduction in volume of the particles. The mathematical description of this model is given as Equation 2.2.

9

$$E_K = K_K \log\left(\frac{x_f}{x_p}\right) \qquad (2.2)$$

where E_K is the specific energy required to reduce feed particles of size x_f to product particles of size x_p and K_K is the rate constant. The development of Kick's theory was based on the stress-strain diagram of cubes under compression. The evenly applied stress in compression is proportional to the volume, and therefore Kick's theory fails to describe the effect of surface energy as described by the theory of Rittinger, under predicting the energy requirements.

Bond (1952) postulated a third theory of comminution. He stated that the useful energy applied in breaking a stated weight of homogeneous material is inversely proportional to the square root of the diameter of the product particles according to Equation 2.3.

$$E_B = K_B\left[\frac{10}{x_p^{0.5}} - \frac{10}{x_f^{0.5}}\right] \qquad (2.3)$$

where K_B is the Bond proportionality constant. Bond argues that his postulate is based on that the work input is utilized in the deformation of the particles and is released as heat. Local deformations beyond the critical strain results in the formation of a crack tip which propagates resulting in breakage. Strain energy level depends on the volume of the particle while crack propagation results in the creation of the new surface area, resulting in a combination of the theories of Rittinger and Kick. A drawback to the theory of Bond is that all the grinding sub-processes are lumped into a single work index term which limits the range of validity for its application.

The above three theories are empirically based and limited when it comes to modeling commercial processes, although Bond's theory is still applied to some extent. The limitations of these models have been attributed to the inability of theories to handle wide particle size distributions, or sub-processes of transportation, in addition to the requirement for normalization of the distribution of breakage products and selectivity limits the theories applications. This has resulted in the development of the population balance model by Bass (1954) which will be discussed in section 2.3.

2.3 THE BREAKAGE EQUATION (POPULATION BALANCE MODEL)

The 20th century saw researchers attempt to develop a mathematical description of the grinding process. Epstein (1947) introduced the two concepts of selection and breakage functions in his continuous probability formulation. Sedlatschek and Bass (1953) introduced the concept of the first law of breakage, that the rate of disappearance of particles from a small size interval is proportional to the weight of particles present in that size interval. This is based on the assumption that the probability of breakage is independent of the proportions of any other sizes present. Bass (1954) was the first to derive the fundamental mass balance as an integro-differential mathematical equation for batch grinding. The result of his derivation is given as equation 2.4.

$$\frac{\partial^2 F(x,t)}{\partial x \partial t} = -k(x)\frac{\partial F(x,t)}{\partial x} + \int_x^{x_0} \frac{\partial B(x,\alpha)}{\partial x}.k(\alpha).\frac{\partial F(\alpha,t)}{\partial x}.\partial\alpha \qquad (2.4)$$

$F(x,t)$ is the weight fraction after grinding a feed of size distribution $F(x,0)$ and maximum size x_0 for time t, and $B(x,\alpha)$ is the cumulative form of the breakage distribution function. The breakage distribution function is the fraction of

material finer than size *x* obtained through the primary breakage of material of size *α*. The fractional rate of breakage *k(x)* is given by either the probability or the selection function.

Equation 2.4 is the integro-differential equation and it states that the net rate of production of material of any size *x* equals the rate of production of that size from breakage of all material initially larger than size *x* minus the rate of breakage of material of size x. That is to say, the net rate of production is given by the difference between the rate of production of the size class of interest and the rate of consumption of the particles in that size class.

Broadbent and Callcott (1956) introduced the concept of a matrix representation of breakage using Epstein's concepts of selection and breakage functions. The classical work of Gardner and Austin (1962) solved the integro-differential equation using the Euler technique to successfully predict experimental results. They used an iterative solution to the integro-differential equation for batch grinding to calculate product size distributions for known feed size distributions and the experimentally determined comminution functions. Gaudin and Meloy (1962) theoretically presented a solution to the integro-differential equation using the matrix notation, Equation 2.5.

$$\boldsymbol{m}_p = (\mathbf{I} + \mathbf{S'b} - \mathbf{S'}).\boldsymbol{m}_f \qquad\qquad (2.5)$$

where $\boldsymbol{m}_p$ and $\boldsymbol{m}_f$ are the product and feed mass fraction distribution vectors respectively, $\mathbf{I}$ is an identity matrix, $\mathbf{S'}$ is the selection function, $\mathbf{b}$ is the breakage distribution function, $\mathbf{I}.\boldsymbol{m}_f$ is the feed material remaining unbroken, $\mathbf{S'b}.\boldsymbol{m}_f$ is the amount of feed material selected and broken into the vector of products and $\mathbf{S'}.\boldsymbol{m}_f$ is the amount of material broken out of its size class.

Reid (1965) presented a finite difference solution to the integro-differential equation. The solution is continuous in the time variable and therefore can be extended to continuous systems. Particle characterisation is achieved by sieving techniques. Discreet size intervals result from these subdivisions which offer an opportunity for finite difference modelling. The population balance model by Reid (1965), Equation 2.6, is the form that will be used for describing product size distributions for our experimental analysis.

$$\frac{dm_i(t)}{dt} = -k_i m_i(t) + \sum_{\substack{j=1 \\ i>j}}^{i-1} k_j b_{ij} m_j(t) \tag{2.6}$$

Herbst and Fuerstenau (1973) have postulated an alternative normalised form of the population balance model, Equation 2.7. This form is independent of mill speed, ball and particle loading. They experimentally verified that the ratio of the selection function to the specific power input to the mill was a constant. The kinetics of the top size interval are normalised with respect to the specific energy input. This kinetics model reduces to a single straight line when the independent variable of grinding time is replaced by specific energy input.

$$\frac{dm_i(\overline{E})}{dE} = -k^{\overline{E}}{}_i m_i(\overline{E}) + \sum_{j=1}^{i-1} k^{\overline{E}}{}_j b_{ij} m_j(\overline{E}) \tag{2.7}$$

The implications of this result are profound in that the specific energy becomes the only variable of interest instead of the equipment specific variables such as kinematic and loading conditions in a ball or roller mill. This concept of specific energy dependency will be further explored later in this thesis.

Having explored the different grinding models such as those proposed by Rittinger, Kick and Bond, the population balance model describes the breakage process more adequately and it is the model of choice in this thesis. The population balance model will be used for the determination of the behaviour of the comminution system.

2.3.1 The breakage distribution function (b_{ij})

The breakage function describes the distribution of feed particles from a grinding event. It is predicted from the analyses of breakage of single sized particles in a laboratory mill. Equation 2.8 describes b_{ij} which ideally should be the ratio of the mass from size class j reporting only to size class i before size class i breaks into size class i+1, which is why it is calculated at initial grind times (Austin et al., 1984).

$$b_{ij} = \frac{mass\ in\ size\ class\ i, t \to 0}{mass\ broken\ from\ size\ class\ j, t \to 0} \qquad (2.8)$$

Shoji et al. (1979) have shown that b_{ij} values are insensitive to the precise mill conditions. Many models have been proposed to describe the distribution of breakage products. Single impact tests at different energy levels are shown in Figure 2.1 (Bourgeois, 1993).

The nth index represents the relative size ratio of the parent size to the progeny size. Increasing the impact energy increases the amount of progeny in the lower size classes. It is postulated that the same relationship between the breakage function and energy will be obtained when the impact involves a bed of particles.
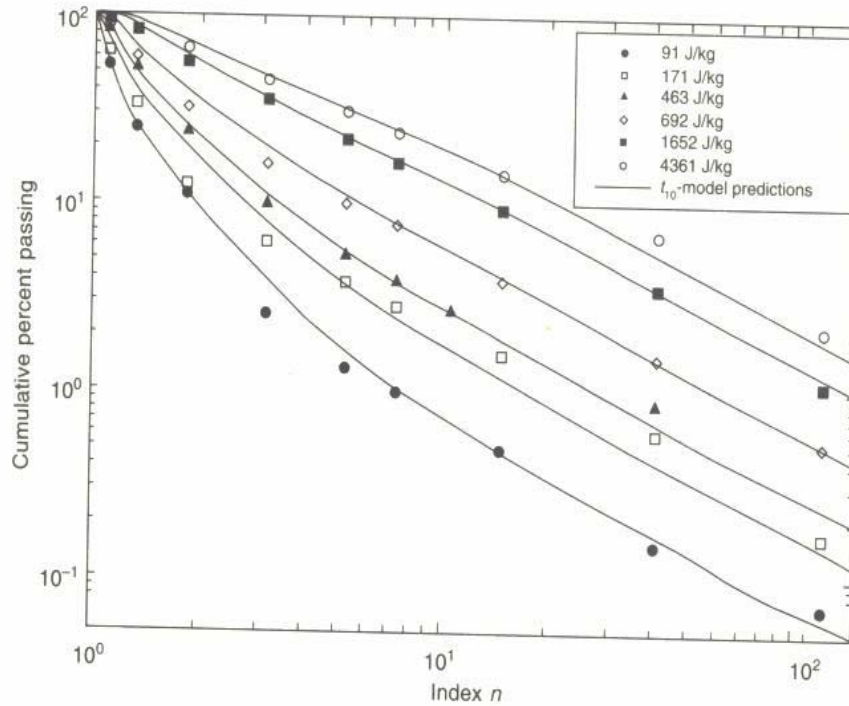
Figure 2.1: The breakage functions measured in single-particle tests at different impact forces for 3.35 - 4.00 mm quartz particles (Bourgeois, 1993).

The breakage function that results from the impact as a whole is the sum total of the individual breakage functions from each particle that absorbs sufficient energy to break. The size distributions can be characterized effectively in terms of the parameter t_{10} which is the mass fraction of the progeny that are smaller than 1/10th of the parent size. The breakage function at any other size can be represented by t_n the mass fraction smaller than 1/n of the parent size (King, 2001). Figure 2.2 shows the agreement between the experimental results and the model predictions.

15
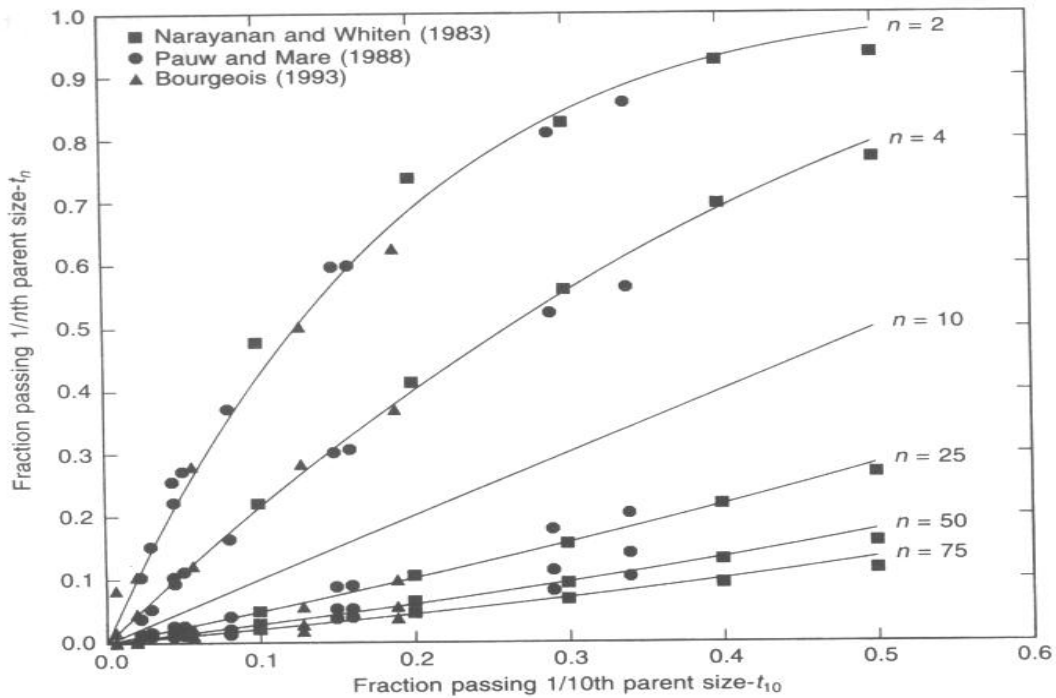
Figure 2.2: Reconstruction plot for the breakage function that is defined in terms of the parameter t_{10}. The solid lines are calculated using Equation 2.10 (King, 2001).

The t_{10} breakage index is determined primarily by the energy that is absorbed during the impact and is modeled using Equation 2.9 (King, 2001).

$$t_{10} = t_{10\,max}\left(1 - exp^{-\frac{\beta E_m}{E_{m\,50}}}\right)$$ (2.9)

where t_{10max} and β are material specific and are obtained using the results of standard drop weight tests. Figure 2.2 shows the entire breakage function regenerated from the single t_{10} value using Equation 2.10 based on the truncated Rosin-Rammler distribution.

$$t_n = 1 - \left(1 - t_{10}\right)^{\left(\frac{9}{n-1}\right)^{\alpha}}$$ (2.10)

Substituting Equation 2.9 into Equation 2.10 enables the modeling of breakage products as a function of specific energy. Figure 2.3 is a result of such an exercise and shows that the cumulative distribution of 4.75 mm quartz particles impacted with increasing specific energy favors the smaller particle size range. This trend continues up to a point where any additional energy has no significant particle size reduction and this condition is known as plastic deformation. Varying the specific energy produces a unique mass distribution and this can, within constraints of the energy input model be manipulated to control product size distributions.
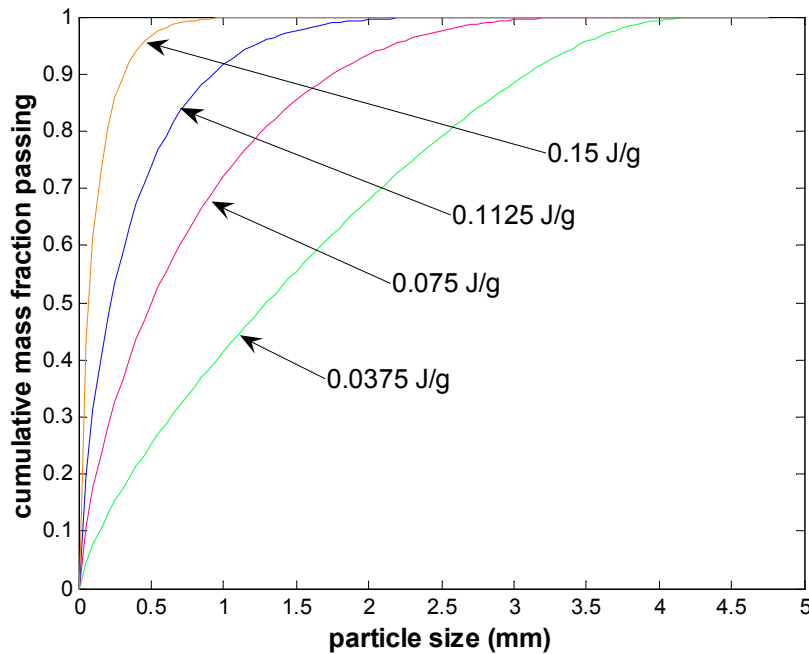
Figure 2.3: The breakage function for 4.75 mm quartz particles for increasing specific energy.

Figure 2.4 describes in a different format the information shown in Figure 2.3. These two formats are the traditional representations of particle size

distributions. Figure 2.4 shows the discreet density function which is the mass of particles retained in each geometric size class. It can be clearly seen that product distributions of higher specific energy are narrower towards the fines range. This would indicate that if the energy addition can be varied it might be possible to achieve certain distributions as required.

The above description of particle size distributions is on a geometric x-coordinate system. Figure 2.4 is geometric in the sense that it is constructed from mass fraction information residing in geometric size intervals. The amount of material in the larger size classes is minute and would be invisible when represented on a constant x-coordinate system. However because of the lumping effect due to the geometric x-coordinate system, the whole particle size distribution is described fairly.
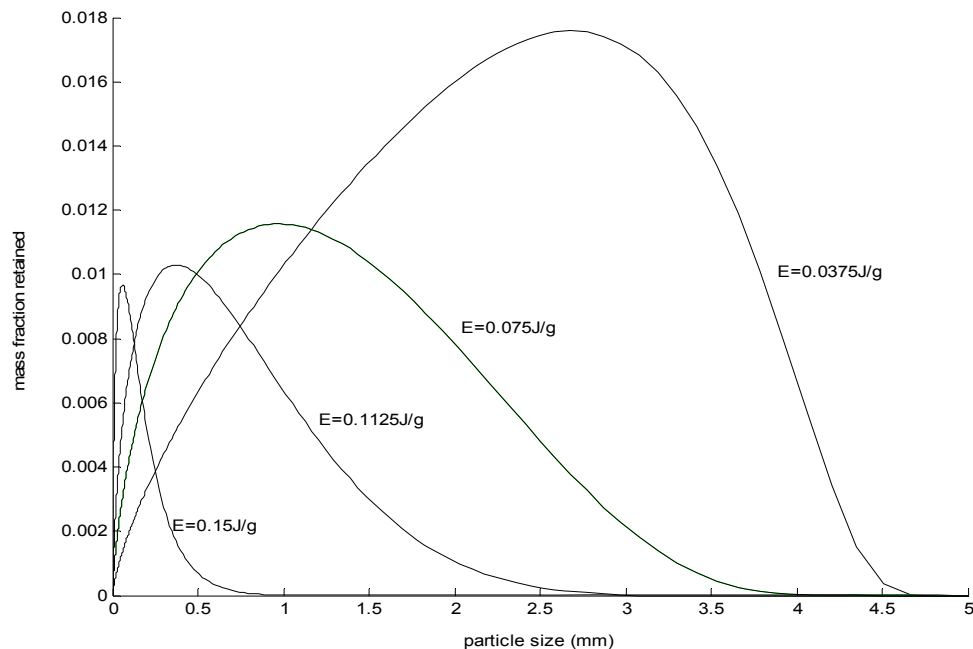
Figure 2.4: Mass fraction retained for 4.75mm quartz particles impacted by increasing specific energy.

2.3.2 The selection function

Section 2.3 introduced the population balance model which consists of the breakage and selection functions as in Equation 2.7. This section now describes in detail the selection function which is defined as the rate or probability of breakage of particles. The particle must be heavily stressed before any substantial breakage occurs. This stress is mostly stored as elastic energy and is lost when the particle fractures. The elastic energy a particle can absorb without fracture is related to its volume and material properties of the particle. The elastic energy in comminution can be described as analogous to the activation energy in chemical reactions. The rate constants depend on particle size according to the Arrhenius form of equation. The rate constant in chemical reactions has an exponential dependence on temperature as depicted by the Arrhenius equation, Equation 2.11.

$$k^R = k^R{}_o \, exp^{\left(-\frac{E}{RT}\right)}$$
(2.11)

In comparison, for comminution the rate of breakage has a power law dependence on the particle size x as in Equation 2.12.

$$k(x) = Ax^{\alpha}$$
(2.12)

As would be expected, the rate of breakage is constant for zero order grinding kinetics. This occurs when the grinding zone is saturated with mono-sized feed material. First order grinding kinetics is observed when statistically independent grinding events are applied to an infinite particle population. The convex combination of zero and first order grinding kinetics can also be considered as physically possible (Grandy et al., 1970). This implies that for

the population balance model the term k_i*m_i (Equation 2.6) remains constant for zero order kinetics and changes for first order kinetics.

The population balance model by Reid (1965), Equation 2.6, was time dependent but now has been modified to be specific energy dependent (Herbst et al., 1973) as in Equation 2.7. This has lead to a change in thinking in that, instead of the selection function being a time dependent rate function, it is now defined as being dependent on the probability of breakage which is a function of the specific energy expended. The time dependence of the Reid equation tells us that the product distribution is a function of time and this is only partly true because breakage is a result of the amount of energy input over time. According to breakage fundamentals, stress response due to energy input results in breakage while time on its own does not break anything.

The log-normal distribution has been successfully used to describe the breakage probability with specific energy for a variety of irregularly shaped brittle materials (Baumgardt et al, 1975; Dan et al, 1990; King et al, 1993a) and is given by Equation 2.13.

$$P(E_m) = \frac{1}{2}\left[1 + erf\left(\frac{\ln E_m - \ln E_{m50}}{\sqrt{2\sigma_E}}\right)\right] \tag{2.13}$$

where P is the breakage probability or selectivity, E_m is the specific energy input, E_{m50} is the median particle fracture energy and σ_E^2 is the geometric variance of the distribution.

Equation 2.13 is used for predicting the probability of breakage of single particles when impacted with different specific energy levels during drop

weight tests. Load cell experiments on similarly sized particles show that the particle fracture energy of similarly sized particles follows a distribution. The median fracture energy E_{m50} is a single value that quantifies the fracture energy of similarly sized particles. Power law relationships between the mass specific particle fracture energy and the particle size have been derived and the model in Equation 2.14 is used for these systems (Tavares & King, 1998).

$$E_{m50} = E_{m\infty} \left[1 + \frac{d_{po}}{d_p} \right]^{\phi} \qquad\qquad (2.14)$$

where $E_{m\infty}$ is the residual particle fracture energy of the material at larger sizes and d_{p0} is a characteristic size of the material microstructure and Φ is a model constant.

The models used for the simulations presented in this thesis, e.g Equation 2.13, are statistical averages of single particle breakage from drop weight tests (Tavares, 1999). Also statistical mechanics stipulates that the macroscopic behavior of a system is identical to the statistical average over all possible micro-states. Each single particle breakage distribution is descriptive of a microscopic state of the system and is equally likely by an assumption of randomness and the statistical average of many single particle breakage distributions is taken as the one which describes the macroscopic behavior of the system. This statistical average assumption will be used later for theoretical simulations and experimental data fitting.

Substituting Equation 2.14 into Equation 2.13 enables the calculation of the selection function for known particle sizes being impacted by known input energy levels resulting in Figure 2.5. Figure 2.5 is a plot of the breakage probability of different sized particles impacted by different specific energy

levels. Figure 2.5 shows that smaller particles have lower probability of being broken for a given specific energy input. Increasing the specific energy input to a system increases the probability of breakage for all particle sizes. Both Equations 2.12 and 2.14 have particle sizes x and d_{po} raised to a power of α and Φ, respectively. Both equations have the form of a product of a pre-multiplier constant and the relative particle size raised to some exponent. It also follows that as the particle mass is proportional to the particle size; and the minimum energy density requirement for new surface generation, that one needs more energy to break a bigger particle than a small one. We can see that the power law dependence of the breakage rate in Equation 2.12 and the specific energy in Equation 2.14 on the particle size are analogous and therefore invariant in their application. The specific particle fracture energy decreases as particle size increases while the particle fracture energy increases at a rate proportional to the particle mass.
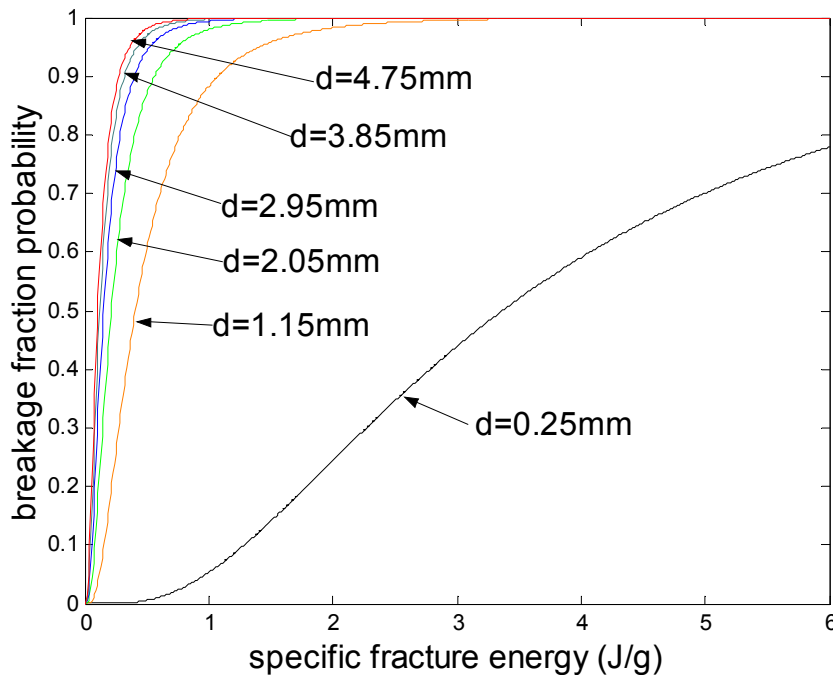
Figure 2.5: The selection function for increasing quartz particle sizes

2.4 GRINDING MECHANISMS

First we need to understand how breakage as a physical and fundamental process occurs without being equipment specific. This is necessary so that we can identify the different breakage mechanisms on the basis of the stress requirements. The proposed breakage mechanisms are classified as abrasion, impact or compression (Prasher, 1987). These can also be classified in terms of the magnitude of the applied stress. The product breakage pattern is a function of the predominant breakage mechanism. Leung et al. (1987) have shown that if the specific energy of the impact is low enough the size distribution of the breakage products is similar to that expected of an abrasion mechanism. For each size class and material, there is a minimum energy level below which abrasion is dominant and above this minimum energy, impact and/or compression becomes the dominant breakage mechanism. There is not significant difference between the magnitude of forces required for both compression and impact mechanism. However, the rate of application of the force is lower in compression than in impact breakage. Shipway & Hutchings (1993) have shown that the stress distributions in elastic spheres subjected to free impact and uniaxial compression loading are broadly similar.

2.4.1 Abrasion/chipping mechanism

The average mass of a particle is related to its characteristic particle size d_p by Equation 2.15 and using a spherical particle model the rate of wear is proportional to the surface area of the particle. Equation 2.16 is the model for the loss of mass of a coarse particle due to abrasion (Unland and Szczelina, 2002).

$$m(d_p) = \beta d_p^{\ 3} \tag{2.15}$$

$$wear \ldots rate = -\frac{K \rho \pi r^{2+\Delta}}{2}$$

$$\frac{dm}{dt} = -3K \frac{m}{d_p^{1-\Delta}}$$

(2.16)

where ρ is the density and r the radius of the particle, m is the mass of the particle, d_p is the geometric mean size (square root of the product of the end particle sizes defining the interval) of the original feed particles and K is the breakage rate function which is proportional to the input specific energy. The size of particles and the load influences the value of the specific wear rate. This implies that the velocity at which a wearing particle moves in phase space is constant and is given by K.

Δ is a constant which varies between 0 and 1. If Δ is equal to zero, the specific surface wear rate is constant and if Δ is greater than zero then the specific wear rate increases as the size of the particle increases. For Δ equal to one, the wear rate is proportional to the mass of the particle and is attributed to the chipping mechanism. For Δ equal to two thirds, the wear rate is proportional to the surface area of the particle and indicates abrasion as the mechanism of breakage. Figure 2.6 shows the increasing wear rate as particle weight increases for Δ equal to two thirds.
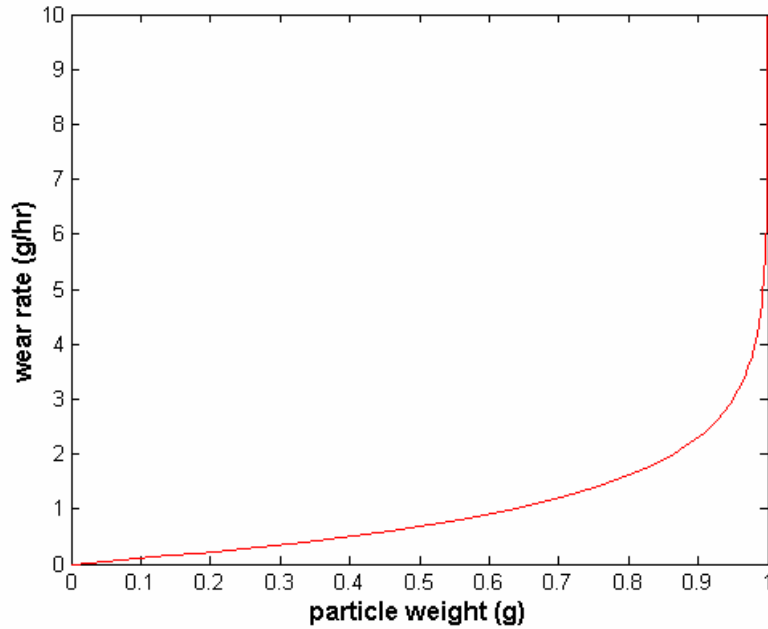
Figure 2.6: Particle wear rate for the abrasion mechanism.

Figure 2.6 shows that the wear rate decreases as the level of fines increase in the load. This can be explained by means of a cushioning effect with time, which is described by the relationship by Goldman et al. (1988) given in Equation 2.17.

$$K = K_0 + K_1 \times (\% \, fines)$$ (2.17)

where K_0 = 0.089 hr^{-1} and K_1=-0.5hr^{-1}.

The abrasion breakage rate increases for a given particle diameter up to a point where sufficient specific energy is imparted to the particles to propagate cracks through them. This leads to a change in the breakage mechanism.

The fraction of the original feed particle/s degraded (P) with time is represented as a plateau on the cumulative size distribution curve. Figure 2.7

25

is a plot of P with time and it represents the points where the cumulative particle size plateaus. These points also represent the abrasion breakage function. So the rest of the particle size distribution is the residue of the worn feed particles. The original feed particles do not change much in size.
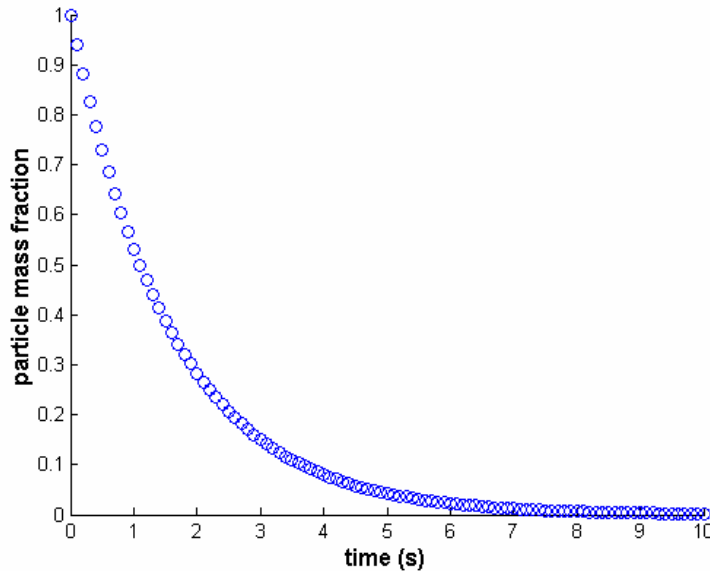
Figure 2.7: Change in mass of a particle being abraded.

2.4.1.1 Modeling of abrasion product size distributions

The cumulative size distribution is typically bimodal. It is linear in the fines range and has a single/double inflexion in the coarse range. The linear section can be represented using a Gaudin-Schumann plot while the single/double inflexion is modeled by a third degree polynomial. The combination of the two functions results in the model with the form of Equation 2.18 (Goldman et al. 1991).

$$\log Y = m \log(\frac{X}{X_{max}}) + a(\frac{X}{X_{max}})^3 + b(\frac{X}{X_{max}})^2 + c(\frac{X}{X_{max}}) + 2 - d \qquad (2.18)$$

where $d=a+b+c$, Y is the cumulative size distribution, X is the particle size (sieve size), and X_{max} is the maximum sieve dimension (100%).
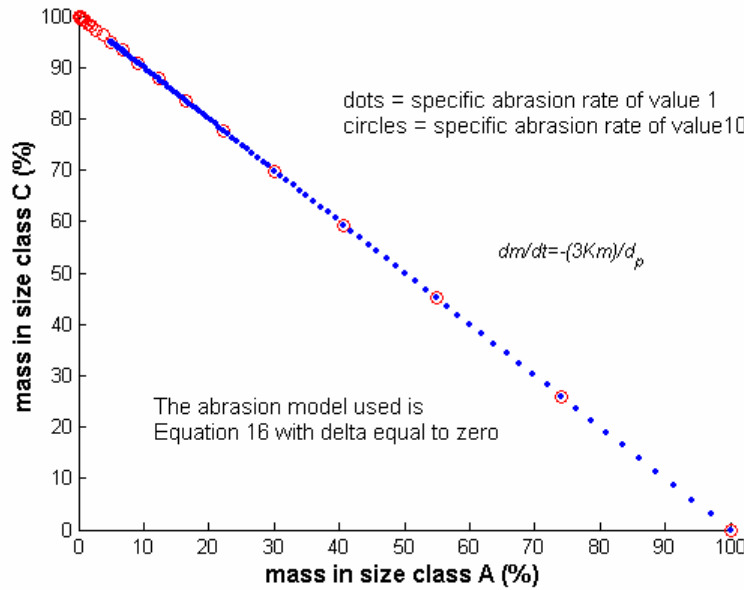
Figure 2.8: Abrasion particle size distribution.

Three size classes are considered and no daughter particles report to the middle size class because abrasion is a surface phenomenon. Therefore the breakage products report to the third size class only as represented in Figure 2.8.

The dotted line is for a lower specific abrasion rate as compared to the higher one represented by circles. The breakage products only distribute themselves within two size classes in time.
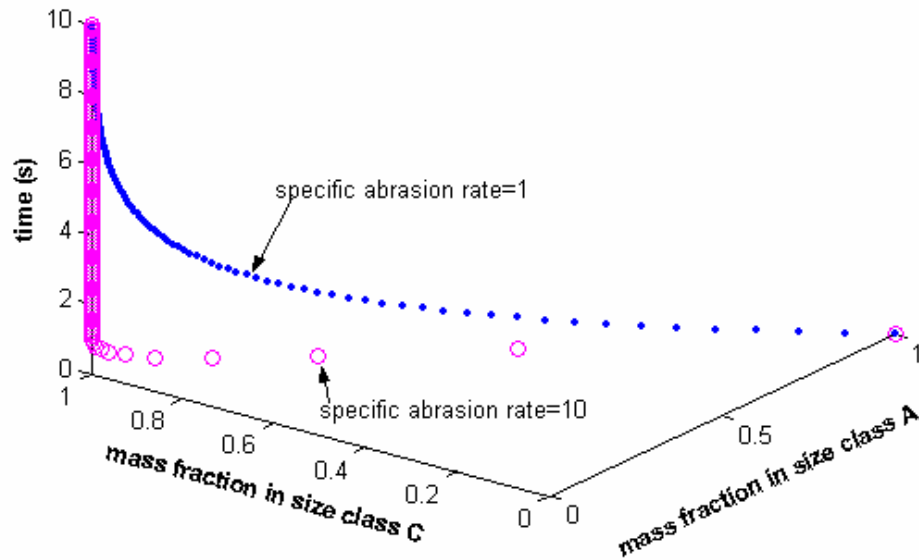
Figure 2.9: Abrasion size distribution with an additional dimension of time.

The same distribution into the two size classes is achieved at different residence times for varying specific attrition rates as seen in Figure 2.9. The level of specific energy is important in analyzing dynamic systems. In Figure 2.9 we can see that increasing the abrasion rate reduces the process time. The dynamic simulation gives insight into the optimal control of an abrasion process. As long as the abrasion rate and its corresponding specific energy does not cross the boundary for mechanism change one should endeavor to operate at a higher specific abrasion rate.

2.4.2 Compression mechanism

In the processing zone the main compression is of individual particles and not of entire particle beds. The level of resistance of a material to breakage is the measure of its compressive strength. In considering compression breakage

we should make a distinction between the fracture mechanism and the crushing mechanism which is a function of the equipment. The stressing factor is the displacement applied to the particles. All breakage is a result of application of force which results in tensile stress to the bonds and pulling them. The magnitude of the resultant stress is what has been classified as breakage mechanisms namely; attrition, impact or compression. Since we now understand how breakage as a physical and fundamental process occurs without being machine specific, we can now assign the different mechanisms of breakage based on the specific energy input.

Experimental work shows that there is a reduced specific crushing work with increasing particle diameter and decreasing enforced displacements h_r. The applied compression displacement h is used in relation to the particle diameter d_p as the relative compression displacement. Equation 2.19 is a good approximation of the dependence of mass specific compression work to particle diameter (Unland et al., 2002).

$$W_m = K_n \times d_p^{-0.7} \tag{2.19}$$

The mass specific compression work applied is a function of the relative displacement. One has to determine the relative displacement required to break all particles when designing the crushing equipment.

There is a close resemblance of the compression work to the impact work as shown in Equations 2.14 & 2.19 respectively and represented in Figure 2.10. The compression and impact breakage mean specific fracture energy have been generalized into the form of Equation 2.20.

$$E = K \times d_p^{-\alpha} \tag{2.20}$$

where K and a are material constants and d_p is the particle diameter. Figure 2.10 shows the variation of the mean fracture energy as a changes.
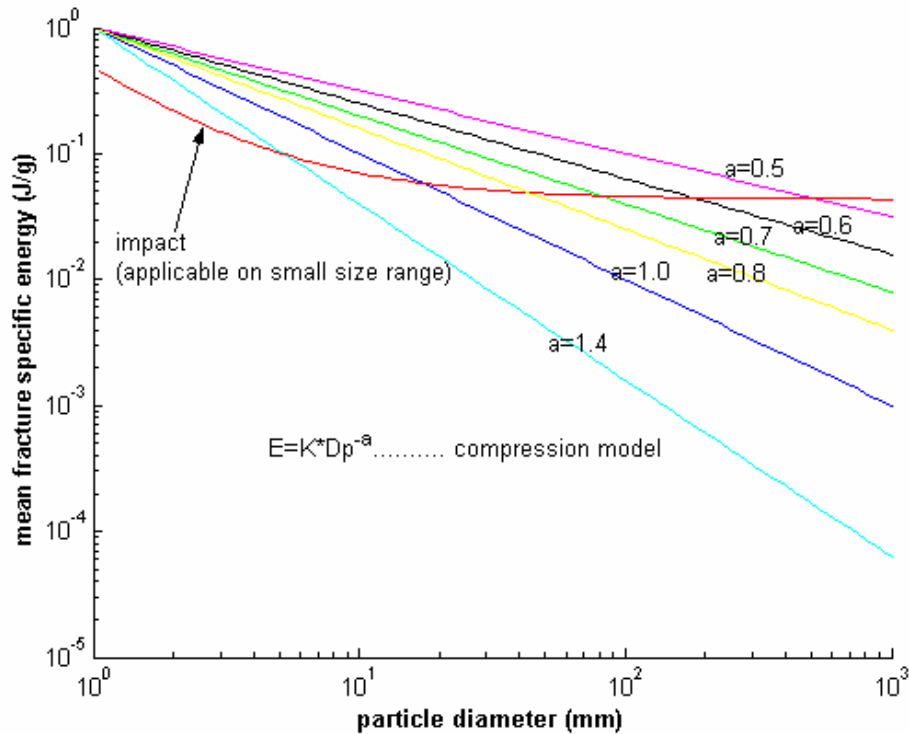
Figure 2.10: Variation of specific fracture energy with particle diameter for impact and compressive stress.

Compression applies a well defined displacement to the rock and the likelihood of breakage is not dependent on the particle diameter. The likelihood of breakage P_b is a function of the relative displacement up to a certain displacement where all the particles are broken. The likelihood of breakage is proportional to the t_{10} breakage index defined as the fraction of the progeny that are smaller than $1/10^{th}$ of the parent size used to describe impact breakage products. There is a unique relationship between t_{10} and t_n the fraction smaller than $1/n^{th}$ of the parent size, Equation 2.10.

The compression displacement h is used in relationship to the particle diameter d_p as the relative compression displacement h_r. Figure 2.11 represents the compression model: where k_1 represent the relative displacement at which all particles are broken. Equation 2.21 is also a representation of the likelihood of breakage.

$$P_b(T_{10}) = k_1 \left(1 - \exp\left(-\frac{h_r}{k_2} \right) \right)$$ (2.21)

The size distribution is well described by a truncated logarithmic normal distribution. Truncated distribution functions refer to particle populations where no progeny particle can have a size larger than the parent so that the size distributions are truncated at the parent size. No agglomeration of particles takes place. Log-normal distributions are described by the geometric mean size which is the 50% passing size and the geometric standard deviation calculated from 0.5*(84% passing size ⁒ 16% passing size). The related mean particle diameter depends on the relative displacement and is not a function of the particle diameter.
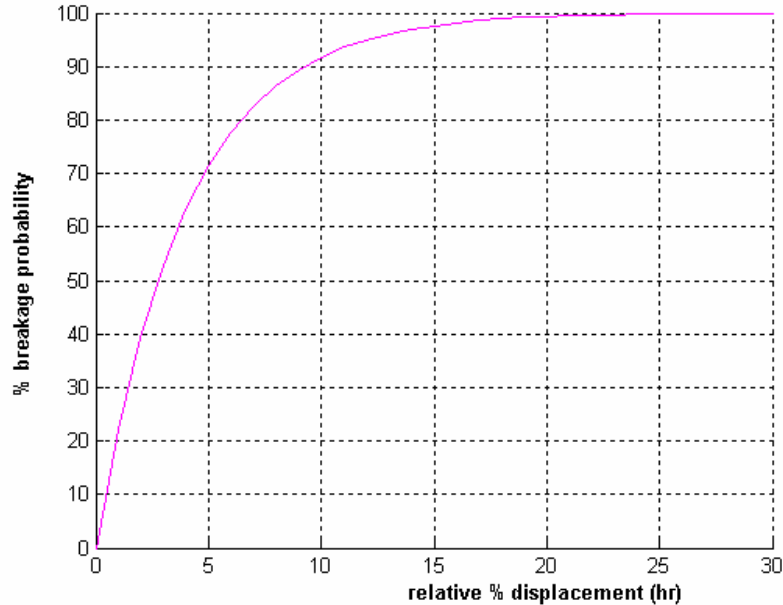
Figure 2.11: The likelihood of breakage with displacement.

The standard deviation increases with relative displacement h_r and is independent of the particle diameter (Unland et al., 2002). A particular relative displacement on any particle diameter gives the same amount of undersize mass percentage. As the relative displacement increases, the cumulative percent passing material also increases. Compression breakage distributions are independent of particle size.

2.4.3 Impact type

The specific particle fracture energy decreases as size increases but the rate of decrease reduces as the particle size increases and eventually becomes a constant for larger particles (Tavares et al., 1998). Therefore the particle fracture energy increases at a rate approximately proportional to the particle mass. For a given impact energy, larger particles have a smaller probability of being broken since the energy that a particle absorbs from the impact must

32

exceed its fracture energy. Equation 2.14 describes the specific energy requirements for impact breakage.

The rate and magnitude of the force determine which mechanism is taking place in breakage. The selection function describes the breakage rate, so the rate of application of force determines the breakage function. All other mechanisms of breakage can be related to impact breakage. The impact breakage mechanism will be used in our study of comminution systems and the same method can be repeated for systems employing abrasion and compression breakage mechanisms depending on the level of the specific energy input. The differences in the observed phenomenon of breakage mechanisms depend on the rate of application of force and the amount of force applied.

2.5 THE CLASSIFICATION PROCESS IN COMMINUTION

Classification is the splitting of product streams from a breakage process into two or more streams (Austin et al., 1984). The classification of particles is based on the physical property of particle size to the relevant product, be it tailings or middlings or course. These recovered streams can be recycled or retained as product according to the desired objective function. It has been noted that repeated grinding stages result in excessive fines production due to over-grinding. There is an optimum point at which the classification process should be introduced to avoid over grinding therefore optimizing energy consumption. The classification process also gives the opportunity for mixing streams of similar distributions so as to get the most efficient use of energy since different particle sizes have different mean specific fracture energies according to Equation 2.14. Introducing inter-stage classification maximises:

    i)   The amount of material that meets the design specification,

ii)   The energy efficiency by reducing the extent of over grinding material beyond the design specification.

Classification is currently used industrially in closed circuit processes and the purpose of our research is to show whether it reduces energy consumption and maximises the objective function. This will provide a target against which actual processes can be measured.

2.5.1 Classification principles

Classification is a result of density, shape and size considerations. A falling particle achieves terminal velocity when the gravitational pull and the fluid resistance force balance out causing the particle to fall at a uniform rate. The fluid resistance force is a result of the drag experienced by the descending particle as it displaces the fluid around it. The drag force pulls the particle upwards while the gravitational force is pulling it down. The particle eventually descends at a constant velocity reaching terminal velocity rapidly. Particles in a sorting column either sink or rise depending on whether their terminal velocity is greater or less than the upward velocity of the fluid. The overflow will consist of particles with terminal velocities which are less than the fluid velocity and conversely, the underflow consists of particles with terminal velocities greater than the rising fluid velocity. For a spherical particle of diameter d_p and density ρ_p falling under gravity in a fluid of viscosity μ_f and density ρ_f under free settling conditions, the terminal velocity v_T is calculated using Stokes' law which assumes the drag force to be entirely due to viscous resistance, Equation 2.22.

$$v_T = \frac{g d_p^{\,2} \left(\rho_p - \rho_f \right)}{18 \mu_f}$$

(2.22)

Newton assumed the drag force was entirely due to turbulent resistance and deduced Newton's law, Equation 2.23 for calculating the terminal velocity.

$$v_T = \left(\frac{3gd_p \left(\rho_p - \rho_f \right)}{\rho_f} \right)^{0.5}$$

(2.23)

These two laws of free settling show that for two particles with the same;

(i)   diameter, the heavier particle achieves a higher terminal velocity and,

(ii)   density, the particle with the larger diameter has the higher terminal velocity.

Hindered settling is encountered as solid particles increase in the pulp resulting in particle crowding. This results in reduced terminal velocities due to the fluid behaving as a heavy liquid whose density is that of the pulp and not the carrier liquid. Equation 2.24 is the modified form of Newton's law that is used to calculate the falling rate of the particles.

$$v_T = k \left[d_p \left(\rho_p - \rho_f \right) \right]^{0.5}$$

(2.24)

Hindered settling reduces the effect of size while increasing the effect of density on classification.

2.5.2 Classification models

Ideally there is no practical classifier which can achieve 100 % separation of the feed into a stream of fines only and another stream of course particles only. Due to stochastic factors of particle collisions and separating medium

turbulence some of the fine particles will report to the stream of course particles and also some of the coarse particles will report to the stream of fine particles. Mathematical models have been developed to quantify the selectivity of particles into the product streams, be they fines or course. The selectivity *s* for size interval *i* is the fraction of size *i* in the feed stream reporting to the coarse stream. The set of s_i values describe how the mass in the various size intervals are split. Ideal classification would achieve s_i equal to zero for the size classes less than the cut-size and s_i equal to one for all size classes greater than the cut-size. The most common way of representing cyclone efficiency is the Tromp curve shown in Figure 2.12.
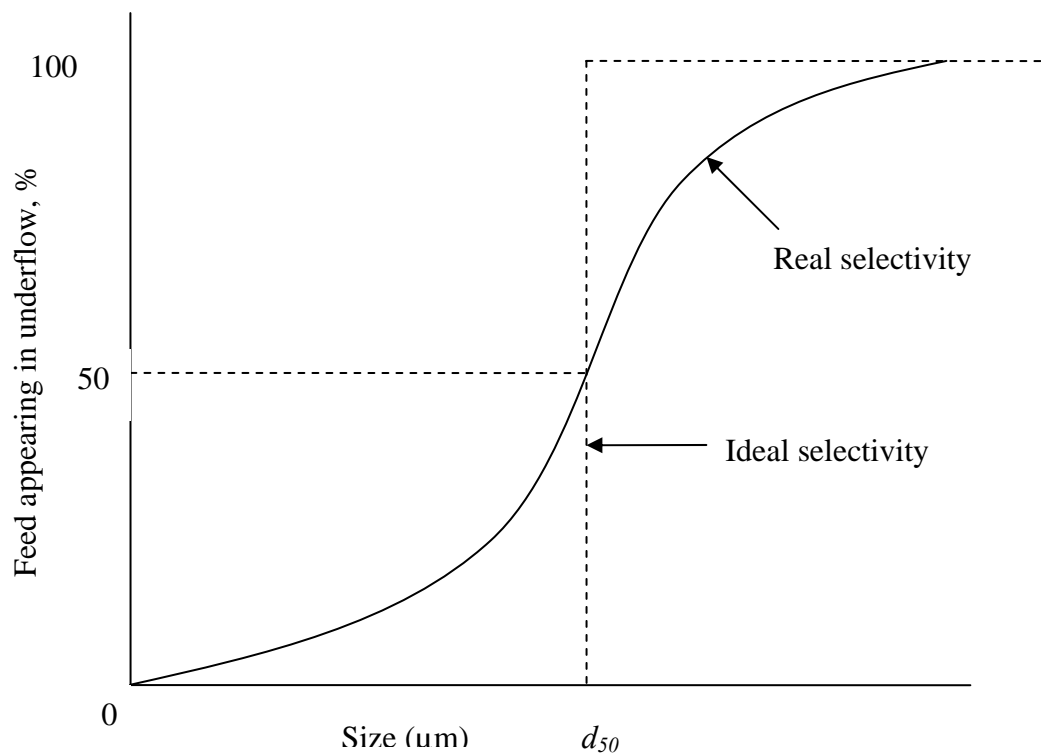
Figure 2.12: Tromp curve for hydrocyclones (Wills, 1981).

The Tromp curve relates the particle size to the mass fraction of each particle in the feed which reports to the overflow or the underflow (Wills, 1981). The

36

cut-size is defined as that point on the Tromp curve for which 50 % of particles in the feed of that size report to the underflow, it is also referred to as the d_{50} size and it is shown in Figure 2.12.

A number of empirical relationships are available to a designer for predicting performance and design of cyclones. Dahlstrom (1954) presented Equation 2.22 for the calculation of the cut size for dilute slurries in small diameter cyclones.

$$d_{50} = \frac{13.7 (D_o D_i)^{0.68}}{Q^{0.53} (S-L)^{0.5}}$$
(2.22)

where d_{50} is the cut-size (µm), D_o is the overflow diameter (cm), D_i is the inlet diameter (cm), Q is the total feed flow rate of the slurry (m^3 h^{-1}), S is the specific gravity of solids and L is the specific gravity of liquid (g cm^{-3}).

Plitt (1976) developed a model Equation 2.23 that is applicable on cyclones with large diameters operating at high solids content over a wide range of operating conditions. This mathematical model can calculate the efficiency of a cyclone accurately without experimental data.

$$d_{50} = \frac{14.2 D_c^{0.46} D_i^{0.6} D_o^{1.21} \, exp(0.063V)}{D_u^{0.71} h^{0.38} Q^{0.45} (S-L)^{0.5}}$$
(2.23)

where D_c, D_i, D_o and D_u are the inside diameters of the hydrocyclone, inlet, vortex finder and apex, respectively (cm), h is the distance from the bottom of the vortex finder to the top of the underflow orifice (cm).

Many empirical correlations have been presented by other researchers in an effort to predict performance and design cyclones (Flintoff et al., 1987;

Nageswararao, 1978; Bradley, 1965; Lynch et al., 1975). However in this research we do not concentrate much on the classification models since our idea is to construct the candidate attainable region for the extreme limits of selectivity, 1 and 0 because we are offering a tool for targeting purposes.

2.5.3 Types of classifiers

Various types of classifiers are used and they generally fall into two categories. There are those that separate by fluid dynamics and those that involve mechanical screening.

2.5.3.1 Mechanical air separator

Mechanical classifiers have widespread use in closed-circuit grinding operations. The mechanical air classifier consists of an outer and inner shell with a rotating plate which disperses the feed within the inner shell. Air is drawn upwards from the outer shell to the inner shell and it carries the suspended finer material into the outer shell. The rotation of suspended material and air in the outer shell results in the discharge of solids and the air re-enters the inner shell for further separation of the feed. Some fine solid material re-enters the inner shell with the air because the separation is not ideal. This results in low selectivity values of the fines particles.

2.5.3.2 The hydrocyclone

It consists of a vertical cylinder with a conical bottom. It is open at its apex or the underflow, with the vortex finder at the top extending below the feed point to avoid the feed reporting directly to the overflow discharge. There are no moving parts and the feed is introduced under pressure resulting in the rotational motion. This devise utilises centrifugal force to accelerate the settling rate of particles. It yields fast settling rates because the gravitational force is replaced by the higher centrifugal force. The hydrocyclone uses water

as the bulk fluid medium that rotates due to a tangential introduction into the vessel. This rotational motion generates a vortex in the cyclone with a low pressure zone along the vertical axis. The particles are subjected to two opposing forces, an outward centrifugal force and an inward acting drag force. Faster settling particles move to the wall of the cyclone where the velocity is lowest and migrate down to the apex of the conical bottom. The slower settling particles move towards the zone of low pressure along the vertical axis and are carried upward through the vortex finder to the overflow.

2.5.3.3 The hydraulic classifier

The classifier consists of a series of sorting columns with water being added in a counter-flow direction to the feed pulp. The direction of flow of the water opposes that of the settling particles carrying out finer particles to the successive columns. The velocity of the water currents decrease downstream with course particles separated out in the early columns and finer particles found from the latter columns (Wills, 1981).

2.5.3.4 Screens

There are different types of screens used for classification. There are rotating screens called trommels, shaking screens, and vibrating screens (Austin et al., 1984). The screens are decked one top of each other with the largest aperture sized screen at the top and decreasing down wards towards the sink where the fine sized particles are collected. This deck of screens is shaken or vibrated resulting in classification by size and shape.

2.6 THE COMMINUTION CIRCUIT

The comminution circuit is a connection of mills, classifiers and mixers by solid streams. The streams are made up of feed, product and recycle material. The combination of the processing units differs depending on the

quality of the feed. The normal closed circuit with a post-classifier is the best comminution circuit for a mono-sized feed. The pre-classifier circuit is most suited to a feed which is normally distributed so that the material that meet the product specification is separated out before entering the grinding unit and bypassed to the mill product. However the general comminution circuit consist of a pre-classifier and a post-classifier (Austin et al., 1984). Figure 2.13 shows the schematic diagram of the general combined closed circuit with pre- and post-classifiers.
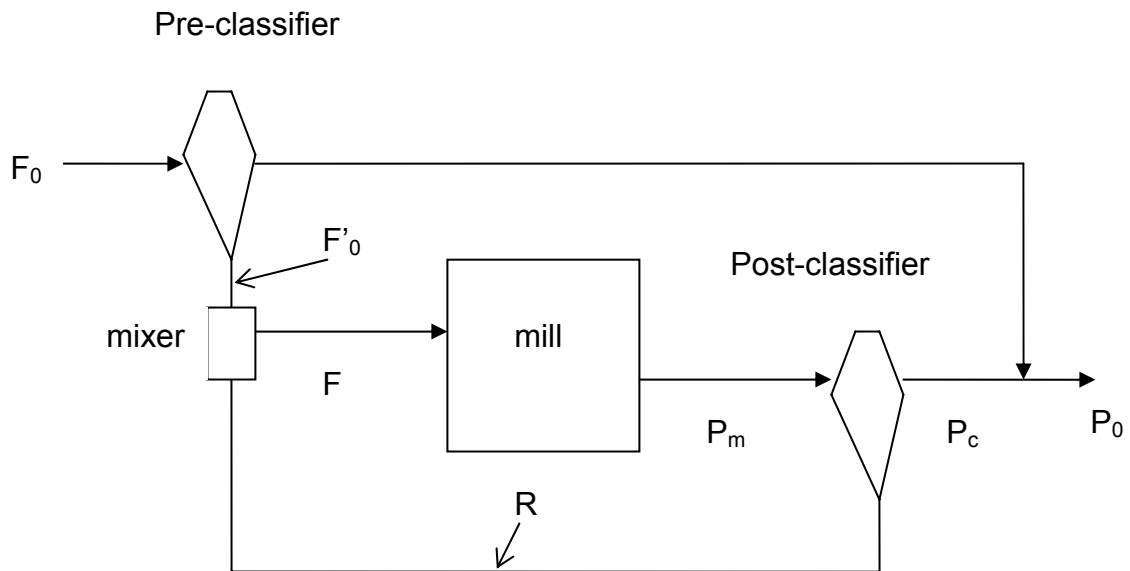
Pre-classifier

Figure 2.13: The combined grinding circuit with pre- and post-classifiers.

The mass balance for the grinding circuit in Figure 2.13 is achieved using the following nomenclature $F=P_m$, $F_0=P_0$, and $F'_0=P_c$. The pre- and post-classifier selectivity are denoted as s_{1i} and s_{2i}, respectively. Equation 2.24 is the pre-classifier makeup mass balance. Equation 2.25 is the mill feed mass balance. Equation 2.26 is the post-classifier mass balance and Equation 2.27 is the overall circuit product mass balance. C is the circulation ratio which is defined

as the relative mass flow rates of the coarse material (R) to the fine product stream (P_c) ($C=R/P_c$). The circulating load is also defined as $F/P_c=1+C$.

$$f_{0i}' = s_{1i} f_{0i} \left(\frac{F_0}{F_0'} \right)$$ (2.24)

$$f_i (1+C) = f_{0i}' + s_{2i} p_i (1+C)$$ (2.25)

$$p_{ci} = (1-s_{2i}) p_i (1+C)$$ (2.26)

$$p_{oi} = (1-s_{1i}) f_{0i} + p_{ci} (F_0'/F_0)$$ (2.27)

The Reid solution, Equation 2.6, calculates the value of p_i sequentially taking into account the new feed rate f_i which is a result of mixing the fresh feed f_{0i}' with the recycle r_i.

2.6.1 Current advances in comminution circuit optimisation

Simulation and optimisation of the comminution circuit depends on each unit having an accurate mathematical model. Figure 2.13 shows the units involved which are the grinding machine, the classifier, the mixer and the material transport of the connecting streams. Optimisation requires the definition of the objective function and the variables of interest. Espig and Reinsch (1996) have provided a survey scheme for the optimisation of grinding circuits and it is given in Table 2.1.

The effect of changing a single variable is not clear without looking at the system as an optimisation problem. There is a need of a methodology for a

process engineer to simulate the result of such a change for design purposes and operating conditions.

Table 2.1: Optimisation of grinding circuits – survey scheme (Espig and Reinsch, 1996).

Optimisation of grinding circuits with tumbling mills					
Objectives: fineness demand, quality assurance					
Objective function: specific energy amount → minimize					
Restrictions: fineness demand, circulating load					
ITEM	Mill specific improvements	Classifier specific improvements	Pre-crushing Pre-grinding	Flow sheet changes	Grinding aids
VARIABLES	Ball composition Ball mass Liner design	Bar basket Air quantity Passing elements	Roller press mill Roller mill Impact crusher	Splitter Pre-classification Bypass	Type Quantity Feed location
Effects	Grinding intensity	Sharpness of cut Bypass fraction Cut size	More homogeneous feed material	Improved utilisation of aggregates	Dispersity agglomeration Agglomeration Grinding intensity Classifier efficiency
ENTIRE SYSTEM	Increased feed rate		Improved process control		Quality assurance
Decision criteria: Cost – profit relation (economy)					
Environmental aspects (ecology)					

There are a number of commercial packages available for simulating and optimising comminution flowsheets. These include METSIM®, USIM PAC$^©$, Limn®, JKSimMet and Matlab/Simulink.

2.6.1.1 METSIM®

METSIM® developed by John Bartlett of Proware is used in comminution to calculate material balances, fit equipment model parameters, simulate and optimise performance of the crushing, screening and grinding processes at steady state. A screen analysis provides information on each stream.

2.6.1.2 USIM PAC$^©$

This package is used in the simulation of steady state mineral processes and it predicts plant operation according to the feed ore and circuit characteristics. It was developed by Broussaud et al. (1988 through 1991) and Guiillaneau et al. (1993). It offers opportunities for data analysis, display of results, material balance computation, model parameter estimation and plant capital investment.

2.6.1.3 Limn®

This package is developed and marketed by David Wiseman Pty Ltd. It provides data structures and models for simulation and analysis of mineral processing operations at steady state. This is a spreadsheet based simulation and the results are saved within the spreadsheet and presented in data blocks on the flowsheet.

2.6.1.4 JKSimMet

JKSimMet was developed at the Julius Kruttschnitt Mineral Research Centre (JKMRC) and it is commercially marketed by JKTech Pty Ltd. It is used for the analysis and simulation of comminution circuits at steady state. The package is able to analyse data, design, simulate and optimise the comminution circuit.

It has screen graphics which acts as a user interface which displays detailed plant flowsheet and the accompanying information.

2.6.1.5 Matlab/Simulink

The MATLAB/SIMULINK is a dynamic simulation approach developed by CSIRO Minerals. Dynamic mathematical models of key grinding and separation devices are linked into various complex dynamic grinding circuits. Real-time dynamic simulation and visualisation of interlinked unit process operations in grinding circuits can readily be achieved.

Continuous, discrete and hybrid models of individual unit operations within the flowsheet can be modified within the MATLAB/SIMULINK programming environment by a powerful in-built suite of equation solvers. The results are analyzed using extensive existing graphical capabilities. The mathematical models can be nonlinear and they are solved using a powerful in-built suite of equation solvers. Liu and Spencer (2004) have shown how the MATLAB/SIMULINK programming environment can be adapted to dynamically simulate mineral processing flowsheets.

These simulation packages are based on in-built unit mathematical models which have different levels of complexity. The level 1 model is based on the Bond's work index. The highly complex models (level 3) are based on the population balance model which requires experimentation to determine the selection and breakage functions.

This thesis aims to provide a simulation algorithm which can be used for the synthesis of the comminution process. Therefore we deem it is necessary to describe the other available packages which have a different method of presentation and have not considered comminution in the way this research has. It is therefore our contention that a review of the available packages is

valuable, by that a critical comparison would be of only academic interest. It is our intent to investigate the integration of the methods with the commercial packages including those discussed above. One of the methods of especial interest is the proposed format of representing particle size distributions as points in space. This will enable the end-user to easily and quickly see the behavioral trends of the system.

2.7 SUMMARY

The aim of this chapter was to understand the comminution process and identify a mathematical model that best describes the physical processes of breakage and classification. The comminution models have come of age from the theoretical size-energy relationships to the current population balance models which is a difference solution to the all inclusive integro-differential equation. The literature review enabled us to select and identify the population balance model as the preferred dynamic model of choice for our specific requirements.

The simulation packages have mathematical models that describe each unit in-built in them. The mathematical models increase in levels of complexity and cost. The steady state simulation packages are necessary for design sizing, capital expenditure costs and optimisation of initial operating conditions. The dynamic simulators are necessary for calculating non-linear behaviour of the comminution system for better process control. The review of the available comminution commercial packages will enable us to propose new ways of making them user-friendly.

2.8 REFERENCES

Austin, L. G., Klimpel, R. R., Luckie, P. T., (1984), Process Engineering for Size Reduction: Ball Milling, Guinn Printing Inc., Hoboken, New Jersey, United States of America.

Bass, L., (1954), Zur theorie der mahlvorgange, *Zeitschrift fur Angewandte Mathematik und Physik* **5**, pp. 283–292.

Baumgardt, S., Buss, B., May, P., Schubert, H., (1975), On the comparison of results in single grain crushing under different kinds of load, Proc. 11th Int. Miner. Process. Congr., Cagliari, 3-32.

Bond, F. C., (1952), The third theory of comminution, Trans. Am. Inst. Min. Metall. Pet. Eng., **193**, pp. 484-494.

Bourgeois, F., (1993), Microscale modeling of comminution processes, Ph.D Thesis, University of Utah.

Bradley, D., (1965), The hydrocyclone, Pergamon Press, Oxford.

Broadbent, S. R., Callcott, T. G., (1956), A matrix analysis of of processes involving particle assemblies, Philosophical Transactions of the Royal Society of London, **A249**, pp. 99-123.

Broussaud, A., 1988. Advanced Computer Methods for Mineral Processing: Their Functions and Potential Impact on Engineering Practices. In: *Proceedings of the XVI International Mineral Processing Congress* Stockholm, Sweden, June 5–10, *Developments in Mineral Processing*, **Vol. 10.A**, Elsevier, pp. 17–44.

Broussaud, A., Fourniguet, G., Franck, J. and Conil, P., 1990. Quantitative Analysis of the Accuracy of Steady State Simulation of Mineral Processing Plants. In: *Proceedings of the CONTROL '90, Mineral and Metallurgical Processing, SME*, pp. 13–21.

Broussaud, A., Guillaneau, J.-C., Guyot, O., Pastol, J.-F. and Villeneuve, J., 1991. Methods and Algorithms to Improve the Usefulness and Realism of Mineral Processing Plant Simulators. In: *Proceedings of the XVII International Mineral Processing Congress*, pp. 229–246.

Dahlstrom, D. A., (1954), Fundamentals and applications of the liquid cyclone, Chem. Engng. Prog. Symp. Series No. 15, **50**, pp. 41.

Dan, C.C., Schubert, H., (1990), Breakage probability, progeny size distribution and energy utilization of comminution by impact, Aufbereit.-Tech., **31**, 241-247.

Epstein, B., (1947), The mathematical description of certain breakage mechanisms leading to the logarithmic-normal distribution, Journal of the Franklin Institute, **244**, pp. 471-477.

Espig, D., Reinsch, V., (1996), Computer aided grinding circuit optimisation utilising a new mill efficiency curve," Int. J. Miner. Process., **44**-**45**, pg. 249-259.

Flintoff, B. C., Plitt, L. R., Turak, A. A., (1987), Cyclone modelling: a review of present technology, *CIM Bulletin*, **80,** 905, pp. 39–50.

Gardner, R. P., Austin, L. G., (1962), A radioactive tracer technique for the determination of breakage functions, Proceedings, 1st European Symposium Zerkleinern, H. Rumpf and D. Behrens, eds., Verlag Chemie, Weinheim, pp. 217-231.

Gaudin, A. M., Meloy, T. P., (1962), Model and comminution distribution equation for repeated fracture, *Transactions of the AIME* **223**, pp. 43–50.

Glasser, D.; Hildebrandt, D. (1987). A geometric approach to steady flow reactors: the attainable region and optimization in concentration space. American Chemical Society, **26**, 1803-1810.

Goldman, M., Barbery, G., (1988), Minerals Engineering, **1**, 67-76.

Goldman, M., Barbery, G., Flament, F., (Feb. 1991), Modelling load and product distribution in autogenous and semi-autogenous mills: pilot plant tests, CIM Bulletin, **84**, pp. 80-86.

Grandy, G.A., Fuerstenau, D.W., (1970), Trans. SME/AIME, **247**, pp. 348-354.

Guillaneau, J.-C., Durance, M.-V., Libaude, J., Ollivier, P., (1993), Computer-aided Optimization of Mineral Processing Plants, a Case Study: Increasing the Capacity of the Shila Gold Mine, Peru, In: *Paper presented at the SME Annual Meeting* Preprint #93–222.

Herbst, J. A., Fuerstenau, D. W., (1973), Trans. SME/AIME, **254**, pp. 343-347.

Kick, F., (1885), Das Gesetz der proportionlen Wilderstande und seine Anwendung, Leipzig.

King, R. P., (2001), Modeling & Simulation of Mineral Processing Systems, Butterworth-Heinemann: Great Britain, pp. 144-151.

King, R.P., Bourgeois, F., (1993a), Measurement of fracture energy during single-particle breakage, Miner. Eng., **6**, pp. 353-367.

Leung, K., Morrison, R.D., Whiten, W.J., (1987), An energy based ore specific model for autogenous and semi-autogenous grinding, Copper '87, Santiago.

Liu, Y., Spencer, S., (November-December 2004), Dynamic simulation of grinding circuits, Minerals Engineering, **17**, Issues 11-12, pages 1189-1198.

Lynch, A. J., Rao, T. C., Bailey, C. W., (1975), The influence of design and operating variables in the capacities of hydrocyclone classifiers, Int. J. Min. Proc., **2**, pp. 29.

Nageswararao, K., (1978), Further developments in the modelling and scale-up of industrial hydrocyclones, Ph.D. Thesis, University of Queensland (JKMRC), Brisbane, Australia.

Plitt, L. R., (December 1976), A mathematical model of the hydrocyclone classifier, *CIM Bull*. **69**, pp. 114.

Prasher, C. L., (1987), Crushing and Grinding Process Handbook, John Wiley & Sons Ltd., Great Britain.

Reid, K. J., (1965), Chemical Engineering Science, **20**, 953-963.

Rittinger, P. R., (1867), Lehrbuch der Aufbereitungskunde, Berlin.

Rose, H. E., (1967), Proceedings, 2nd European Symposium Zerkleinern, H. Rumpf and W. Pietsch, eds., Dechema Monographien 57, Nr. 993-1026, Verlag Chemie, Weinheim, pp. 27-62.

Schonert, K., (1988), Fundamentals of particle breakage. Course notes, University of the Witwatersrand, Division of Continuing Engineering Education, Johannesburg, Section F6.

Sedlatschek, L., Bass, L., (1953), Contribution to theory of milling processes, Powder Tech. Bull., **6**, pp. 148-153.

Shipway, P. H., Hutchings, I. M., (1993), Attrition of brittle spheres by fracture under compression and impact loading, *Powder Technology*, **76**, pp. 23–30.

Shoji, K., Lohrasb, S., Austin, L. G., (1979), The variation of breakage parameters with ball and powder loading in dry ball milling, Powder Technology, **25**, pp. 109-114.

Tavares, L. M., King, R. P., (1998), Single-particle fracture under impact loading, Int. J. Miner. Process., **54**, pp. 1-28.

Tavares, L.M., (1999), Energy absorbed in breakage of single particles in drop weight testing, Minerals Engineering, **12**, pp. 43-50.

Unland, G., Szczelina, P., (2-5 September 2002), Coarse crushing of brittle rocks by compression, 10th European Symposium on Comminution, Heidelberg, Germany.

Wills, B. A., (1981), Mineral Processing Technology, 2nd Edition: An introduction to the practical aspects of ore treatment and mineral recovery, Pergamon Press, Oxford, Great Britain.

CHAPTER 3

LITERATURE REVIEW: THE ATTAINABLE REGIONS THEORY

3.1 INTRODUCTION

The attainable region analysis is a method which allows us to solve optimization problems simultaneously with the process synthesis formulation. It uses a geometric based construction approach together with necessary conditions to check the boundary of the AR. The AR is defined as the set of all possible outcomes for the system under consideration that can be achieved by the use of fundamental processes operating within the system and that satisfies all the constraints placed on the system.

3.2 HISTORY OF CHEMICAL PROCESS OPTIMISATION

The question of choosing and/ or optimizing the best equipment configuration has been dealt with in chemical reaction engineering. Until recently, choosing and optimizing the best chemical reactor configuration has been a difficult task. In the literature there are many optimization techniques that have been employed to optimize such systems. For instance Chitra and Govind (1985) looked at the series of recycle reactors. Paynter and Haskins (1970) looked at what value of the axial mixing coefficient as a function of reactor length would give the optimum for a chosen objective function. Horn (1964), addressed the issue of finding the optimal reactor structure. He noted that for given kinetics and given feeds, it might be possible to find the set of all possible output concentrations from all possible reactor systems. He called the set of all possible outputs the *Attainable Region (*AR) (Horn, 1964). If one knows the AR, one can then search over the region to find the output conditions that maximize a given objective function. One would therefore be in a position to

determine the maximum of the given objective function, which in reactor design could be selectivity or maximum concentration of a product.

This approach would be useful for two reasons. Firstly, it would simplify the optimization problem, as searching over a defined set for the maximum of an objective function is a fairly standard and simple procedure. Secondly, the value of the objective function could be used as a target for designers and operators to measure their process against. Therefore if the reactor structure being considered had an optimal of the objective function that was quite different from the target value of the objective, found by searching the AR, the designers would then be in a position to know that significant improvements in performance were possible. Having a target against which to compare current operation or designs is extremely valuable for the engineer. Horn (1964) and subsequent researchers were however unable to find a systematic method of finding the AR and so this concept languished for about 20 years.

Glasser and Hildebrandt (1987) re-looked at the problem of finding the AR and approached the problem from a very different angle. They looked at the fundamental physical processes occurring in a reactor rather than looking at equipment, which is what had been done previously. The fundamental processes in a simple homogeneous reactor are for instance reaction and mixing. They described these processes (reaction and mixing) in terms of vectors in the concentration space. By using a growing algorithm together with some necessary conditions, they were able to determine candidates for the AR. They were able to search the AR to find the maximum of a given objective function, and hence specify the maximum value or target for the objective function. Using this approach they were able to find the maximum output concentrations of several well known problems in the literature, such as that posed by van de Vusse (1964), and by so doing finally and

convincingly ended the 20 year search for the answer to this problem. An unexpected, but very important outcome from the approach was that not only was the optimal value of the objective function found, but also the flow-sheet or reactor type required to achieve this output as well. Hence the optimal equipment was found as part of the solution to the problem, which was the first time this could be done.

3.3 CLASSICAL OPTIMISATION

A chemical engineering problem has many possible solutions but optimisation identifies the optimum depending on the objective function. An optimisation problem usually contains;

(i)   an objective function,
(ii)   equality constraints (equations),
(iii)   inequality constraints (inequalities).

Classical optimisation is based on linear and non-linear mixed integer programming of superstructures of all possible units connected by a number of interlinking streams (Kokossis and Floudas, 1990, 1991, 1994). Papalexandri and Pistikopoulos (1994, 1996) have generalised the processing units of the superstructure as mass and heat exchanger modules. The program uses integer variables to choose or discard a processing unit or interlinking stream. Linear or non linear programming is used to control the process variables of temperature, pressure, reactor volume and flow rates. The superstructure however cannot be proved to be all inclusive of the optimum process layout.

3.4 CURRENT KNOWLEDGE ON THE APPLICATION OF THE ATTAINABLE REGIONS THEORY

Interest in the application of the attainable region for process synthesis has increased in the last two decades. Currently researchers are moving in the direction of automating the construction of the AR. This means that for known kinetics for a system of fundamental processes the algorithm will generate the optimum process layout and processing conditions.

Rooney et al. (2000) developed the Iso-state Algorithm. Burri et al. (2000) proposed the IDEAS formulation which used linear programming formulations of the CSTR, PFR and mixing lines. A combination of CSTRs and mixing lines can represent any known reactor structure and Kauchali et al., (2002) capitalised on this in their linear programming formulation to construct the AR systematically. Abraham and Feinberg (2004) proposed the method of Bounding Hyperplanes to construct the AR from the exterior points. Seodigeng (2006) has developed a systematic numerical formulation for the AR. He considered combinations of various fundamental processes of reaction, mixing and heat transfer. He proposed two systematic numerical formulations for identifying process unit networks.

3.5 PROCEDURE FOR DETERMINING THE CANDIDATE ATTAINABLE REGION

Certain steps are performed to build an attainable region. As an illustration we look at the problem posed by van de Vusse (1964). We wish to consider the reaction system of Equation 3.1 and determine the maximum concentration of component B (c_B). This problem was solved by Glasser and Hildebrandt, 1987.

$$A \xrightarrow{k_1} B \xrightarrow{k_2} C$$
$$2A \xrightarrow{k_3} D$$

(3.1)

The feed to this system is pure A, the reactions are elementary and the rate constants are given. Furthermore it is assumed that there are no volume changes on reaction. We outline the approach outlined by Hildebrandt (1989) for finding the AR to solve this classic reaction problem, Equation 3.1. MacGregor (1998) has given a more elaborate step by step procedure for solving the process synthesis problem of reactor network synthesis using the AR as outlined in the following section.

3.5.1 Specify the fundamental process/es

For the above chemical reaction system the fundamental processes are reaction and mixing.

3.5.2 Specify the state variables

The variables which characterize the output state of the system and the fundamental processes are chosen. These states can be, for example, concentrations of reactants and products, and mass fraction distributions. The rate of reaction depends on the concentration of A and B, c_A and c_B respectively, while the objective function, which maximize the concentration of B, c_B, depends on c_B only. Thus the variables c_A and c_B are sufficient to completely describe the kinetics and the objective function. The characteristic vector c is denoted as $c = [c_A, c_B]$. This can be represented as a vector in two-dimensional space.

56

3.5.3 Define the fundamental process vectors

The fundamental processes are defined such that they give an instantaneous change in the characteristic vector *c* if the fundamental process occurs. In section 3.5.1 we identified the fundamental processes as reaction and mixing. We will now consider the vector description of each of these processes.

- *The mixing vector*: Under the assumption of no change in density on reaction, the mixing of streams with different concentrations are described by the lever arm rule. Thus when mixing material of composition *cₘ* with material of composition *c*, the mixing vector describing this, *v(c)*, is given by Equation 3.2.

$$v(c) = c\text{-}c_m \tag{3.2}$$

*Therefore the mixing vector at **c** points from the state of the system **c** to the state that we are mixing with, **cₘ**.*

- *The reaction vector*: The reaction vector *r(c)* at some point *c* points in the direction of the instantaneous change in *c*, if material of composition *c* is allowed to react as in Equation 3.3.

$$\frac{dc}{dt} = r(c) \tag{3.3}$$

Therefore the rate vector is tangent to the trajectory of a plug-flow reactor (PFR) for all points on the trajectory.

3.5.4 Determine the necessary conditions

The attainable region should include the feed point(s). No process vectors on the boundary of the AR should point outwards. In this case, because of mixing and the constant density assumption, the region should be convex.

3.5.5 Construct the region

The region is constructed using a growing algorithm. We first use a reaction only process from the feed point to generate a set of points achievable with reaction only. We then use mixing to generate a convex region. We check the boundary of the region to see if reaction vectors point outwards. If they do, we consider a reaction process from the points on the boundary of the region where the reaction vectors point outwards. We continue to alternate between convexifying the region (i.e. using mixing) and reaction from the boundary points where the reaction vectors point outwards. When we have a region that satisfies the necessary conditions, we can claim that we have a candidate region for the AR. The candidate region for this problem is given in Figure 3.1, and it is the region enclosed by the:

i)   line from the feed point to point **B**,

ii)   curve from point **B** passing through point **A** to point (0,0) and

iii)   line from point (0,0) to the feed point.

3.5.6 Finding the optimum

Once the boundary of the candidate attainable region is known, the maximum concentration of B can be found at point ***A*** on Figure 3.1.
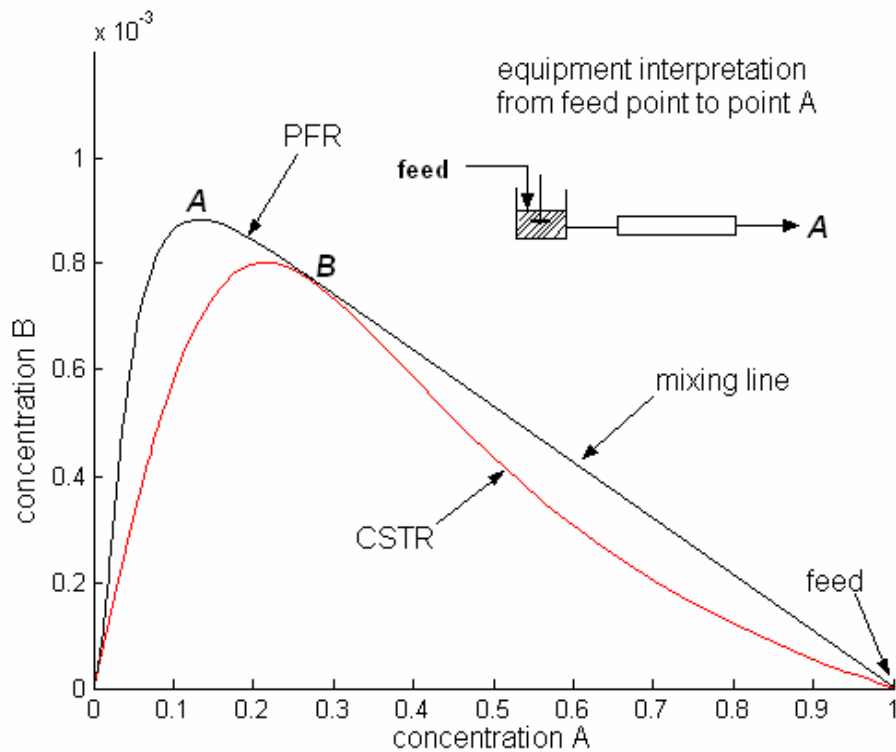
Figure 3.1: Change of concentration for the processes of reaction and mixing.

3.5.7 Interpretation of the AR for the optimal reactor structure

We trace the path or combination of reaction and mixing that allowed us to move between the feed point and point **A**. We are then able to interpret this combination of reaction and mixing as process equipment. Hence we are able to show that the optimal reactor structure to achieve the maximum concentration of B is a CSTR operating at point **B** in Figure 3.1, followed by a PFR operating from point **B** to point **A**. Thus we are not only able to determine the maximum achievable concentration of product B but the optimal reactor structure to achieve this concentration as well.

3.6 SUMMARY

Hildebrandt, Glasser and co-workers have over the years improved and refined the growing algorithm. The AR has been used to solve classical optimization problems in higher dimensions and with multiple fundamental processes (Seodigeng, 2003). Feinberg and Hildebrandt (1997) and Feinberg (2000) have found some interesting results for the boundary of the AR that have influenced and been incorporated in process synthesis research (Biegler, 1997 and Nisoli, 1997).

3.7 REFERENCES

Abraham, T. K., Feinberg, M., (2004), Kinetic Bounds on Attainability in the Reactor Synthesis Problem, Ind. Eng. Chem. Res., **43**, pp. 449-457.

Biegler, L. T., Grossman, I.E., Westerberg, A. W., (1997), Systematic methods of Chemical Process Design, New Jersey: Prentice Hall.

Burri, J. F., Wilson, S. D., Manousiouthakis, V. I., (2000), Infinite DimEnsionAl State-space approach to reactor network synthesis: application to attainable region construction, Comp. & Chem. Eng., **26**, no. 6, pp. 849-862.

Chitra, S. P., Govind, R., (1985), AICHE J., **31**, 177.

Feinberg, M., Hildebrant, D., (1997), Optimal reactor design from a geometric viewpoint. Part I. Universal properties of the attainable region, Chemical Engineering Science, **52**, 1637-1665.

Feinberg, M., (2000), Optimal reactor design from a geometric viewpoint. Part II. Critical side-stream reactors, Chemical Engineering Science, **55**, 2455-2479.

Glasser, D., Hildebrandt, D., (1987), A geometric approach to steady flow reactors: the attainable region and optimization in concentration space, American Chemical Society, **26**, 1803-1810.

Hildebrandt, D., (1989), The Attainable region generated by Reaction and Mixing, PhD Thesis, Republic of South Africa: University of the Witwatersrand.

Horn, F., (1964), Attainable and non-attainable regions in chemical reaction technique. 3rd European Symposium on "Chemical Reaction Engineering", Pergamon Press Ltd., Great Britain.

Kauchali, S., Rooney, W. C., Biegler, L. T., Glasser, D., Hildebrandt, D., (2002), Linear programming formulations for attainable region analysis, Chem. Eng. Sci., **57** (11), pp. 2015-2228.

Kokossis, A. C., Floudas, C. A., (1990), Optimisation of complex reactor networks I: Isothermal operation, Chem. Eng. Sci., **45** (3), pp. 595.

Kokossis, A. C., Floudas, C. A., (1991), Synthesis of Isothermal Reactor-Separator-Recycle Systems, Chem. Eng. Sci., **45**, pp. 1361-1383.

Kokossis, A. C., Floudas, C. A., (1994), Optimisation of complex reactor networks II: Non-isothermal operation, Chem. Eng. Sci., **49** (7), pp.1037.

MacGregor, C., (1998), Choosing the optimal system structure using the attainable region approach for systems involving reaction and separation, PhD Thesis, Republic of South Africa: University of the Witwatersrand.

Nisoli, A., Malone, M. F., Doherty, M. F., (1997), Attainable Region for Reaction and Separation, AICHE J., **43** (2), February 1997, pp. 374-387.

Papalexandri, K. P., Pistikopoulos, E. N. (1994), A Multiperiod MINLP Model for the synthesis of Flexible Heat and Mass Exchange Networks, Comp. Chem. Eng., **18** (11/12), pp. 1125-1139.

Papalexandri, K. P., Pistikopoulos, E. N. (1996), Generalised Modular Representation Framework for Process Synthesis, AICHE J. **42** (4), pp. 1010 -1032.

Paynter, J. D., Haskins, D. E., (1970), Chem. Eng. Sci., **25**, 1415.

Rooney, W. C., Hausberger, B. P., Biegler, L. T., Glasser, D., (2000), Convex attainable region projections for reactor network synthesis, Comp. Chem. Eng., **24**, no. 2-7, pp. 225 – 229.

Seodigeng, T., Hausberger, B., Hildebrandt, D., Glasser, D., (3-5 September 2003) DSR Algorithm for Attainable Regions Analysis: Higher Dimensional Problems, South African Chemical Engineering Congress, Sun City, South Africa.

Seodigeng, T., (2006), Numerical formulations for attainable region analysis, PhD Thesis, Republic of South Africa: University of the Witwatersrand.

Van de Vusse, (1964), Plug-flow type reactor versus tank reactor, Chemical Engineering Science, **19**, pp. 994-997.

CHAPTER 4

THE APPLICATION OF THE ATTAINABLE REGION ANALYSIS TO COMMINUTION*

4.1 INTRODUCTION

Energy is consumed for size reduction of solid materials in the mineral processing industry during comminution. The cost of energy required for size reduction is one of the major costs in the surface operations of a mine. Three classical laws of comminution have been postulated by Rittinger (1867), Kick (1885) and Bond (1952) relating change of particle size with input energy. The first law of comminution postulated by Rittinger (1867) states that the energy required for size reduction is proportional to the newly created surface area. Schonert (1988) has calculated the energy efficiency for grinding processes to be in the range of 4-8% assessed on the basis of surface area produced. However the calculation of energy efficiency based on the breakage of inter-particle bonds of the resulting surfaces disregards the presence of cracks in the solid material, but it is a good indicator of how inefficient comminution equipments are in terms of energy consumption.

Energy costs account for more than 50% of the operational cost of a grinding circuit. Therefore any slight increase in the energy efficiency offers an opportunity to increase profitability. Furthermore, the product size distribution that is achieved is very important, with the particles that are either too fine or too coarse both causing complications in the downstream processing of the ore and often leading to increased waste and lowered efficiency of the minerals recovery process. There is thus a very strong incentive to investigate

---

the comminution process with the aim of increasing energy efficiency and improving control of the product size distribution (*PSD*).

Walker et al. (1937) described a general differential law, Equation 4.1, which is the classical approach to the relationship between size reduction and energy.

$$\frac{dE}{dX} = -\frac{C}{X^n}$$

(4.1)

where *dE* is an infinitesimal amount of energy required to bring about an infinitesimal size reduction *dX*, and *C* and *n* are constants for a given mill and material system. Kapur and Fuerstenau (1987) points out that for Walker's equation to hold, the infinitesimal increment of overall energy *dE* should be related to the infinitesimal change in size reduction *dX* thus introducing the concepts of:

   (i)   the breakage trajectory of the particle size distributions – the trajectory in this case is a path followed by the breakage vectors.
   (ii)   quantification of specific energy for size reduction - energy consumed per unit mass of solid material.

The choice of specific energy for mill design and scale up has been employed for the past quarter of a century. It allows mills of different sizes to yield identical products for the same specific energy when fed with the same material (Herbst and Fuerstenau, 1980). Single particle studies have been used to study fracture of different materials and the associated energy consumption (Gilvarry et al., 1961; Bergstrom, 1962; Rumpf, 1973). These studies have shown that the specific energy and therefore the stress required to initiate fracture for smaller particles is greater because of fewer defects, mainly. The fracture energy (which is the maximum energy which can be

absorbed and stored by the particle before fracture occurs) is useful as a guide for the design of the comminution device to reduce feed particles of different sizes. The best comminution device is one which could provide the correct fracture energy to each particle resulting in the fracture energy giving the target product particle size distributions for given energy inputs and feed material.

The classical grinding laws could not account for comminution sub-processes of transportation and classification. A model was sought which could take into account all sub-processes of breakage kinetics, material transport and size classification. Reid (1965) presented the population balance model, Equation 4.2, which can be used to describe the evolution of mass fractions with size class intervals in a linear size-discretized manner.

$$\frac{dm_i(t)}{dt} = -S_i m_i(t) + \sum_{j=1}^{i-1} S_j b_{ij} m_j(t) \qquad (4.2)$$

where $m_i(t)$ is the mass fraction of particles in the ith size class interval, S_i is the breakage rate function and b_{ij} is the breakage distribution function. The breakage rate function describes the rate at which material is broken out of a particular discretized size class, whereas the breakage distribution function (b_{ij}) represents the fraction of the primary breakage product of material in size class interval j which appears in size class interval i. Herbst and Fuerstenau (1973) have improved on the population balance model by incorporating the specific energy ($\overline{E}$) for a batch mill drawing constant power (P). The quantity (Pt/m) is equal to the specific energy, $\overline{E}$. The attainable region ideas are applied to comminution using the improved population balance model which is specific energy dependent. Equation 4.3 is the modified population balance model and it predicts that for a given feed material, identical product size

distributions in different mills are achieved by the same specific energy into each mill. This removes the dependence of the model on mill dimensions and mill operating variables, enabling the model to describe the fundamental comminution sub-processes more adequately.

$$\frac{dm_i\left(\overline{E}\right)}{dE} = -S'_i\, m_i\left(\overline{E}\right) + \sum_{j=1}^{i-1} S'_j\, b_{ij} m_j\left(\overline{E}\right) \tag{4.3}$$

Having defined the general concepts of comminution, we move on to describe the concept of the attainable regions which is based on fundamental process trajectories in space. The resulting boundary process trajectories show the extreme paths to achieve the stated output. By assessing these boundary processes with a continuous objective function we can select the optimal process combination and operational conditions. Typical objective functions could be maximizing material in a particular size class or minimizing energy consumption to the grinding circuit. The fact that different sized particles have different strengths is an indication that materials of similar size should be fed to the same mill. The grinding circuits should therefore at least consist of series and/or parallel processing equipment configurations. Thus a detailed and fundamental understanding of the basic particulate fracture process as described above is used to ensure that the technology developed here leads to better comminution process flow-sheets.

4.1.1 Review of the AR method in Reaction Engineering

The question of choosing and/ or optimizing the best equipment configuration has been a difficult one in chemical reaction engineering. Mathematical optimization techniques such as mixed integer non-linear programming (MINLP) have been used to optimize superstructures, which are a complex

layout of all possible units and connecting streams (Kokosis and Floudas, 1990, 1991, 1994). There are many techniques in the literature that have been employed for process synthesis and optimization. For instance Chitra and Govind (1985) looked at the series of recycle reactors. Paynter and Haskins (1970) looked at what value of the axial mixing coefficient as a function of reactor length would give the optimum for a chosen objective function. The objective function may be achieved more efficiently through a linear combination of various fundamental processes which can lead to the extension of the possible states.

Horn (1964) addressed the issue of finding the optimal reactor structure. He noted that for given kinetics and given feeds, it might be possible to find the set of all possible output concentrations from all possible reactor systems. He called the set of all possible outputs the *Attainable Region (AR)* (Horn, 1964). If one knows the *AR*, one can then search over the region (often the boundary) to find the output conditions that maximize an objective function. One would thus be in a position to determine the maximum of the given objective function, which in reactor design could be, for example, selectivity or maximum concentration of a product.

This approach would be useful for two reasons. Firstly, it would simplify the optimization problem, as searching over a defined set for the maximum of an objective function is a fairly standard and simple procedure. Secondly, the value of the objective function could be used as a target for designers and operators against which to measure their process. Thus if the reactor structure being considered had an optimal of the objective function that was quite different from the target value of the objective, found by searching the *AR*, the designers would then be in a position to know that significant improvements in performance were possible. Thus having a target against

which to compare current operation or designs is extremely valuable for the engineer. Horn and subsequent researchers were however unable to find a systematic method of finding the *AR* and so this concept languished for about 20 years.

Glasser and Hildebrandt (1987) re-examined the problem of constructing the *AR* and approached the problem from a very different angle. They looked at the fundamental physical processes occurring in a reactor rather than looking at equipment, which is what had been done previously. The fundamental processes in a simple homogeneous reactor are for instance reaction and mixing. They described these processes (reaction and mixing) in terms of vectors in concentration space. By using a growing algorithm together with some necessary conditions, they were able to determine candidates for the *AR*. Thus they were able to search the *AR* to find the maximum of a given objective function, and hence specify the maximum value or target for the objective function. Using this approach they were able to find the maximum output concentrations of several well known problems in the literature, such as that posed by van de *Vusse (1964)*, and by so doing finally and convincingly ended the 20 year search for the answer to this problem. An unexpected, but very important outcome from the approach was that not only was the optimal value of the objective function found, but the flow-sheet or reactor type required. Hence the optimal equipment was found as part of the solution to the problem, which was the first time this could be done.

The *AR* method is capable of handling both dynamic/transient and steady state systems; this allows the *AR* approach to separate the dynamic behavior of the system from the optimization. It determines all the states that can be achieved by the system of fundamental processes, which is equivalent to considering all possible curves that obey the dynamic constraints (Godorr,

1998). Once the bounds on the system performance have been determined, the selection of the optimal set of processes and conditions is easily performed as a subsequent process. The dynamic behavior of the system is important in that it gives the control variable settings associated with the limits of system performance.

4.1.2 Aims of this Paper

In this paper we will look at the fundamental comminution processes with respect to applying the attainable region approach, as previously introduced by Khumalo (Khumalo et al, 2003). We will use the fundamental processes occurring in comminution and then use geometric concepts to construct the *AR* for the comminution of a specified *PSD* of solids. We will examine the optimal targets for objectives such as minimizing energy input or maximizing a product size distribution. We will interpret the combination of processes used to achieve the optimal value of the objective function in terms of equipment. Hence we will be able to determine what the optimal equipment in terms of the selected objective function is. Designers and operators of comminution equipment could use these results to determine how close the operation of the equipment is to the target values and what room for improvement there is in the design and operation of existing equipment.

The purpose of this paper is to apply the AR approach to the comminution process. While we have tried to use a credible model for the analysis, criticisms of the details of the model do not affect the validity of the AR approach. If a different or "better" model were to be used the details of the results would be affected but not the approach.

4.2 APPLICATION OF THE AR APPROACH TO COMMINUTION

Glasser and Hildebrandt (1987) and other co-workers have shown how the *AR* can be constructed using the necessary conditions for process synthesis and optimization of a system. These methods apply in the following fashion; in place of a reaction from component *A* to component *B*, we have particles being broken from size class 1 to size class 2 as in Equation 4.4. Likewise the process of classification is synonymous with separation, and mixing is common to both comminution and standard reactor systems.

$$class1 \xrightarrow{\ k_1\ } class2$$
$$class2 \xrightarrow{\ k_2\ } class3 \qquad\qquad (4.4)$$
$$class1 \xrightarrow{\ k_3\ } class3$$

The following sections show how the *AR* can also be constructed for the comminution system as in reaction engineering to enable simultaneous process synthesis and optimization.

4.2.1 The fundamental processes in comminution

The *AR* approach requires that the fundamental processes taking place in a system be identified. The following three fundamental processes are identified for the comminution system:

i)   breakage,
ii)   mixing, and
iii)   separation.

In this paper we consider only the first two processes. Separation will be studied as a further fundamental process in a later paper.

The power of the *AR* approach is that it looks at the fundamental processes without being equipment specific. Thus we need to define the breakage process independently of the machine or equipment being used. This is not simple to define, as much of the literature quotes breakage rates or functions that are machine specific (Grandy et al. (1970); Fuerstenau et al. (1991); De (1995)). We thus have to look at a fundamental model of breakage and we will, when we define the breakage vector, use the concept of fracture energy as first described by Baumgardt et al. (1975).

4.2.2 The state variables in comminution

The next step is to choose the state variables which describe the breakage and mixing processes as well as characterize the objective function that we are trying to optimize. Our objective function could, for example, be to achieve a specified particle size distribution (*PSD*) or to minimize total energy consumption in the circuit. We expect the breakage process to depend on the *PSD* as well as the specific energy ($\overline{E}$) because breakage can only occur as a result of energy input. $\overline{E}$ is the specific energy and is defined as the supplied energy per unit mass of material. The power of this *AR* approach is that it can represent concentrations or *PSD*s as single points in space allowing connectivity of the points through the Markov property.

Let us review the traditional ways of representing *PSD*s and then move on to how we propose *PSD*s should be represented geometrically for clarity of connectivity for simultaneous process synthesis and optimization.

4.2.2.1 Traditional Representation of Particle Size Distribution (PSD)

Traditionally, particle size distributions are described by cumulative distribution functions and/or probability density functions (Hulburt and Katz, 1964). The three main statistical models used to describe the breakage distribution products are:

i)   Gates-Gaudin Schumann plots

ii)   Rosin-Rammler plots

iii)   Log-probability plots.

The type of plot used usually depends on the distribution of sizes and the model to which the data fits best.
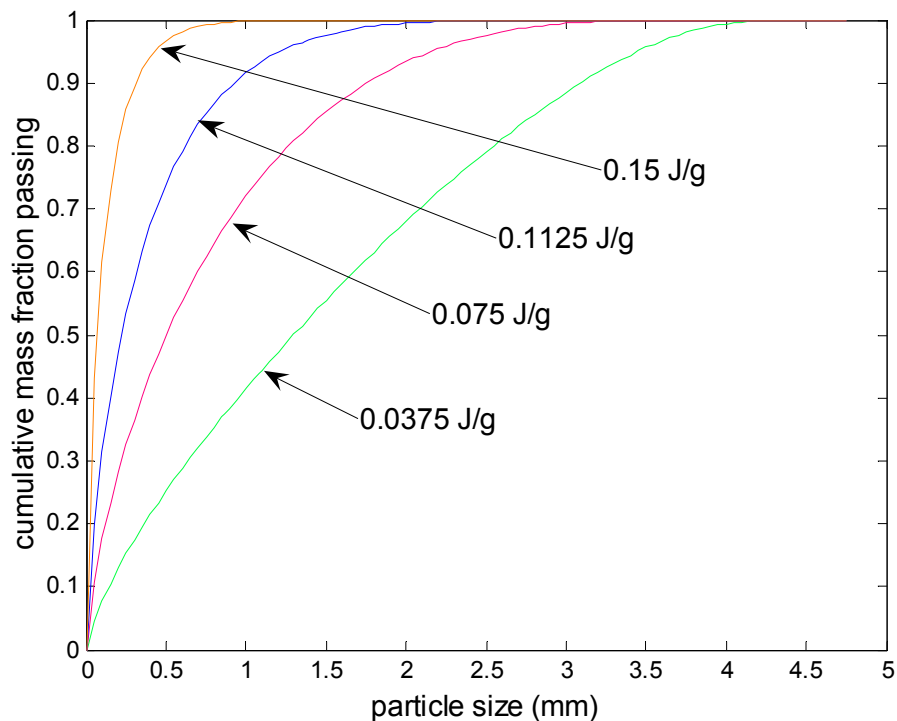
Figure 4.1: The cumulative distribution graph, for 4.75mm quartz particles for varying specific energy inputs.

Size analysis data is traditionally represented by plotting a graph of the cumulative mass fraction passing versus the particle size diameter which is equivalent to aperture size. Figure 4.1 shows the cumulative distribution representation of 4.75mm quartz particles impacted with increasing $\overline{E}$ input. It can clearly be seen that as the input $\overline{E}$ increases, the slope of the graphs become sharper tending to the left towards the lower size classes. This means that the lower size classes retain more mass than the upper size classes for increased $\overline{E}$ input. In most industrial operations the particles are reduced in size to fit a certain percent by mass below a desired size, based on these plots.

4.2.2.2 Representing the PSD in mass fraction space

Single point product specifications have played a major role in the minerals processing industry without people being perhaps all that aware of it. This approach provides the opportunity to utilize single point representation to build and control the comminution process better.

We find in literature that the specification of an objective for a product *PSD* can be defined by:

i)   a single point for example 80% by weight passes a certain size such as 75µm (Bond, 1952),

ii)   two points for instance 50% by weight less than 38µm but no more than 5% by weight greater than 208µm,

iii)   an equivalent specific surface area of the distribution (Rittinger, 1867).

In the light of these single point representations of desired product *PSD*, we propose a way of representing *PSD*s' in *n*-dimensional space using the geometrical approach of the attainable region technique. This improves on the determination of control policies because we can track the change of mass fraction in each size class with a given $\overline{E}$ input in an *n*-dimensional space as will be explained for Figure 4.2 later.

The AR approach can be extended to n-dimensional size classes. However since single points are used industrially to specify the desired output, the characteristic equation will mostly comprise of the feed size class and that desired size class. This condition limits the system to a 2-dimensional one. The number of size classes considered in a problem would depend on the accuracy of the answer required. We, for the purposes of illustration, choose to limit the number of size classes. We then can work in a smaller dimensional space and represent the results graphically. For example if we wish to consider three size classes in a specific problem, we can reduce the size class problem to a 2-dimensional one. The sizes are grouped as the:

i)   feed size class which truncates the subsequent distributions. This is taken as the top size class or size class 1 in our terminology,

ii)   middling size class which is a result of moderate breakage extents. This is termed size class 2 and could be the desired product thereby defining the objective function of the breakage system,

iii)   fines size class which is a result of a relatively large breakage extent. This is termed size class 3 and could also be the objective of the breakage system.

If we decide to consider 3 size classes only, and the objective function is maximizing the mass fraction in size class 2, then size classes 1 and 2 will

describe the output state of the process as well as the objective function fully. Hence the *AR* is constructed in a 2-dimensional space, with mass fraction in size classes 1 and 2 as the two axes in space.

We have used the concept of a single point to represent mass fractions in space which are properties of a process stream in comminution. This representation, as opposed to the cumulative distribution function representations that are often used in this field, allows us to follow the change in the process stream properties as different fundamental processes operate on the stream. The *AR* is so versatile that it can handle the addition of other processes and the change in process conditions easily. This explains why the *AR* also answers the dynamic optimization problem because it is inclusive. In particular the concept that a system can be represented as curve/s of process vectors in terms of mass fractions is extremely powerful and allows both process synthesis and optimization of the comminution circuits and/or equipment.

4.2.2.3 Analogy between concentration in reaction and mass fraction in comminution

A chemical reaction does not always convert the reactants to products completely. Similarly, in size reduction, for a given population of particles being impacted with some energy, not all of the particles are broken. Furthermore, there is still some mass fraction of the top size class remaining.

The second point is that a chemical reaction may give numerous reaction products depending on the reaction system. Similarly in comminution, the breakage process gives rise to numerous particle sizes. In this way we have managed to treat each size interval analogously to a species in a chemical

reaction system. The size classes other than the feed size class contain the products from the formation of new progeny sizes through division of the larger particles into two or more distinct smaller particles.

4.2.2.4 Geometrical representation of the characteristic and process vector in comminution

The characteristic vector is the set of all state variables that describe the output state of the system. Hence if we wish to achieve some specified *PSD* in terms of *i* particle size classes, the characteristic vector would be the vector of dimension *i*-1. Geometrically each mass fraction of material of a given size interval represents an axis in space. So for three size classes (i.e. *i* = 3) the mass fraction (m_i) in each size class is represented in 2-dimensional (i.e. *i*-1 dimensions) space with the third mass fraction in size class 3 being inferred by mass balance. The mass fraction of some product stream can be represented as a single point in the 2-dimensional space.

Similarly, if we wished to consider 4 size classes (i.e. *i* = 4), the mass fraction (m_i) in each size class is represented in 3-dimensional space with the fourth mass fraction in size class 4 being found by mass balance.

Again in an analogous manner, the mass fraction of some product stream can be represented as a single point in the 3-dimensional space. Thus in this case the characteristic vector, and hence the space that the *AR* is determined in, would be defined by Equation 4.5.

$$\boldsymbol{m_i} = [m_1,\ m_2,\ m_3] \hspace{4cm} (4.5)$$

One of the necessary conditions of the attainable region is that the candidate attainable region should include the feed point. So for a system in which we wish to consider 4 size classes, as an example, we can represent as described above an output state of a comminution process in 3-dimensional space as shown in Figure 4.2.

The feed must be in the Attainable Region and so must be represented as a point in the space, in this case marked point *A* in Figure 4.2. The product might be point *B* for instance, and the outputs from the processes used to get from *A* to *B* would be represented by the path or the curve joining *A* and *B*.

The material breaks as the process continues and it distributes itself into these four size classes. Each distribution into the four size classes is represented as a single point in the mass fraction space. It is easy to track the path followed by the distribution with $\overline{\overline{E}}$ input per batch grinding stage.

m_2 size class 2

Outputs, with time, from applied processes to achieve point B

B

A

m_1 size class 1
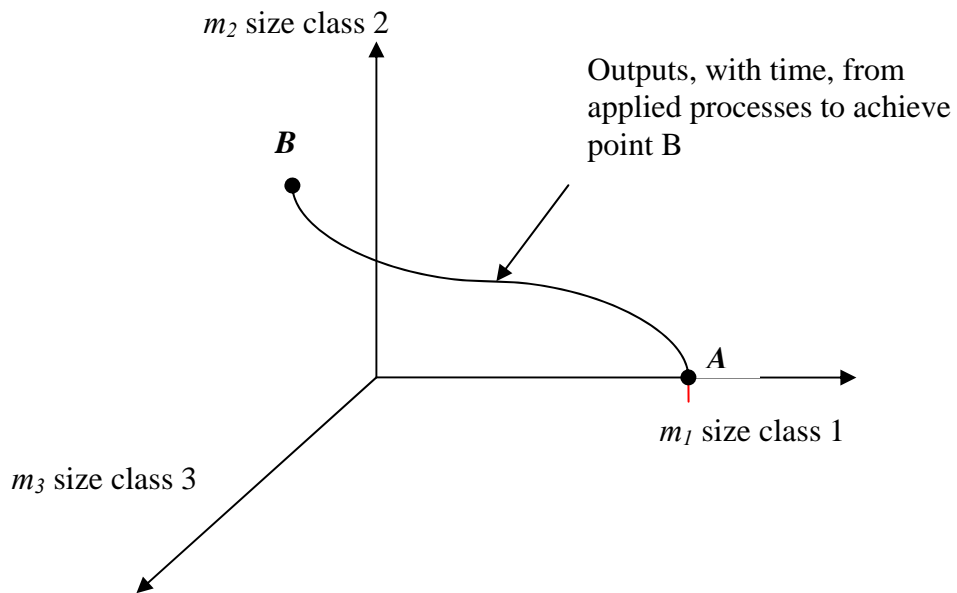
m_3 size class 3

Figure 4.2: An example of the geometrical representation of a feed and product point in a 3-dimensional mass fraction space.

If the objective function is to maximize the mass fraction in size class 2, then this is a 2-dimensional problem. The variables of interest would be given by the characteristic vector in Equation 4.6.

$$\boldsymbol{m_i} = [m_1, m_2] \tag{4.6}$$

The power of the attainable region technique is that it looks at the fundamental breakage process and determines the set of all achievable distributions at the process conditions. It thereby provides the designer with the best path required to achieve a specific objective function from the system feed. The fundamental processes of breakage, mixing and separation can be manipulated to get each single point in the mass fraction space.

Another variable which could be included in the characteristic vector is $\overline{E}$. We have not included it as a variable in this paper as including this variable increases the dimensionality of the problem by one. We have rather taken the approach as used by Godorr et al. (1994) where we consider $\overline{E}$ as a control variable that we have at our disposal. This will be discussed below in detail when we define the breakage vector.

4.2.3 Definition of process vectors: The breakage vector and mixing vector

Once one has defined the characteristic vector, the next step is to define the process vectors. The process vector $\boldsymbol{p(m_i)}$ is defined such that a process operating on material described by the characteristic vector $\boldsymbol{m_i}$ points in the direction of change of $\boldsymbol{m_i}$. The specific fracture energy of particles is an important fundamental property. Impact tests on single particles and/or

particle populations are used to determine the fracture characteristics of particles. The specific energy associated with this single stage operation is equivalent to Equation 4.7.

$$\overline{E} = \frac{Mgh}{m} \tag{4.7}$$

where M is the mass of the falling ball, g is the gravitational acceleration, h is the height of fall and m is the mass of the particle being impacted.

We will now introduce the concept that the process vector $\boldsymbol{p}_i$ depends on the characteristic vector $\boldsymbol{m}_i$ of the system as well as the control variable $\overline{E}$ (Godorr et al., 1994). For our system the value of the control variable can be chosen at every point m_i, and can hence be considered as an optimization variable.

Let us first consider the **<u>breakage process</u>** and define the breakage vector i.e. $\boldsymbol{b}_i$. The breakage depends on the mass distribution of the material, i.e. $\boldsymbol{m}_i$ as defined above, as well as $\overline{E}$.

$$\boldsymbol{p}_i(\boldsymbol{m},\ \overline{E}) = \frac{\Delta m_i}{\Delta E} = \boldsymbol{b}_i \tag{4.8}$$

The population balance model Equation 4.2 first proposed by Reid (Reid, 1965) provides the mathematical formulation which describes the evolution of the instantaneous change in mass fraction with time. Herbst and Fuerstenau (1973) have used a modified form which is $\overline{E}$ dependent as in Equation 4.3. Free, McCarter and King (2004) have used the form of Equation 4.3 to estimate size distributions from a single-particle impact of known $\overline{E}$.

b relates the output of each batch grinding stage without mixing for the net specific energy expended, *m* is the vector of mass fraction of material in size class *i*. The breakage rate function S_i describes the proportion of particles in each size interval, *i*, selected for breakage. The breakage distribution function B_{ij} is a lower triangular matrix giving the fraction of progeny particles reporting to size interval *i* when unit mass fraction of particles of size *j* is broken, where the size of class *j* is greater than the size of class *i*. If we consider, for instance, three size class intervals then both functions are 3x3 matrices.

For the purposes of this research, we have made both S_i and B_{ij} functions of $\overline{E}$. The rate at which particles break and the breakage extents should increase with $\overline{E}$. This is consistent with what we observe in operational and test systems. The product *PSD*s' for our batch grinding stages are fundamentally described by the difference form of Equation 4.3, which is a differential equation describing a continuous system. The Euler mathematical technique is used for the solution of Equation 4.3 in the matrix form as in Equation 4.9. A modified selection function S^E is defined as the amount of breakage that takes place when a small ΔE is applied, as introduced in our previous paper (Khumalo et al., 2003). Equation 4.9 is the resulting mass balance for the batch grinding equation whose solution represents our grinding stage.

$$m_{\text{out}}\left(\overline{E}\right) = \left(I + S^E B - S^E\right) m_{\text{in}}(0) \tag{4.9}$$

I is an identity matrix, m_{out} and m_{in} are the feed and product vectors respectively from each stage of breakage while $\overline{E}$ *(J/g)* is the specific energy input into each hypothetical breakage stage described by Equation 4.8. The

product of the number of breakage stages with $\overline{E}$ is the net specific energy requirement into the system.

Considering the first batch grinding stage, the breakage vector transforms the feed vector into the product vector and it is given by Equation 4.10.

$$\boldsymbol{b}_1 = \boldsymbol{m}_{out} - \boldsymbol{m}_{in} = \left(S^E B - S^E\right)\boldsymbol{m}_{in} \qquad (4.10)$$

When the fracture of individual particles in a sample of particles is measured, a large scatter of the data results and it is described statistically. Tavares (1998) has shown that the log-normal statistical distribution is successful in describing particle fracture energy data of a variety of irregularly shaped brittle materials. The experiments were carried out on single particles of different sizes and also on particle populations. The conclusion was that the specific particle fracture energy decreases as the particle size increases. The fracture energy increases at a rate proportional to the mass of the particle. In the light of the relevance of the specific energy, it is safe to assume that the breakage rate function must be a function of $\overline{E}$. The breakage rate function is also particle size dependent through its dependence on the $\overline{E}$. The probability of breakage is represented as a mathematical expression of the form in Equation 4.11 which is in the form of the log-normal statistical distribution.

$$S_i(\overline{E}) = 0.5 * \{1 + \operatorname{erf}(\frac{ln(\overline{E}) - lnE_{m50,i}}{\sqrt{2\sigma_E}})\} \qquad (4.11)$$

where σ_E is the geometric variance of the distribution and $\overline{E}$ is the specific energy which is a variable in our case. E_{m50} is the median specific fracture energy which is a function of particle size ($d_{p,i}$) as in Equation 4.12.

$$E_{m50,i} = E_{m\infty} \left[1 + \frac{d_{po}}{d_{p,i}} \right]^{\phi} \qquad (4.12)$$

where d_{po} is a characteristic size of the material microstructure, Φ is a fitting parameter, and $E_{m\infty}$ represents the residual particle fracture energy. Equation 4.12 has been fitted to particle fracture energy data on a variety of materials over a range of particle sizes. Table 4.1 provides the values for the constants in Equation 4.12 especially the quartz values as used in our theoretical simulations. The breakage distribution function describes the product breakage distribution into the relevant size class intervals. The breakage products fall into numerous size class intervals which are regarded as the particle effective diameters. So to try and describe the breakage products by considering each particle size would be a truly enormous task considering the fact that in industrial operations and even in the laboratory scale quite substantial amounts of material are handled, all with different effective diameters. In the light of this limitation the quantification of the mass of material falling into a certain size class interval has been the norm in dealing with products of breakage processes. We propose that the formulation of the population balance model is representative of the objectives of this research in describing the change in mass fraction distribution in every size class interval with specific energy ($\overline{E}$) as in Equation 4.9.

The theoretical basis for describing the breakage distribution function is that it is determined by the energy available to break the material during the impact. Higher energy impacts produce finer progeny particles. Bourgeois (1993) carried out some work to describe the breakage distribution function. From the results of the experiments it is shown that the measured size distributions

can be characterized effectively in terms of the parameter T_{10}. T_{10} is defined
as the fraction of the progeny that are smaller than the $1/10^{th}$ of the top size.
The mathematical formulation is of the form of Equation 4.13 and the
constants are found in King (2001).

$$T_{10,i} = T_{10_{max}} \left(1 - exp^{-\frac{\beta \bar{E}}{E_{m50,i}}} \right) \qquad (4.13)$$

where T_{10max} and β are material specific and can be determined easily in the
laboratory using standard drop weight apparatus. Some of the constants
found in Equation 4.13 are presented in Table 4.1.

Table 4.1: Parameters used to fit Equations 4.12 and 4.13 (Tavares, 1998; King, 2001)

Material	$E_{m\infty}$ (J/kg)	d_{po} (mm)	T_{10max}	β	Φ	Size range (mm)
Apatite	1.50	19.30	45.4	0.0115	1.62	0.25-8.00
Galena	3.19	7.31	44.5	0.0176	1.03	0.70-7.60
Gilsonite	5.50	7.03			1.60	1.18-10.0
Quartz	**43.40**	**3.48**	**38.8**	**0.0176**	**1.61**	**0.25-4.75**
Sphalerite	7.00	8.24			1.16	0.35-10.0
Magnetite	9.56	3.93	47.1	0.0098	1.96	0.25-7.20
Copper ore	96.10	1.17	44.8	0.0263	1.26	0.25-15.8
Iron ore	47.30	1.08			2.30	0.25-15.0
Limestone	114.20	0.49	54.5	0.0176	2.05	0.35-5.60
Marble	45.90	0.882			2.66	0.50-15.0
Tarconite (BM)	235.90	0.803			1.42	0.35-6.00
Taconite (CC)	163.30	0.856			1.76	0.35-10.0
Hematite			45.6	0.0164		
Basalt			52.0	0.0252		
Titanium ore			51.0	00269		

The entire breakage distribution function is regenerated from the single value
of T_{10} using the standard truncated distribution functions. The truncated

Rosin-Rammler distribution is specifically used to regenerate the entire breakage distribution function as represented in Equation 4.14.

$$b_{ij} = \left(1 - T_{10,i}\right)\left(\frac{9}{i-1}\right)^{\alpha}$$

(4.14)

Equations 4.13 and 4.14 fully describe the breakage distribution function. It follows that Equation 4.9 now fully describes how material breaks out into different size intervals for each breakage stage. Use and verification of the model will be dealt with in a future paper.

The input specific energy $\overline{E}$ is incorporated in the functions, S_i and B_{ij} and thus both vary with $\overline{E}$. In some published modeling work the breakage function is found to be constant (Herbst and Fuerstenau, 1973) but in this paper the breakage distribution function varies with $\overline{E}$. Our model has the advantage that energy distributions can be simulated, as this is a fundamental property of most grinding environments. Understanding the desired energy input distribution is critical to the selection and design of equipment to satisfy the objective function.

4.3.1 Example 1: AR for breakage process only with constant specific energy

We will initially consider only a breakage process with $\overline{E}$ held constant through the batch grinding stages. For purposes of this paper we consider 3 size classes: the feed size class 1, median size class 2 and the fines size class 3. The objective is to maximize the proportion of material in size class 2.

We start by considering a simple process where particles are continually broken by applying a fixed $\overline{E}$ according to Equation 4.8. We begin with a given mass of material of size class 1, and we do not separate or add material, thus the mass of material that we are breaking remains constant. For ease of representation, we could imagine this process as a number of batch grinding stages in series. We introduce the feed material in stage 1 and we use a known amount of energy and determine the extent of breakage.
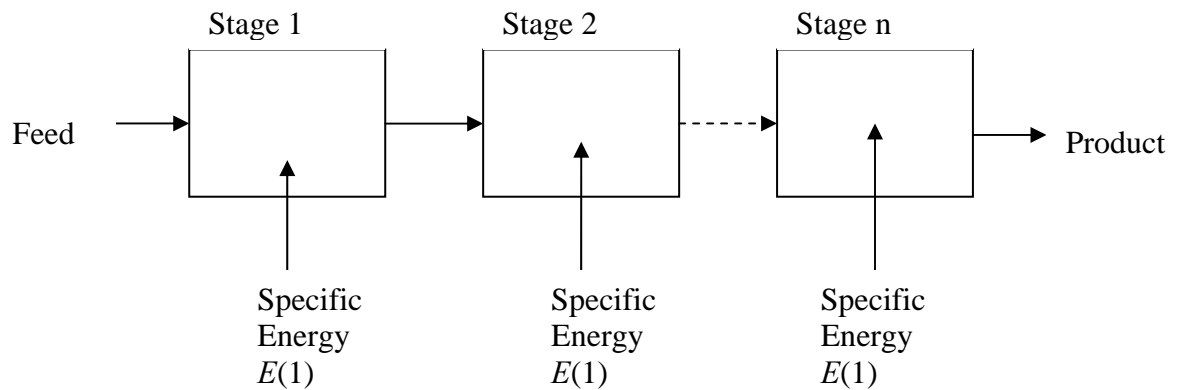
Figure 4.3: Illustration of the breakage only process considered in Examples 1 and 2

The broken material from the first batch grinding stage is introduced into stage two where we again subject the material to the same $\overline{E}$ causing further extent of breakage. We continue similarly to stage 3 and so on as illustrated in Figure 4.3. The total mass of material in each of the batch grinding stages is constant.

For a known particle size Equation 4.12 calculates the median specific fracture energy which is substituted into Equations 4.11 and 4.13. Once we know the T_{10} breakage index we now can calculate the breakage distribution function using Equation 4.14. The result of Equation 4.11 is a vector and it is converted to a diagonal square matrix, **S**. The result of Equation 4.14 is a

vector and it is converted to a lower triangular square matrix, **B**, whose dimensions are equal to the number of size class intervals describing the feed and product *PSD*s', *i*. The results of Equation 4.11 and Equation 4.14 are substituted into Equation 4.9 which calculates the mass fraction in each size class for each batch grinding stage as explained below. A Matlab® algorithm found in Appendix A is used to calculate the mass fraction distributions for every batch grinding stage.

We track the product mass distributions after each stage of breakage by keeping track of the mass of material in each of the size classes under consideration. We are thus in this first simple example considering a breakage only process with a fixed $\overline{E}$.

If we consider only three size classes, then we can consider the output of this breakage only process in a 2-dimensional figure, with axes of mass fraction of size 1 (feed size class) versus mass fraction of the medium size class 2. The breakage vector is described by Equation 4.10. If we choose an input $\overline{E}$ of 2 J/g, we find that the set of outputs from the breakage process is as shown in Figure 4.4.
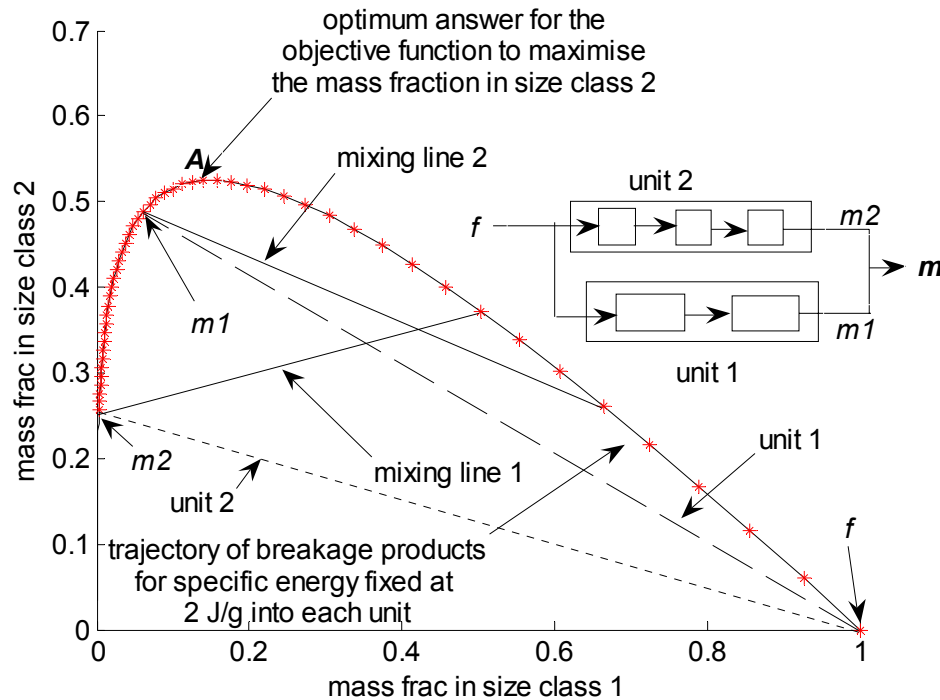
Figure 4.4: The effect of proportionally mixing products from two parallel unit structures with different residence times.

The output from stage 1 to 100, marked by asterisks, is shown to indicate how the product distribution changes with number of stages. Figure 4.4 clearly shows that as the number of stages is increased the mass of material in size class 2, the intermediate size class, increases while the mass fraction of material in the feed size class, size class 1, decreases. This increase in the amount of material in size class 2 continues until at point **A** the mass fraction of material in size class 2 reaches a maximum and then starts to decrease with the addition of further batch grinding stages as the material in the smallest size class 3 accumulates even more.

Thus for an objective to maximize the mass of material in size class 2, using a breakage only process with a constant $\overline{E}$ input of 2 J/g, Figure 4.4 shows that we would achieve a maximum mass fraction of size class 2 of 0.52 after 20

breakage stages. Over-design or under-designing of equipment will adversely affect the output *PSD*.

The region found is convex but other models of breakage or other substances may not give this result.

4.3.2 Example 2: The effect of mixing for parallel units

Mixing obeys a linear mixing rule such that the mixing vector describing this, *v(m)*, is defined by Equation 4.16.

$$\boldsymbol{m} = \alpha m_1 + (1\text{-}\alpha)\, m_2 = m_2 + \alpha\,(m_1\text{-}m_2) \qquad 0 \leq \alpha \leq 1 \qquad\qquad (4.15)$$

$$\boldsymbol{v(m)} = m_1 - m_2 \qquad\qquad (4.16)$$

The mixing vector, *v*, operating at *m* points from the state of the system m_1 to the state that we are mixing with m_2.

Figure 4.4 shows that by running stages in a series-parallel arrangement, we can in the limit achieve all the *PSD*s' inside the curve. Given feed *f*, m_1 is the output from the series arrangement of unit 1. Also m_2 is the output from the same feed *f* from the series arrangement of unit 2. The dashed and dotted lines serve to show the end points of the individual units 1 and 2, respectively. The curve of mass fraction distributions and the dashed or dotted lines describe the candidate attainable region for the respective units 1 and 2. Unit 1 and unit 2 are parallel arrangements whose combined output is the mixing vector *m* described by Equation 4.16. The parallel units will not allow us to achieve a higher mass fraction of size class 2, as the highest value is found on the boundary using the set of 20 stages in series. However the parallel

units of structures would allow one to achieve the *PSD*s' inside the region, which would not have been achievable by stages in series alone. The products can be mixed such that we get a set of resultant product mass fraction distributions. Also for a 2-dimensional convex structure all interior points can be obtained with feed bypass, eliminating the requirement for parallel processes as shown in Figure 4.4.

The same breakage vector as in Equation 4.10 is used to describe the change of mass fraction in each unit with $\overline{E}$. The mixing line 1 in Figure 4.4 shows the resultant distributions when the product of 8 breakage stages from the first unit is mixed with the product of 100 breakage stages in the second unit in all proportions. Mixing line 2 also shows the resultant distribution when the product from the fifth breakage stage in the first unit is mixed according to Equation 4.15 with the product from the twenty-seventh breakage stage in the second unit in all proportions.

The region achieved by the breakage only process is convex; no breakage vector for $\overline{E}$ held constant point outwards. Hence we have the candidate *AR* for a fixed $\overline{E}$ of 2 J/g. This means that we have determined the maximum achievable mass fraction in size class 2. The required equipment would not use mixing in order to optimize the mass fraction in size class 2.

4.3.3 Example 3: The effect of constant specific energy density input

We now reconsider the system considered for Examples 1 and 2, but remove the condition that the input $\overline{E}$ is kept fixed at a value of 2 J/g as used in the previous cases. Initially for simplicity, we allow the input $\overline{E}$ to be kept constant for all stages of the comminution process. The input $\overline{E}$ is then

varied for the next set of breakage stages. Considering that we have a fixed mass of mono-sized particles as the feed to the process, again all the material from one batch grinding stage is fed to the next batch grinding stage. Thus the mass flow-rate would be the same along the process.

As in Examples 1 and 2, we track the product mass distributions after each batch grinding stage by keeping track of the mass of material in each of the size classes under consideration. We are thus in this example considering a breakage only process where the input $\overline{E}$, although kept fixed, can be set at different levels. If we again consider only three size classes, then we can consider the output of this breakage only process in a 2-dimensional figure, with axes of mass fraction of feed size 1 versus mass fraction of the intermediate size class 2. The breakage vector is still described by Equation 4.10. Figure 4.4 is a series of *n* breakage stages and it effectively constitutes a continuous process in plug flow. The product from each stage acts as a hypothetical feed to the next stage and is further subjected to further breakage at the same $\overline{E}$.
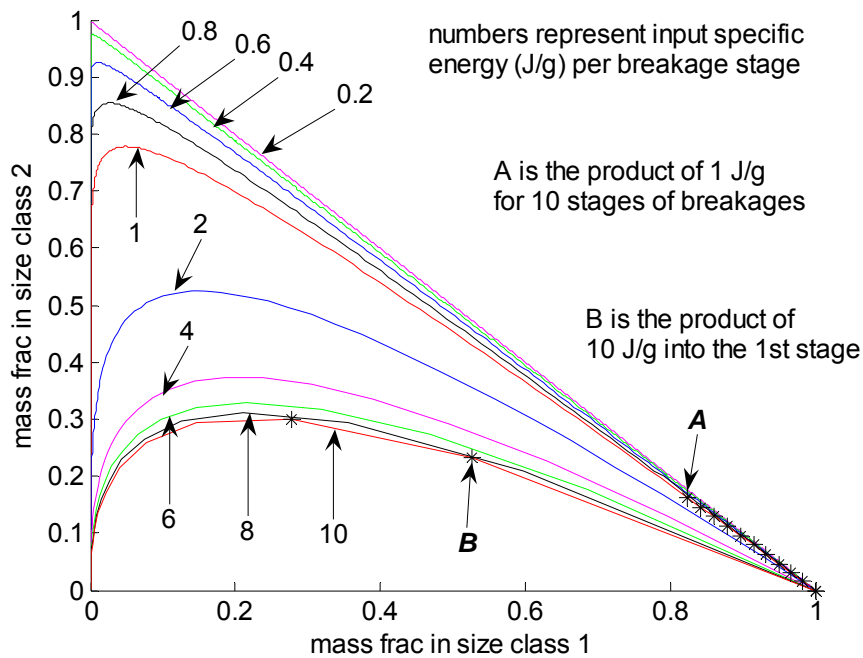
Figure 4.5: Mass fraction distributions for 3 size classes for increasing specific energy input.

For a set of fixed $\overline{E}$ values Figure 4.5 shows the resultant product mass fraction distributions for each stage of breakage represented geometrically as a family of trajectories for size class 1 (the feed size material) and size class 2 (the intermediate size material). There are a number of points that can be noted from this figure.

i) Different $\overline{E}$ values produce different mass fraction distributions. If the objective function was to maximize the mass fraction of material in size class 2, this is achieved in the limit as the $\overline{E}$ approaches the specific fracture energy for that particle size. Furthermore in the limit, using the model outlined in this paper to describe breakage, as $\overline{E}$ approaches the specific fracture energy, the maximum mass fraction of particles of size class 2 approaches

92

1. Thus an interesting result is that if we wish to maximize the mass fraction of material in size class 2, we can achieve a mass fraction of 1 for size class 2, that is, convert all the feed which is size class 1 to size class 2, without producing fines (i.e. size class 3). This is achieved by reducing the input $\overline{E}$ in the breakage process to match the specific fracture energy and use the optimal (infinite) number of stages.

ii)   Increasing the input $\overline{E}$ used in the breakage process reduces the maximum amount of material achieved in size class 2. For example from Figure 4.5, if we supply 2 J/g specific energy, the maximum mass fraction in size class 2 is 0.52 after 20 breakage stages, a reduction of close to 48% of the target value of 1. As the input $\overline{E}$ is increased further to 10 J/g, the maximum mass fraction of particles of size class 2 is only about 30%.

iii)   As $\overline{E}$ increases, we see a tendency for the mass fraction of material in size class 3 to increase, resulting in the trajectories flattening out as they all end in the origin. Hence if we wished to make only fines, we should try to use a high value of $\overline{E}$. However, the higher values of $\overline{E}$ achieve almost the same distributions as the curves come close almost reaching an asymptote. This point continues to emphasize the need to control $\overline{E}$ to increase the energy efficiency of a comminution circuit.

iv)   If we consider the Attainable Region for comminution, we see that the trajectories are convex. Hence the boundary will be the trajectory achieved in the limit as the input $\overline{E}$ approaches E_{m50} (J/g). This region also has no breakage vectors pointing out of it and so it satisfies the necessary conditions for the boundary of the *AR* (Glasser and Hildebrandt, 1987).

v)   We can see that the design of the equipment to control the input $\overline{E}$ is very important in controlling the output *PSD*. We can see that *n* breakage stages with an input $\overline{E}$ (J/g), achieves a different mass fraction of material of size class 2 than one stage of input $n^*\overline{E}$ (J/g). Figure 4.5 shows that re-breaking the material 10 times at an input $\overline{E}$ of 1 J/g achieves 0.16 mass fraction in size class 2, point **A**, while breaking the same material once with $\overline{E}$ 10 J/g achieves 0.23 mass fraction in size class 2, point **B**. *Thus, in the design and operation of comminution equipment, (if we wish to control the PSD) it is very important to control the $\overline{E}$ at all points of the equipment rather than just the total energy.*

vi)   The sensitivity of the product size distribution to input $\overline{E}$ varies along the trajectories. Thus for example, for mass fraction of size class 1 from 1 to 0.7, there is not much effect on the *PSD* for different input $\overline{E}$ values between E_{m50} to about 1 J/g. Thus to reduce size of equipment one could start with a higher input $\overline{E}$ and then reduce $\overline{E}$ at an appropriate point in the trajectory. This concept is examined in more detail in the subsequent examples.

This new approach obviously is versatile in that it provides information on the progress of the breakage event. It shows the evolution of the breakage products with input $\overline{E}$. It also provides geometric evidence of the number of breakage stages required to achieve certain optimum objectives.

It has been shown that it is important to control the input $\overline{E}$ in the comminution process. We could ask how this could be done. Some of the ways in which this could be achieved is by using mills in series with different size balls and/or different rotational speeds.

4.3.4 Example 4: The effect of varying input specific energy density

The comminution process falls under a class of stochastic processes which exhibit a form of state dependency which satisfies the Markov property (Mitrani, 1998). The Markov property states that the future state of a process depends on the past only through its dependence on the present state. This allows us to change process control variables, such as input $\bar{E}$, as the process is in progress as in Figure 4.6. Thus by changing the input $\bar{E}$ (J/g) at some point **A** one could equivalently change the direction and magnitude of the breakage vector as shown in Figures 4.7 and 4.8. Thus we could in principle look at choosing the input $\bar{E}$ at every point along the trajectory or process path so as to achieve some objective such as *PSD*.

Generally, as mentioned previously, the higher $\bar{E}$ applied for fracture the larger the proportion of smaller particle sizes achieved from the process. This can be seen by reference to Equation 4.12 and we can deduce that the median specific fracture energy density of particles E_{m50}, increases as the particle size d_{pi} decreases.
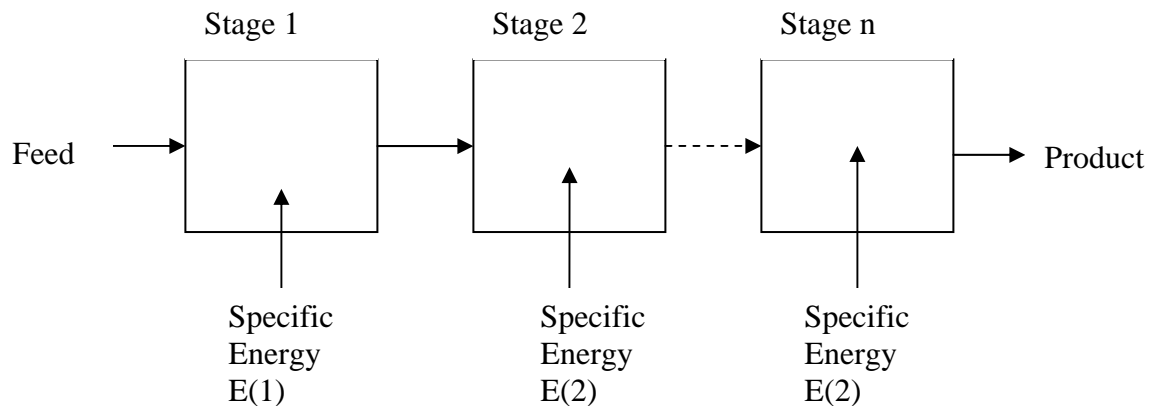
Figure 4.6: Illustration of the breakage flow-sheet for changing specific energy.

Applying an input $\bar{E}$ of 2 J/g for every grinding stage to our system of Figure
4.6 we get the trajectory described by the dotted line in both Figures 4.7 and
4.8. The input $\bar{E}$ is varied from 0.2 to 10 J/g and the resulting trajectories are
represented in both Figures 4.7 and 4.8.
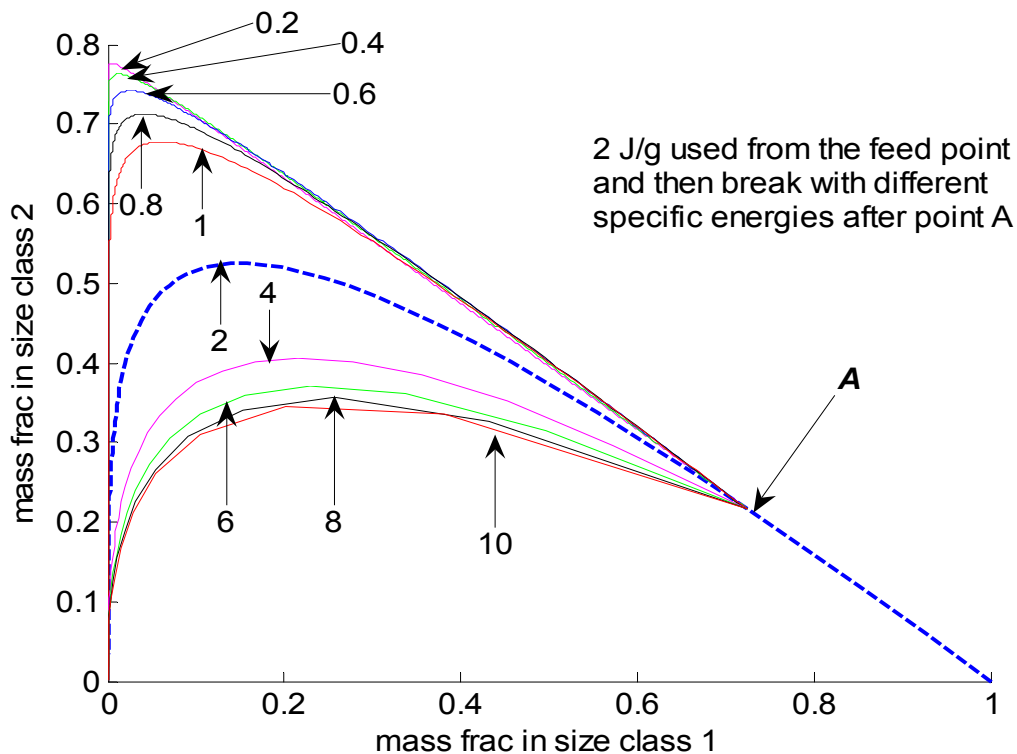
**Figure 4.7: The effect of changing specific energy from the constant 2 J/g at point A
after four stages of breakage.**

We see in Figure 4.7 that when changing the input $\bar{E}$ after point **A**, the mass
fraction of material of size class 2 increases whether we increase or decrease
the input $\bar{E}$ in subsequent stages. In line with what we found in the previous
examples, the lower the $\bar{E}$ used after point **A**, the higher the maximum mass
fraction of material of size class 2. The drop in the value of maximum mass

fraction of material in size class 2 is fairly small when we use a policy of an input $\overline{E}$ of 2 J/g up to point **A** and then switching to a $\overline{E}$ of 0.2 J/g thereafter, compared to following a constant $\overline{E}$ input policy of 0.2 J/g along the entire process.
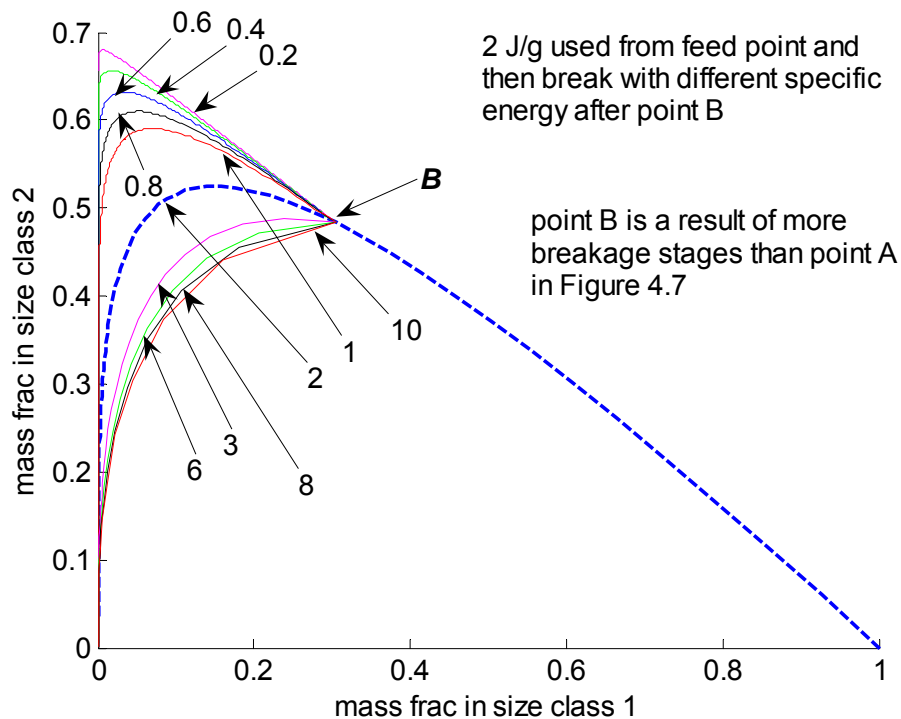
Figure 4.8: The effect of changing specific energy from the constant 2 J/g at point B after thirteen stages of breakage.

We see however that if we had continued with a constant $\overline{E}$ of 2 J/g up to point **B**, as shown in Figure 4.8, and then switched to a constant $\overline{E}$ of 0.2 J/g thereafter, there would have been a much larger difference (of the order of 20%) compared to if we had followed a constant $\overline{E}$ of 0.2 J/g along the entire trajectory. However we see in Figure 4.8 that if we used $\overline{E}$ values higher than 2 J/g after point **B**, the mass fraction of material in size class 2 actually decreases.

From this we can draw two important conclusions:

i) We can achieve as close to maximum mass fraction of material in size class 2 as we wish by following a *decreasing* $\overline{E}$ trajectory which has a value greater than the specific fracture energy.

ii) We however have to carefully control the $\overline{E}$ along the trajectory, since if we increase it, we can decrease the mass fraction of material in the intermediate class.

4.3.5 Example 5: The output *PSD* for constant total energy input

From the previous results we can see that the use of input $\overline{E}$ is very important in controlling size distributions. We now look at how the total energy input E_T affects size distributions of product. We compare systems of *n* batch grinding stages where the input $\overline{E}$ is E_T/n per stage. Thus all the systems will have the same energy available but the input $\overline{E}$ in the various processes is controlled.
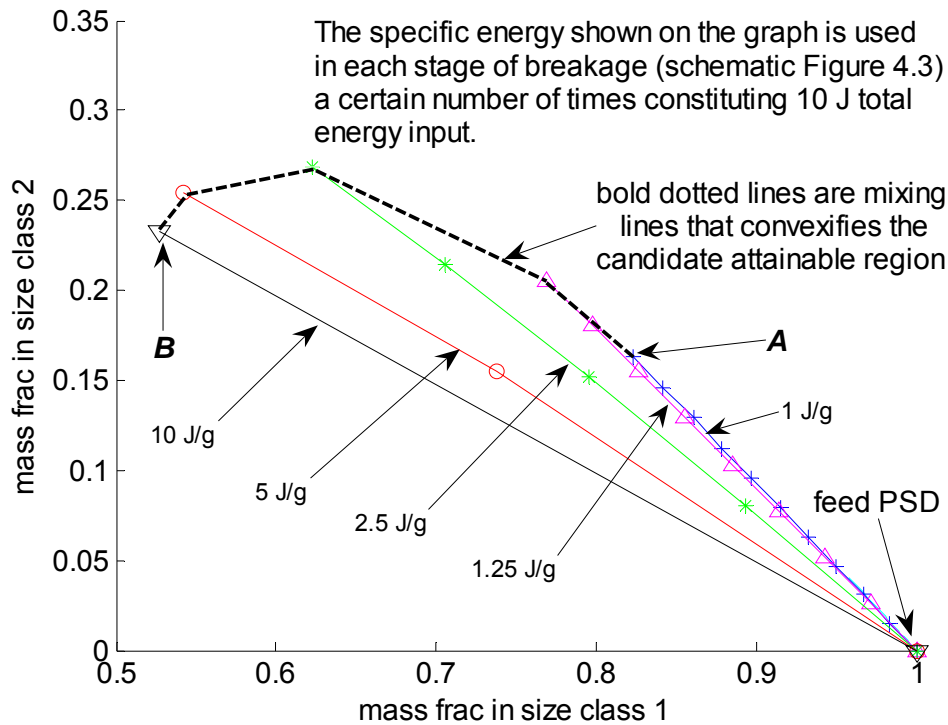
Figure 4.9: Achievable Mass Fraction Distributions for a Total Energy of 10J.

In Figure 4.9 we represent all the possible output states for the application of an energy value of 10 J for the breakage trajectories while incorporating the mixing process as well by dotted lines. The path from the feed point to point *A* is the process trajectory for 1 J/g $\overline{E}$ applied 10 times to 1g feed and the maximum achieved is 0.16 mass fraction in size class 2. The process of mixing convexifies the region to achieve other distributions which could not have been achieved by the breakage process alone.

The path from the feed *PSD* to point *B* is the process trajectory for 10 J/g $\overline{E}$ applied once to 1 gram feed and the maximum achieved is 0.23 mass fraction in size class 2 as shown in Figure 9. We can for the same net energy input vary the mass fraction of material in size class 2 from 0.16 to 0.27 by choice of the input $\overline{E}$ level in the equipment, emphasizing how important design of

equipment is. Thus if we know the energy input into a communition process, we can by seeing where it lies on the contour, decide on how much room for improvement there is for the design or operation of the circuit.
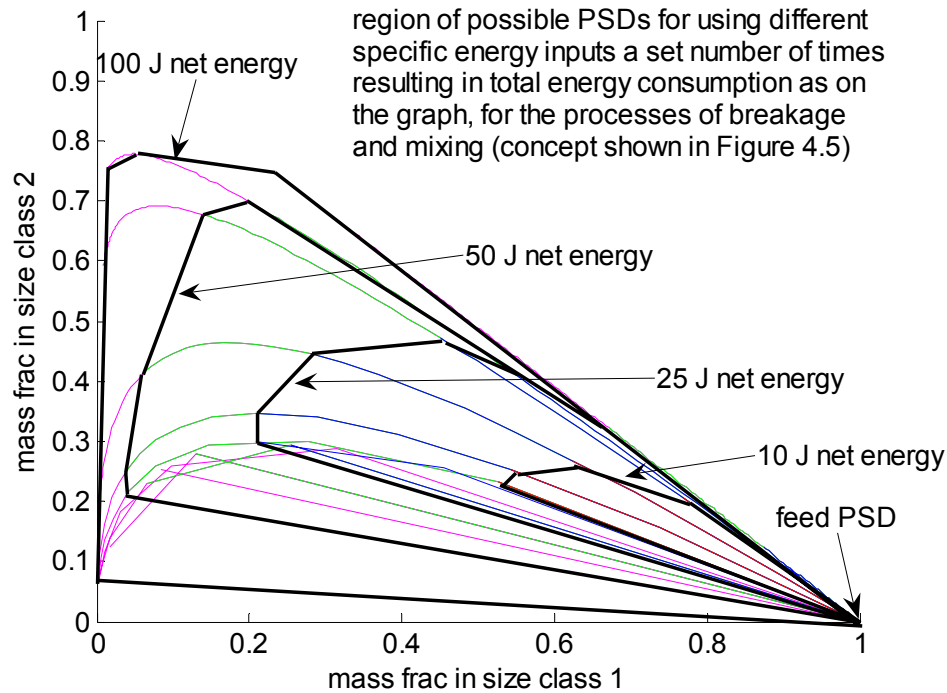
Figure 4.10: Achievable Distributions for Increasing Total Energy in Joules.

We next look at the contours for all possible energy inputs as shown in Figure 4.10. The contours represent the set of all achievable mass fraction distributions for a given total energy as a result of different input $\overline{E}$ being applied a set number of times.

We also notice the region where breakage of size class 1 is small, i.e. this implies that most specific energy inputs for the initial stages are less important for control of particle size distributions. The only difference is that the number of stages required differs with $\overline{E}$, the specific energy.

We note that as the available energy increases, we can achieve a higher maximum value of mass fraction in size class 2. A lower value is also achieved as the contours for higher energy contains the contours for lower energy. Thus, it can be noted that in order to increase the mass of material in size class 2 we need to increase the energy input at the expense of increasing the number of batch grinding stages, n. The contours on the locus get closer and closer, implying that eventually for smaller increases in mass fraction of size class 2 we need large increases in energy.

Another interesting feature of the contours is that as the number of breakage stages are continuously increased, the contours reach a maximum turning point where mass fraction in size class 2 decreases as mass fraction in size class 3 increases. This implies that if the number of stages is not optimized properly, this could result in more quantities of fines at the expense of intermediates.

Figure 4.10 shows how the mass fraction of material in size class 2 can be varied as the total energy is increased and that by controlling the input $\overline{E}$ we can for the same available total energy achieve very different products. Again this gives us targets that we can use in the evaluation of existing equipment/s and circuits.

4.4 SUMMARY

A new method of representing particle size distributions as points in space is successfully presented. This enables batch grinding products to be connected, enabling close control of the process. The power of this method is that the characteristic equation comprise of the required size class (objective

function), the feed size class and the control variable. This reduces the dimensionality of the geometric representation considerably. However any number of size classes can be handled using this approach if necessary, when more than one objective function is prescribed. We have used a simple three particle size system to illustrate the results. Importantly, there is nothing inherent in the approach other than the visualization of the results that stops them from being used on much higher dimensional systems.

Instead of using parallel equipment, we propose that comminution systems should use equipment in series so that the value of $\bar{E}$ can be varied along the circuit. This is recommended because larger particles break along the available cracks resulting in stronger smaller particles with fewer cracks. Breakage and mixing are necessary to achieve the mass fraction distributions below the candidate *AR* by using the equipment in series with feed bypass.

The candidate *AR* for comminution is found to be convex. This means that the region obtained cannot be extended further, and the fundamental process of breakage alone is sufficient to describe it. However the control variable $\bar{\bar{E}}$ can be used to extend the region but still using breakage as the only fundamental process. The models imply that to get maximum amount of intermediate size class low specific energy along the length of the process is needed. High production of fines could be the objective function and therefore a high specific energy input would be recommended.

The candidate *AR* once obtained is interpreted as pieces of equipment and optimum process conditions. This simultaneously solves the process synthesis and optimization problems for comminution systems. The optimum conditions obtained from the *AR* determine the target against which the efficiency of the actual process should be measured.

An experimental validation of this work has been carried out and it is the scope of the subsequent paper.

4.5 REFERENCES

Austin, L. G.; Klimpel, R. R.; Luckie, P. T. (1984). Process Engineering for Size Reduction: Ball Milling. Guinn Printing Inc., Hoboken, New Jersey, United States of America.

Baumgardt, S.; Buss, B.; May, P.; Schubert, H. (1975). On the comparison of results in single grain crushing under different kinds of load. Proc. 11th Int. Miner. Process. Congr., Cagliari, 3-32.

Bergstrom, B.H. (1962). Energy and size distribution aspects of single particle crushing. Proc. 5th Symp. Rock Mechanics, 155-172.Bond, F. C. (1952). The third theory of comminution. Mining Engineering, **4**, 484-494.

Biegler, L. T.; Grossman, I.E.; Westerberg, A. W. (1997). Systematic methods of Chemical Process Design. New Jersey: Prentice Hall.

Bond, F. C. (1952). The third theory of comminution. Trans. Am. Inst. Min. Metall. Pet. Eng., **193**, 484-494.

Bourgeois, F. (1993). Microscale modeling of comminution processes. PhD Thesis, University of Utah.

Chitra, S. P.; Govind, R. (1985). AICHE J., **31**, 177.

Cho, H.; Austin, L. G. (2003). An equation for the breakage of particles under impact. Powder Technology, **132**, 161-166.

Cleary, P. W. (1998). Predicting charge motion, power draw, segregation, wear and particle breakage in ball mills using discrete element methods. Miner. Eng., **11**, 1061-1080.

De, A. (1995). Modeling and Optimization of fine grinding of minerals in high-pressure roll mill/ball mill hybrid comminution circuits, Ph.D. Thesis, University of California, Berkeley.

Feinberg, M.; Hildebrant, D. (1997). Optimal reactor design from a geometric viewpoint. Part I. Universal properties of the attainable region. Chemical Engineering Science, **52**, 1637-1665.

Feinberg, M. (2000). Optimal reactor design from a geometric viewpoint. Part II. Critical side-stream reactors. Chemical Engineering Science, **55**, 2455-2479.

Free, K. S.;McCarter, M. K.; King, R. P. (23-25 February 2004). Evaluation of a new method for work index estimation using single particle impact tests. SME Annual Meeting, Denver, Colorado.

Fuerstenau, D. W.; Shukla, A.; Kapur, P. C. (1991). International Journal of Mineral Processing, **32**, 59-79.

Glasser, D.; Hildebrandt, D. (1987). A geometric approach to steady flow reactors: the attainable region and optimization in concentration space. American Chemical Society, **26**, 1803-1810.

Godorr, S. A.; Hildebrandt, D.; Glasser, D. (1994). The attainable region for systems with mixing and multi-rate processes: finding optimal reactor structures. The Chemical Engineering Journal, **54**, 175-186.

Grandy, G.A.; Fuerstenau, D.W. (1970). Trans. SME/AIME, **247**, 348-354.

Herbst, J. A.; Fuerstenau, D. W. (1973). Trans. SME/AIME, **254**, 343-347.

Herbst, J. A.; Fuerstenau, D. W. (1980). Scale-up procedure for continuous grinding mill design using population balance models. International Journal of Mineral Processing, **7**, 1-31.

Horn, F. (1964). Attainable and non-attainable regions in chemical reaction technique. 3rd European Symposium on "Chemical Reaction Engineering". Pergamon Press Ltd. Great Britain.

Hulburt, H. M.; Katz, S. (1964). Some problems in particle technology. A statistical mechanical formulation. Chemical Engineering Science, **19**, pp. 555-574.

Kapur, P. C.; Fuerstenau, D. W. (1987). Energy-size reduction "laws" revisited. International Journal of Mineral Processing, **20**, 45-57.

Kick, F. (1885). Das Gesetz der proportionlen Wilderstande und seine Anwendung, Leipzig.

King, R. P. (2001). Modeling & Simulation of Mineral Processing Systems. Butterworth-Heinemann: Great Britain. 144-151.

Khumalo, N.; Hausberger, B.; Kauchali, S.; Hildebrandt, D.; Glasser, D. (3-5 September 2003). The Attainable Region in the Particle Size Distribution Space for Steady Flow Processes in Comminution. South African Chemical Engineering Congress, Sun City, South Africa.

Mishra, B. K.; Rajamani, R. K. (1992). The discrete element method for the simulation of ball mills. App. Math. Modelling, **16**, 598-604.

Mitrani, I. (1998). Probabilistic modeling; University Press: Cambridge, pp. 156-168.

Moys, M. H.; Skorupa, J. (1993). Measurement of the radial and tangential forces exerted by the load on a liner in a ball mill, as a function of load volume and mill speed. Int. J. of Mineral Proc., **37**, 329-356.

Nisoli, A.; Malone, M. F.; Doherty, M. F. (1997). Attainable Region for Reaction and Separation, AICHE J., **43** (2), February 1997, pp. 374-387.

Paynter, J. D.; Haskins, D. E. (1970). Chem. Eng. Sci., **25**, 1415.

Rajamani, R. K.; Mishra, B. K. (1996). Dynamics of ball and rock charge in sag mills. Proc. SAG 1996, Department of Mining and Mineral process Engineering, University of British Columbia.

Reid, K. J. (1965). Chemical Engineering Science, **20**, 953-963.

Rittinger, P. R. (1867). Lehrbuch der Aufbereitungskunde, Berlin.

107

Rumpf, H. (1973). Physical aspects of comminution and new formulation of a law of comminution. Powder Technology, **7**, 145-159.

Schonert, K. (1988). Fundamentals of particle breakage. Course notes, University of the Witwatersrand, Division of Continuing Engineering Education, Johannesburg, Section F6.

Seodigeng, T.; Hausberger, B.; Hildebrandt, D.; Glasser, D. (3-5 September 2003) DSR Algorithm for Attainable Regions Analysis: Higher Dimensional Problems. South African Chemical Engineering Congress, Sun City, South Africa.

Tavares, L. M.; King, R. P. (1998). Single-particle fracture under impact loading. Int. J. Miner. Process., **54**, 1-28.

Van de Vusse, (1964). Plug-flow type reactor versus tank reactor. Chemical Engineering Science, **19**, pp. 994-997.

4.6 LIST OF SYMBOLS

AR	attainable regions
b_{ij}	breakage distribution function: lower 3X3 triangular matrix.
E_{m50}	median specific fracture energy.
$\overline{E}$	specific energy.
i	number of size classes.
m	total mass of material being ground.
m_i	mass fraction in size class *i*.
PSD	particle size distribution.
P	power (W)
S_i	breakage rate of particles in size class *i*.
S_i^E	modified breakage rate of particles in size class *i* with $\overline{E}$

CHAPTER 5

AN EXPERIMENTAL VALIDATION OF A SPECIFIC ENERGY BASED APPROACH FOR COMMINUTION[‡]

Khumalo, N., Glasser, D., Hildebrandt, D., Hausberger, B.

University of the Witwatersrand

Ngangezwe Khumalo

University of the Witwatersrand

School of Process and Materials Engineering

Private Bag 3

Wits, 2050

August 14, 2006

Tel: +27(011)7177584

Fax: +27(011)7177557

Email: zwekhums@hotmail.com

ABSTRACT

In a recent paper (Khumalo et al., 2006) it was shown that the attainable region approach could prove useful in designing better comminution circuits. Fundamental to this approach was the assumption that the rate of comminution was only determined by the specific energy within the device. This paper shows experimentally that this assumption holds for a batch ball mill.

The system presented here considered breakage of mono-sized feed particles in a laboratory ball mill into two distinct progeny size classes. The population balance model was successfully used to model the experimental products and the results were represented geometrically in a 2-dimensional space. The resulting geometric structure can be used to solve process synthesis and optimization problems simultaneously.

It was found that the breakage rate parameter out of size class 1, changes with time but exhibits an exponential relationship with an asymptote. It is hypothesized that this asymptote is the rate of breakage at long grind times or in well mixed, steady state continuous systems. It is shown that the parameters of the process depend only on the specific energy. This was one of the assumptions that were made in the construction of the attainable region. Thus equipment selection and operating conditions only requires one to match the required specific energy.

Keywords: attainable region (*AR*); comminution; ball filling; mill rotational speed; laboratory ball mill; particle size distribution; specific energy

5.1 INTRODUCTION

The comminution process is energy intensive and highly inefficient. This is particularly the case for grinding. Schonert (1988) calculated the energy efficiency for grinding processes to be in the range of 4-8% assessed on the basis of surface area produced. Much effort has been expended to try and understand the breakage of single particles in order to increase energy utilization. Tests done on single particles show that the specific fracture energy decrease as the particle size increase, according to a power law (Tavares et al., 1998).

The aim of any industrial comminution process is to reduce particle sizes efficiently. Verma and Rajamani (1995) have shown that breakage rates of particles in a dry ball mill change with time. This means that equipment selection as well as knowledge of the operating conditions is vital for efficient process synthesis. We endeavor in this work to use the ideas of the attainable region to achieve this.

The attainable region analysis has been successfully applied in chemical reactor engineering for choosing and optimizing the best reactor configurations (Glasser et al., 1987). The *AR* approach allows the development of algorithms that determine the set of all output states from specific fundamental processes without being equipment specific.

The close resemblance between chemical reaction and size reduction processes has prompted the idea that the same *AR* principles can be applied in size reduction. Both processes involve the conversion of material from one form to another which could be size or chemical structure. Just as in chemical

reactions where we have reactant and product species, so is the case with size reduction when we assign each particle size class to represent a species. This work cements the application of the concept of speciation of particle size distributions. Each particle size class is represented as a single state (element) in a vector. We note that i particle size classes can be represented in i-1 dimensional space with the ith state being found by mass balance.

The breakage process rate vectors can be used to show how the instantaneous mass fraction distributions vary with volume percent ball filling and mill rotational speed by classifying the progeny into, for instance, three size classes which are grouped as species called;

iv)   The feed size class which truncates the subsequent distributions. This is taken as the top size class or size class 1 in our terminology.

v)   The medium size class termed size class 2, smaller in size than size class 1 since no progeny particle can have a size larger than the parent size (King, 2001).

vi)   The fines size class which is a result of relatively large breakage extents. This is termed size class 3.

A point to note is that the consideration of the three size classes does not affect the generality of the results. The characteristic equation for constructing the attainable region requires the inclusion of the feed point and that size interval to be maximised. In this case the objective function was either minimizing energy consumption or maximising mass in size class 2. However the broken material coming out of the laboratory mill was sieved into 6

different size classes. Any size class could have been chosen as long as it is part of the desired output describing the objective function. Therefore any number of size classes can in principle be handled using this technique by solving the population balance model into the number of size classes required.
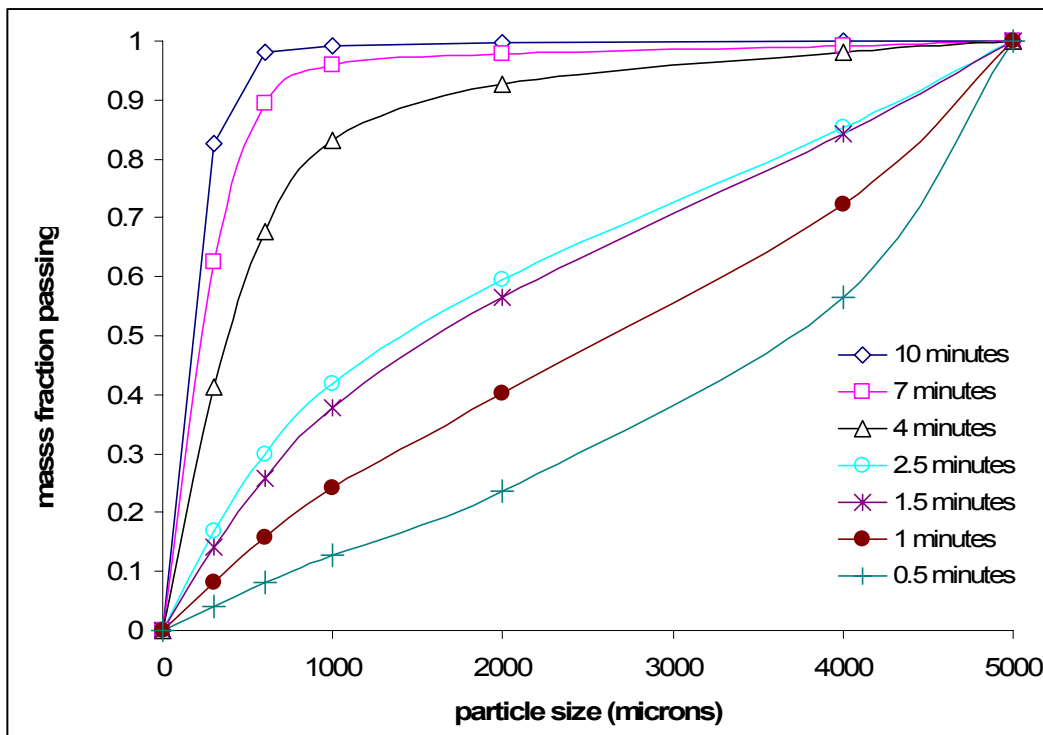
Figure 5.1: Cumulative particle size distributions as one increase the grinding time for a laboratory ball mill at 92 rotations per minute and 20 % ball loading.

The way the *AR* approach has been implemented is also robust in that it creates a way of tracking the states of a process. As an example, up to now particle size distributions have been represented in the form of cumulative weight percent passing vs. particle size as in Figure 5.1.

This representation is limiting in that it does not provide connectivity between product states for a process. We believe dynamic systems are not adequately represented by the traditional cumulative plots. We have suggested a simple way of taking each discreet size class and representing it as a unique species. Thus a point in the space of all of these variables can be used to represent a complete particle size distribution. Any number of discreet size classes can in principle be handled. In the case of our results we consider only three size classes as the third size class can be found by mass balance we can represent our results in a 2- dimensional plot.

Figure 5.2 is our proposed method of representing the particle size distributions in Figure 5.1 as single points in space. For the purpose of illustrating how our method works, three size classes are chosen as;

i)   size class 1 to retain material with particle sizes greater than 4000 μm,

ii)   size class 2 to retain material with particle sizes lying between 4000-2000 μm, and

iii)   size class 3 to retain material with particle sizes less than 2000 μm.
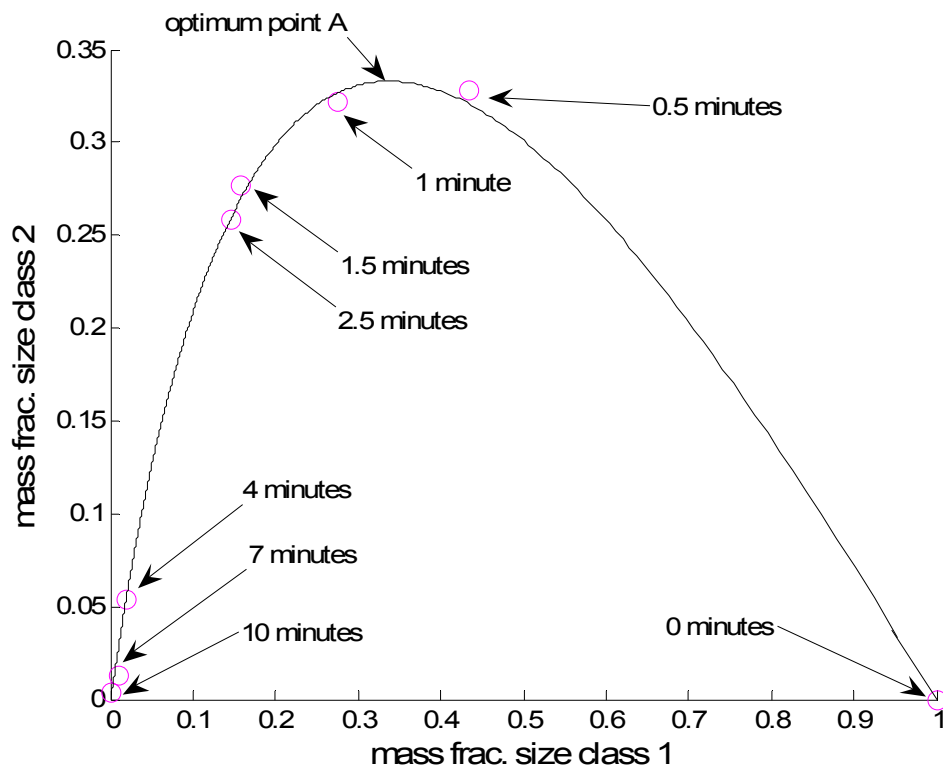
Figure 5.2: Our new proposed method for representing the eight product particle size distributions in Figure 5.1 as a single path.

Figure 5.2 shows the amount of material retained on size class 1 and size class 2 with size class 3 found by mass balance. This offers an opportunity to connect the points into a single trajectory from which the objective function can be drawn for optimization purposes.

Comminution falls under the class of Markov processes. The Markov property states that the future state of a process depends on the past state only through its dependence on the present state (Mitrani, 1998). The process direction is transient in that given the state *p*, the following transition distributions from state to state finally arrive at state *q*, but state *p* is not achievable from state *q* (Mitrani, 1998). In comminution the transient states

represent all possible mass fractions in each size class, which we call species. The Markov property allows for process integration as process products can be interlinked. This connectivity shown in Figure 5.2 allows the handling of successive products from a single unit or many units with constant or varying process conditions. This also means that the breakage of material does not depend on the history but on the present state of particle size distribution and process conditions. This is based on that all the samples have the same material structure and also that the grinding conditions do not change. The behavior of breakage and mixing as fundamental processes as described in Chapter 4 is well supported by both our and other researchers' experimental results. The purpose of this research is to develop a methodology and that this demonstration is shown to be representative. Figure 5.2 clearly shows that at the process conditions, for an objective to maximize the mass in size class 2, the residence time is about 0.75 minutes. Further grinding would result in loss of energy efficiency and production time. The extent of grinding can now easily be interpreted from this simple geometric plot of Figure 5.2, unlike Figure 5.1 whose interpretation is not straight forward.

In this paper the algorithm describing breakage into size class 2 and size class 3 is described using the solution of the batch grinding model. Secondly, the experimental investigation and results are presented and then compared with the theoretical analysis.

5.2 THE BATCH GRINDING EQUATION

The population balance model takes into account all sub-processes of breakage kinetics, material transport and size classification. Reid (1965)

presented a linear population balance model, Equation 5.1, which can be used to describe the evolution of mass fractions within size class intervals as a function of time.

$$\frac{dm_i(t)}{dt} = -k_i m_i(t) + \sum_{j=1}^{i-1} k_j b_{ij} m_j(t)$$
(5.1)

where $m_i(t)$ is the mass fraction of particles in the ith size class, k_i are the breakage rate parameters and b_{ij} are the breakage distribution parameters and t is time. The breakage rate parameters describe the rate at which material is broken out of a particular discretized size class, whereas the breakage distribution parameters (b_{ij}) represent the fraction of the primary breakage product of material in size class interval j which appears in size class interval i.

The change of mass in size class 1 is described by Equation 5.2a. If the breakage rate parameter k_1 is a constant then it can be calculated from the experimental results using Equation 5.2b.

$$\frac{dm_1(t)}{dt} = -k_1 m_1(t)$$
(5.2a)

$$m_1(t) = m_1(0) exp(-k_1 t)$$
(5.2b)

The population balance model describes the evolution of mass from size class 2 according to Equation 5.3a. If the breakage parameters k_2 and b_{21} are constant then one can use Equation 5.3b to calculate their values from the experimental results. Size class 3 is found by mass balance for a three size class interval system.

$$\frac{dm_2(t)}{dt} = -k_2 m_2(t) + k_1 b_{21} m_1(t) \tag{5.3a}$$

$$m_2(t) = m_2(0)\exp(-k_2 t) + \frac{b_{21} k_1 m_1(0)}{k_2 - k_1}[\exp(-k_1 t) - \exp(-k_2 t)] \tag{5.3b}$$

Once the breakage rate parameter from size class 1, k_1, is determined, it can be used in Equation 5.3b which remains with two unknowns, k_2 and b_{21}. The next step is to determine b_{21} the breakage distribution parameter. Equation 5.4 describes b_{21}. Ideally it should be the ratio of the mass from size class 1 reporting only to size class 2 at all times. However this is difficult to find in practice which is why it is calculated at initial grind times (Austin et al., 1984).

$$b_{21} = \frac{mass\ in\ size\ class\ 2, t \to 0}{mass\ broken\ from\ size\ class\ 1, t \to 0} \tag{5.4}$$

Once b_{21} is determined the only unknown left is k_2 and it can be calculated using least squares fitting of the model, Equation 5.3b, to the experimental results.

We will test the hypothesis that the two breakage rates, k_1 and k_2, should be constant with time once we have carried out experiments on our system of silica sand or quartz particles. Equations 5.2b and 5.3b will be used to represent the product mass fraction distributions as points in space instead of the traditional cumulative plots. Our aim is to ultimately show that we can use the results to generate a candidate attainable region, AR^c, in the way that was described in a previous paper (Khumalo et al., 2006).

5.3 EXPERIMENTAL PROCEDURE

5.3.1 Preparation of experimental material

Large fragments of silica sand and quartzite were crushed in a cone crusher and classified by sieving using a rotational and tapping shaker (Ro-Tap shaker). The ground material was sieved for 10 minutes into the 5600-4000 µm size class range as preparation for the feed to the laboratory ball mill.

5.3.2 Mill and experimental method

The mill used in this experiment was made of steel. It had an inside diameter of 180 mm and was 255 mm long. 45 mm diameter steel balls were used. The mass of feed was set constant for all experimental runs at 365 grams. The first sets of tests were carried out on the silica sand by varying the ball filling from 0 to 30% by volume at a constant mill speed of 37 revolutions per minute. The next sets of tests were carried out on the silica sand at a constant volume ball filling of 20% while varying the mill rotational speed from 13 to 92 rpm. For comparison, quartzite was tested in the same ball mill at fixed conditions of 30% ball filling and 37 revolutions per minute mill speed.

A series of batch grinding tests were carried out in the laboratory ball mill at constant conditions of ball filling and mill rotational speed while the grinding time was increased for each sample. For example, the first batch sample was ground for 5 minutes and the next batch ground for 7 minutes at the same milling conditions. The assumption made here was that at 5 minutes the mass fraction distributions are the same in both batches though the other batch is ground for an extra 2 minutes. The ground material was classified by sieving

using a vibratory sieve shaker into 6 size classes and the mass of material in each size class determined by weighing on a laboratory scale. The ratio of aperture size of adjacent screens used was 2.

The empirical Equation 5.5 was used to calculate the mill critical speed N_c as 99.7rpm (Austin et al., 1984). The critical speed is defined as the rotational speed at which balls just start to centrifuge on the ball mill shell and not tumble, which causes the grinding media energy to be wasted causing energy inefficiencies.

$$N_c = 42.2/\sqrt{D-d} \hspace{5cm} (5.5)$$

where D is the internal mill diameter and d is the maximum diameter of the grinding media which are the steel balls in this case.

5.4 THE EFFECT OF SPECIFIC ENERGY ON BREAKAGE

The logarithm of mass fraction in size class 1 was plotted as a function of time in Figure 5.3. A straight line would be expected for Equation 5.2b to hold. It can be seen that the experimental points are not well fitted by straight lines.

We will return to this issue at a later stage. At this point we wish to ascertain whether we can correlate all the results in terms of specific energy. This is the key assumption that was made in the AR paper (Khumalo et al., 2006). If we scaled our time variable by the specific energy input we would get the total amount of energy we have put into the mill up to that point. We would like to examine whether we could correlate the data on this basis.
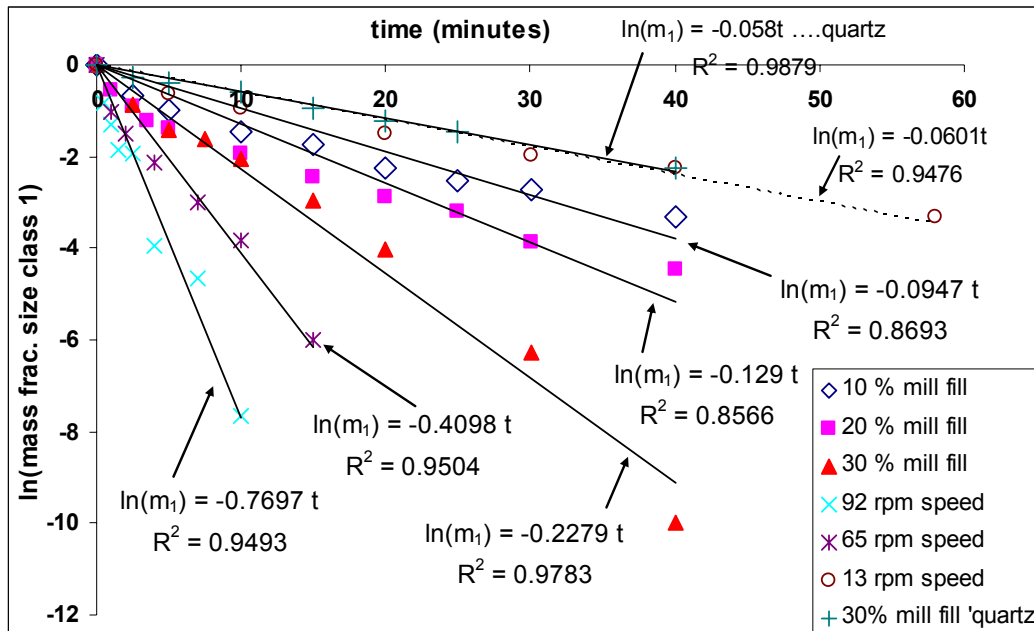
Figure 5.3: Semi-log plot of the mass fraction in size class 1 vs. time.

The laboratory ball mill did not have a power measuring device so the experimental specific power was calculated using Equation 5.6, Beeck's (1970) empirical correlation for dry grinding of cement.

$$\frac{P}{m_{total}} = 42.3(0.374 - 0.47J)D^{0.5}\Phi_c \qquad (5.6)$$

where m_{total} is the mass of the grinding media in metric tonnes, P is the power in kW, J is the fractional ball volume filling, D is the mill inside diameter and Φ_c is the fraction of the actual mill rotational speed to the critical speed N_c (determined using Equation 5.5).

The total energy going into the material in size class 1 ($E_{total,m1}$) up to that point in time is calculated using Equation 5.7. Equation 5.7 apportions power into a size class in direct proportion to the mass in that size class.

$$E_{total,m1} = \frac{Ptm_1(t)}{m_{total}}$$
(5.7)
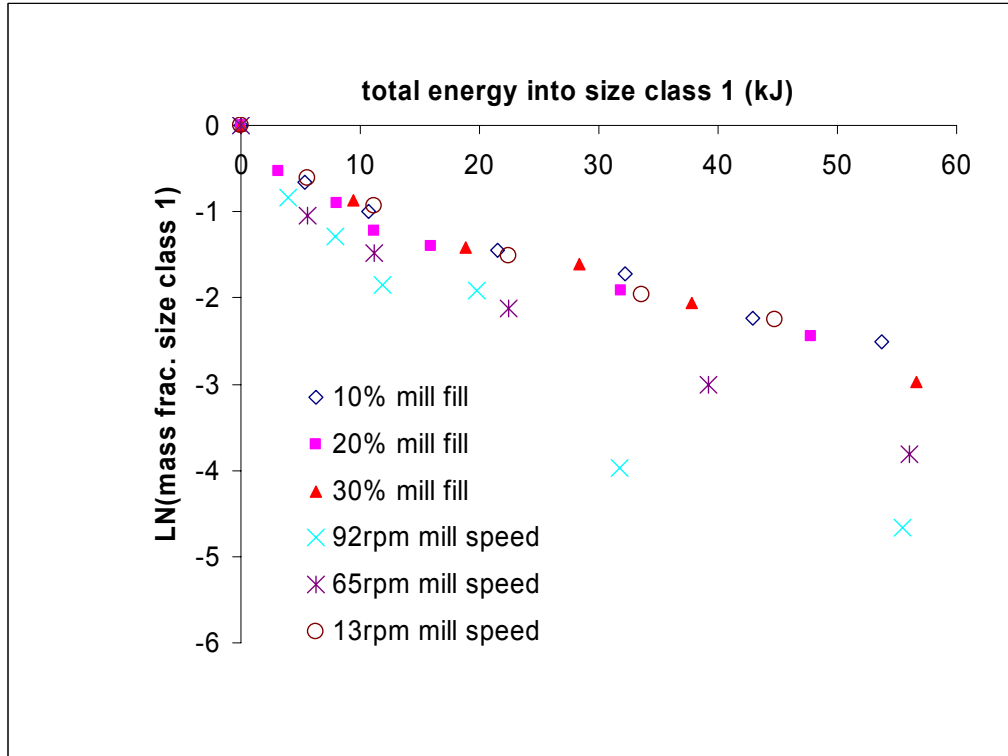
Figure 5.4: Semi-log plot of the mass fraction in size class 1 vs. total energy input into size class 1 calculated using Equations 5.6 and 5.7.

Figure 5.4 shows the plot of the total energy into size class 1 up to that time ($m_1(t)$) based on the literature correlation of Equation 5.6, against the logarithm of the mass fraction in the discreet size class 1, the feed size. Since the same specific energy might give identical products, the products from the six experiments could lie on top of each other for the same total energy input. Figure 5.4 clearly shows that products from four but not all of the experimental conditions lie nearly on top of each other.

123

We then investigated why the results from the 65 rpm and 92 rpm mill rotational speeds deviate from the rest of the experiments. A quadratic function was fitted to the four results in Figure 5.4 which essentially lie on top of each other. A least squares fitting method was employed to determine the power that would cause the products of the 65 rpm and 92 rpm mill rotational speed experiments to be identical with the rest.
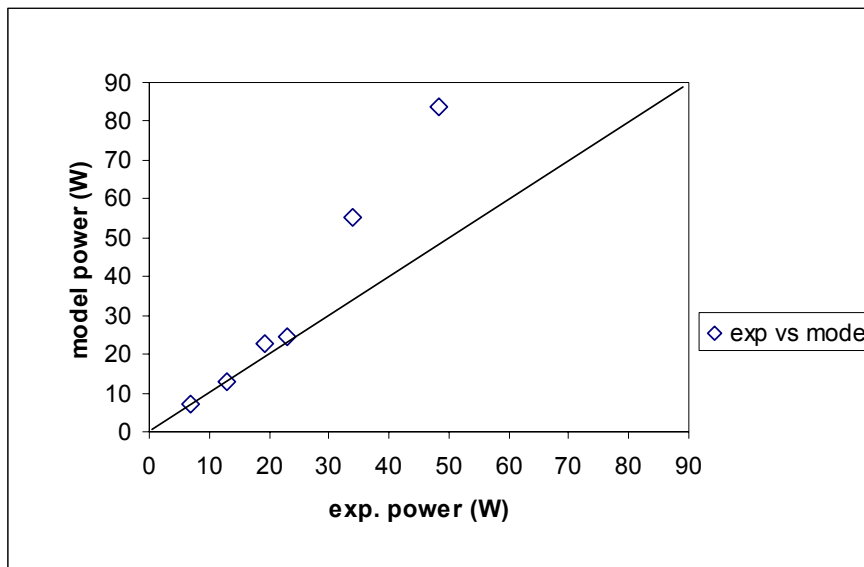
Figure 5.5: The comparison of the experimental specific power (Equation 5.6) to the new model specific power.

Figure 5.5 shows a parity plot of the experimental power which is calculated from Equation 5.6 and the estimated power that is necessary to cause identical products for the same total energy, that is to cause the graphs in Figure 5.4 to lie on top of each other. The literature specific power from the empirical correlation of Equation 5.6 at first follows the 45° diagonal line and appears to be accurate for the lower kinematic conditions. Higher kinematic conditions result in a deviation from linearity of the specific power. This

124

suggests that Equation 5.6 the literature based model we have used may not be accurate for higher specific energy inputs.
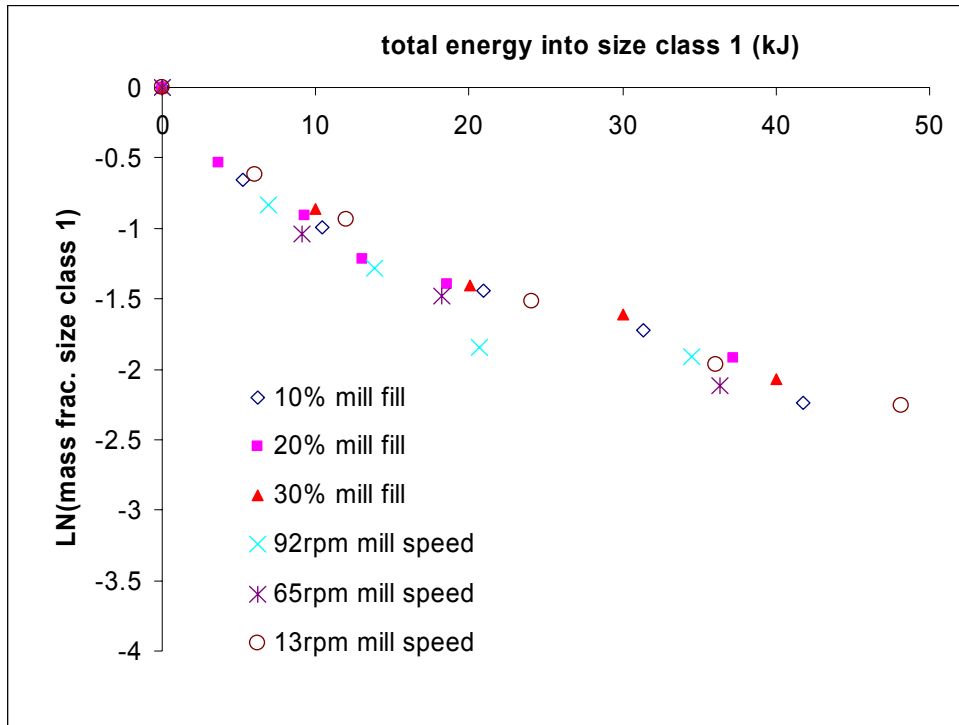
Figure 5.6: Semi-log plot of size class 1 vs. corrected total energy input.

Figure 5.6 clearly shows that the adjusted value of power effectively causes all experimental points, within experimental error, to lie on top of each other for the same total energy. This is the first step in experimentally justifying our use of specific energy only in the construction of the candidate attainable region. The product points however do not lie on a straight line as would be expected from equation 2b if k_1 was a constant.

The use of the same total energy input up to that time, instead of time removes the dependence of the design on kinematic and loading conditions. This makes the construction of the candidate attainable region using specific

energy input to the mill feasible. Equipment selection becomes an event after the construction of the candidate attainable region in order to match the specific energy that achieves the required objective function. This simplifies the design considerably since the required specific energy can, for instance, be achieved by the appropriate combination of mill speed and loading.

5.5 DETERMINATION OF BREAKAGE KINETICS

5.5.1 Mass fraction in size class 1 for a constant k_1

Equation 5.2a which is derived from the population balance model (Reid, 1965) shows that for a linear breakage model the breakage rate parameter k_1 is the only unknown parameter for describing the change in mass for the top size class 1. Ideally according to Equation 5.2b the experimental points in Figure 5.3 should fit a straight line for first order breakage systems, the gradient of the straight line being the breakage rate parameter k_1. However we can clearly see that all the experimental points for silica sand and quartzite do not fit a straight line. An alternative way of calculating the breakage rate k_1 was then sought and is presented in the next section.

5.5.2 An alternative way of handling a varying k_1

Figure 5.3 clearly shows that k_1 is not a constant for both silica sand and quartzite. We then calculated k_1 for each experimental point using Equation 5.2b.

126
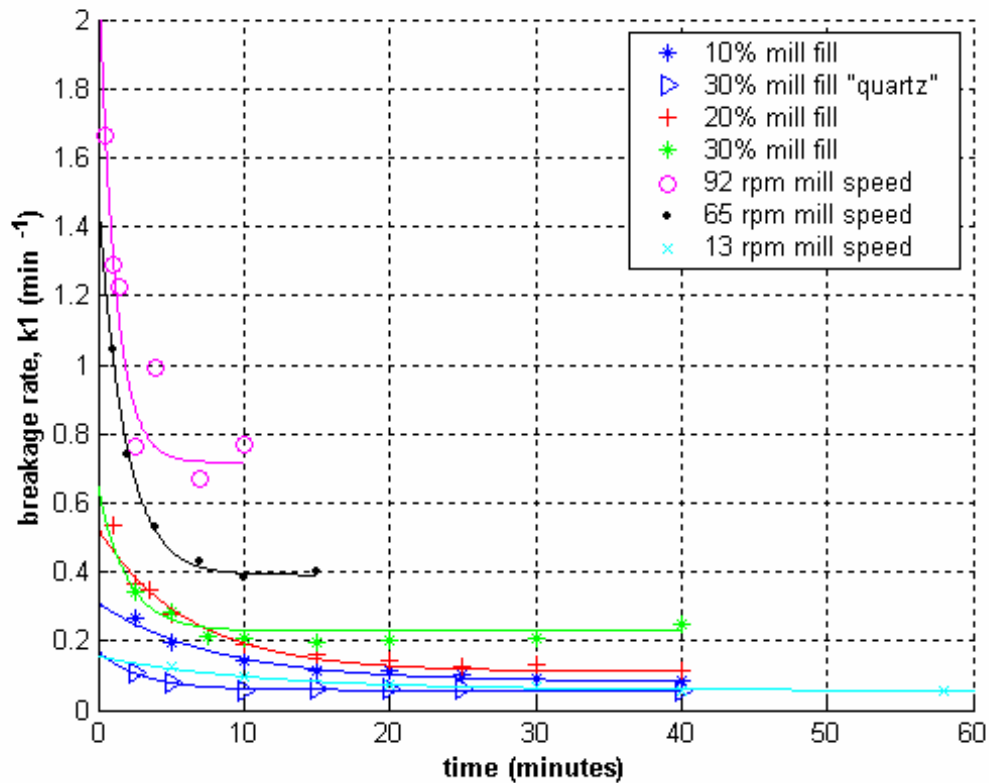
Figure 5.7: Calculated values of k_1 vs. time.

Figure 5.7 clearly shows that k_1 is not constant with time, but decreases rapidly at initial grinding times reaching an asymptote at long grind times. The breakage rate parameter k_1 is clearly a function of time, and it decreases towards an asymptote. We fitted the results according to an exponential law as in Equation 5.8 where *a* and *b* are fitting parameters as shown in Table 1.

$$k_1(t) = k_1(t \rightarrow \infty) + a \exp(-bt)$$ (5.8)

The solid lines in Figure 5.7 represent the best fits using Equation 5.8 and clearly are a good fit to the data.

Table 5.1: Fitting parameters for determination of the breakage rate k_1 using Equation 5.8 and the values of k_2.

Mill speed (rpm)	ball filling (%)	a	b	k_1^∞	k_2
37	10	0.2286	0.1228	0.0825	0.0772
37	20	0.4141	0.1605	0.1114	0.1758
37	30	0.4192	0.5016	0.2295	0.1892
37	30 - quartzite	0.1142	0.3311	0.0580	0.0769
Ball filling (%)	mill speed (rpm)	a	b	k_1^∞	k_2
20	92	1.4777	0.8813	0.7170	0.8778
20	65	1.1045	0.5462	0.3912	0.5523
20	37	0.4141	0.1605	0.1114	0.1758
20	13	0.0987	0.0893	0.0571	0.0316

The breakage rate k_1 decreases rapidly at initial grind times and then flattens out approaching an asymptote, for relatively long grind times. This could be as a result of feed particles breaking more rapidly initially in the absence of progeny particles. Once there is a build up of breakage fragments, these could have a cushioning effect resulting in constant breakage rates of the feed particles, at relatively long grind times. This asymptote $k_1(t \rightarrow \infty)$ could be assumed to be the value of the breakage rate parameter k_1 in continuous grinding environments where there will always be other breakage fragments present. If our assumption is valid we could for the sake of simplicity represent k_1 by k_1^∞. This value k_1^∞ is independent of time and could then be

used in the construction of the candidate attainable region for continuous steady state grinding systems.

We note the breakage rate parameter, k_1^{∞}, increases to a small extent from 0.1 to 0.2 min^{-1} when the volume ball filling increases from 10 to 30%. However the mill rotational speed clearly has a larger effect. For example, k_1^{∞} increases from 0.1 to 0.7 min^{-1} when the mill rotational speed increases from 13 to 92 rpm (at 20% constant ball filling).

Equation 5.2a shows that once the value of the breakage rate function k_1 is known, then the mass fraction in size class 1 can be determined for any grind time. Figure 5.8 clearly shows that Equation 5.2a is sufficient to model the mass fraction in size class 1 with time.
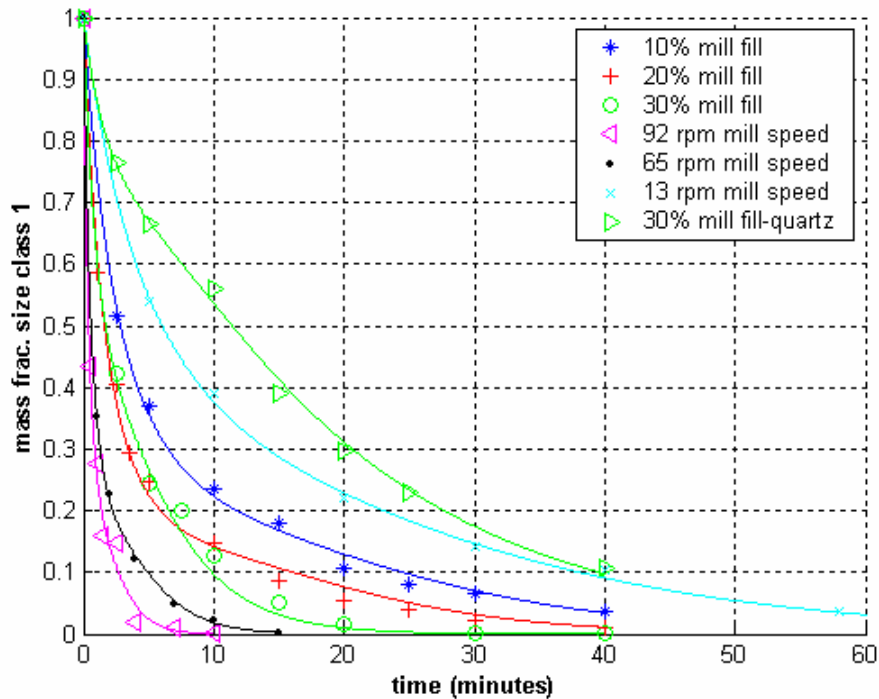
Figure 5.8: Prediction and experimental mass fraction in size class 1 with time for different operating conditions.

Figure 5.9 is a parity plot of the experimental mass fraction in size class 1 versus the model prediction. All the points lie close to the 45° diagonal line and this indicates the good agreement between the experimental data and the model prediction for the mass in size class 1.
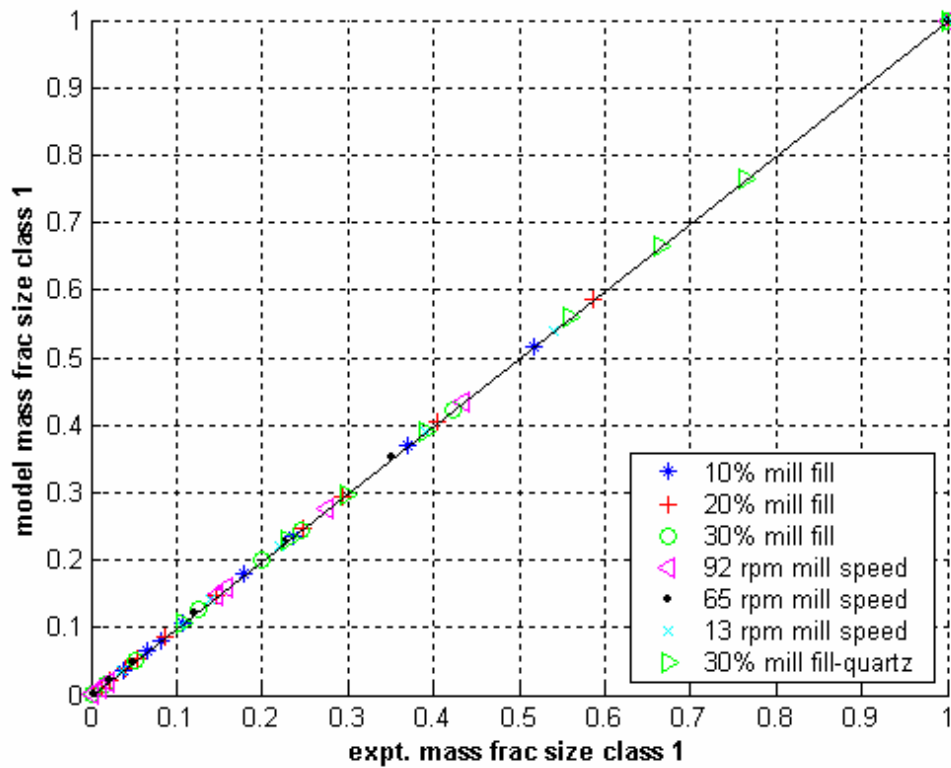
Figure 5.9: Parity plot of the experimental vs. model mass fraction in size class 1.

5.5.3 Prediction of the mass fraction in size class 2 using Equation 5.3a

Equation 5.3a shows that two unknown parameters need to be determined for the mass fraction in size class 2 to be calculated. The first is the breakage distribution parameter b_{21} which is the amount reporting to size class 2 as a

result of breakage of mass in size class 1. This is calculated at short grind times as in Equation 5.4 for reasons that will be explained. The second is the breakage rate parameter of size class 2, k_2. The value of k_1 is known from the calculation of mass in size class 1.

Equation 5.4 was used to calculate the ratio of the experimental mass fraction in size class 2 with mass fraction in size class 1 at every point in time, and this result is denoted as $b_{21}(t)$ taking note that this is not the final b_{21} but a means to calculate it.
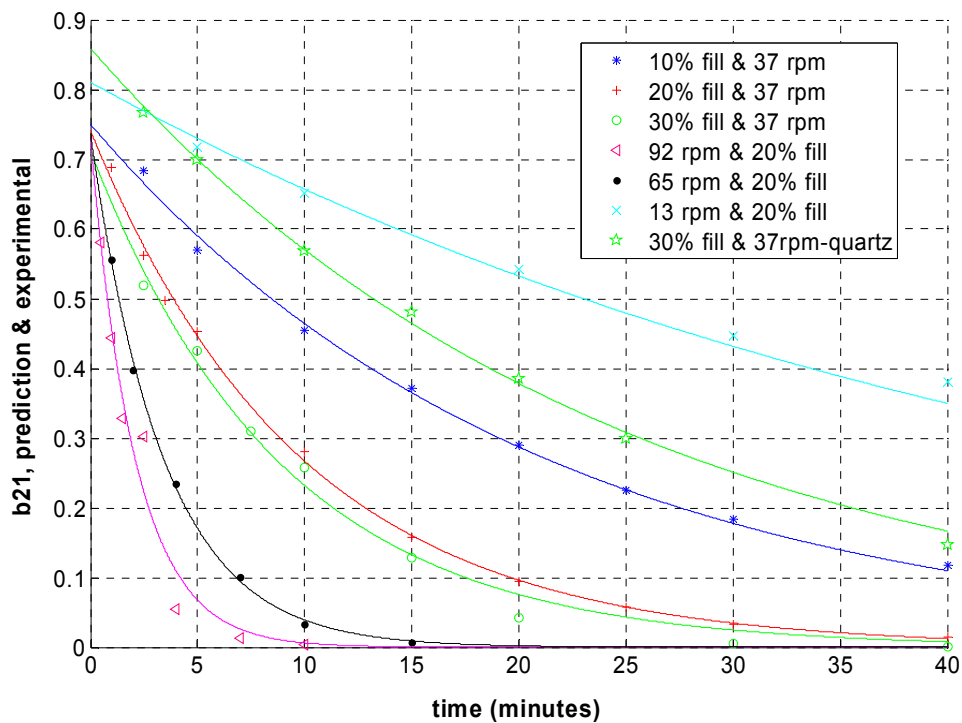
Figure 5.10: Prediction and experimental evolution of b_{21} which is the mass fraction reporting to size class 2 from breakage of size class 1 with time.

Figure 5.10 shows the ratio of the mass fraction in size class 2 to mass fraction in size class 1 as a function of time. Again we considered fitting the results with an exponential function as in Equation 5.9. Table 5.2 provides the

fitting parameter values, p and q, together with the goodness of fit. The breakage distribution parameter b_{21} was determined by extrapolating the fitted exponential function to zero grind time. The values of p were used as b_{21} values. Clearly the fit between the model and the experimental results are good confirming our assumption of the form in Equation 5.9.

$$b_{21} = p \times exp(-qt)$$ (5.9)

Table 5.2: p and q fitting parameters to Equation 5.9.

Mill speed (rpm)	ball filling (%)	p	q	Sum of squared error
37	10	0.751	0.048	0.0010
37	20	0.742	0.102	0.0012
37	30	0.713	0.112	0.0029
37	30 - quartzite	0.860	0.041	0.0008
Ball filling (%)	mill speed (rpm)			
20	92	0.730	0.475	0.0105
20	65	0.737	0.293	0.0003
20	37	0.742	0.102	0.0012
20	13	0.811	0.021	0.0032

Once the values of b_{21} are determined, the next step was to fit the experimental data for k_2. A least squares fitting method was implemented using Matlab®, first for k_2 changing with time and then secondly for k_2 constant. The breakage rate parameter of the particles in size class two, k_2, was found to be approximately constant with grind time as in Table 5.1. This

can be explained by the analysis that particles in size class two starts to break in the presence of other size class/es which offer a cushioning effect resulting in linear breakage kinetics.

The breakage rate k_2 increases slightly with volume percent ball filling up to 0.1892 min^{-1} and it increases significantly to 0.8778 min^{-1} with mill rotational speed. This shows that the mill rotational speed is still a major variable.
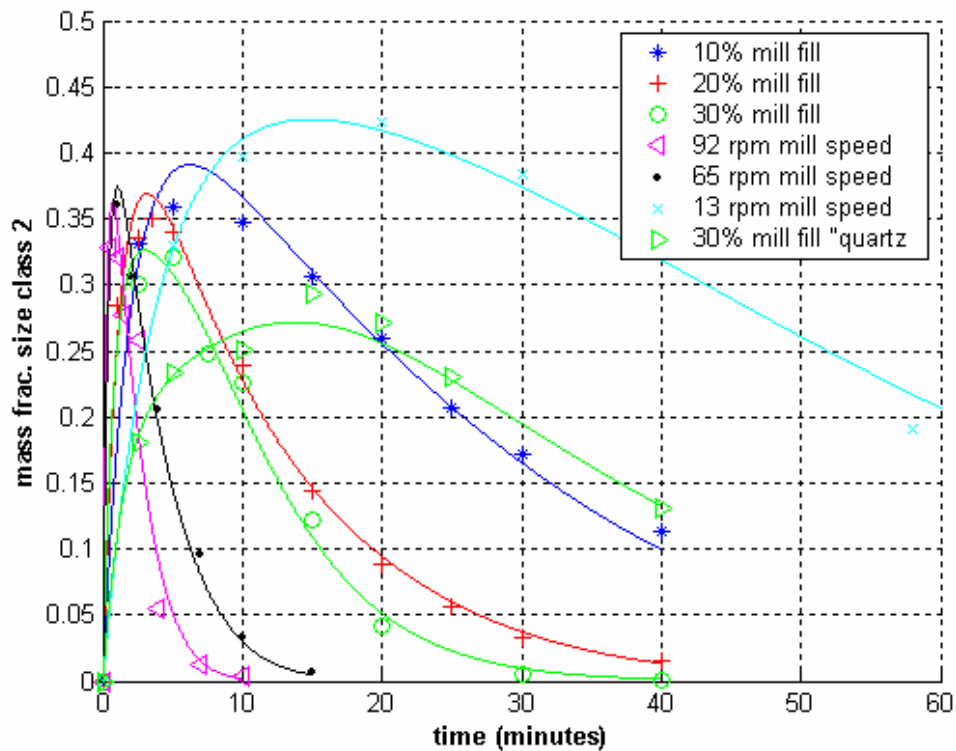
Figure 5.11: Prediction and experimental mass fraction in size class 2 with time for different milling conditions.

Once k_1, k_2 and b_{21} values are known then the mass fraction in size class 2 can be calculated using Equation 5.2b. Figure 5.11 shows the plot of size class 2 against time for different operating conditions. It can be seen that the

133

fit between the experimental data and the model is quite good. This can be best illustrated by the parity plot shown in Figure 5.12.
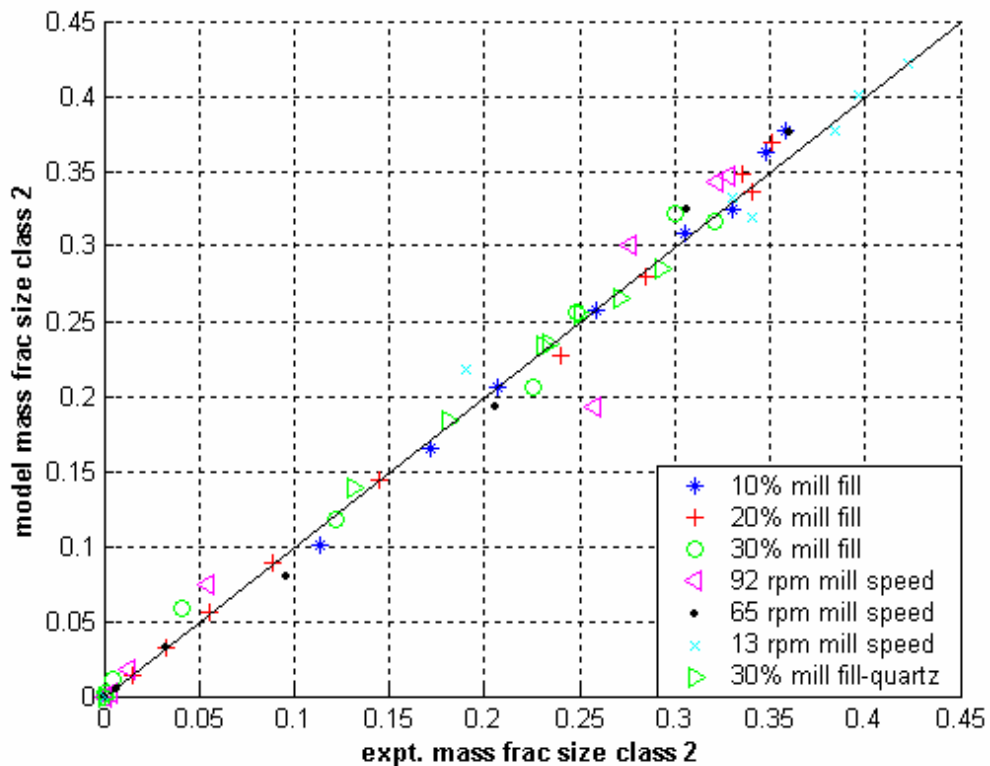
Figure 5.12: Parity plot of the experimental vs. model mass fraction in size class 2.

Once the values of k_1, b_{21} and k_2 were determined, the candidate attainable region was in principle ready to be constructed. For three size classes the characteristic equation is a vector of mass fractions in size class 1 and size class 2. The mass fraction in size class 3 is found by mass balance. In Figure 5.13 we have plotted the mass fraction in size class 2 vs. that in size class 1 for all the runs.

Firstly it can be seen that the curve for 13rpm encloses all the others and secondly that this region is bounded by convex process trajectories. A convex region means that the process of mixing cannot extend the region further. Therefore breakage is the only fundamental process necessary to achieve this region and it is a candidate attainable region. Increasing the volume ball filling or mill rotational speed only serves as control policies for process optimization.
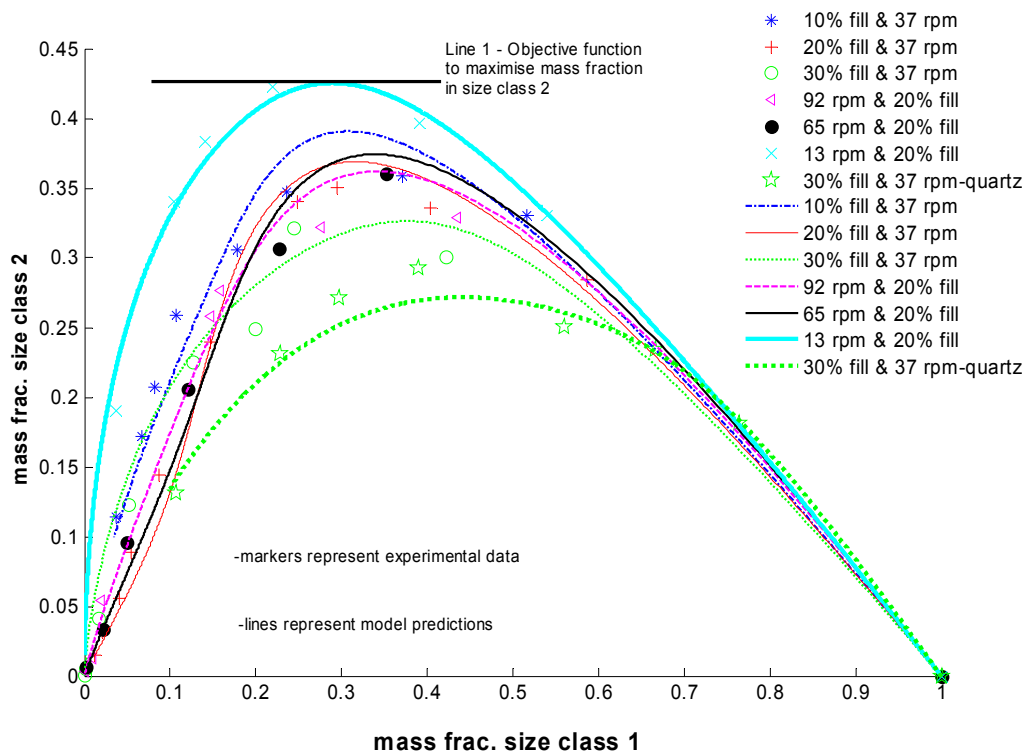
Figure 5.13: Mass fraction in size class 1 vs. mass fraction in size class 2.

Figure 5.13 thus shows the experimental candidate attainable region for the breakage system under the process constraints of ball filling and mill rotational speed. The region is given by the solid thick line 1 constructed from the breakage products of the mill with a rotational speed of 13 rpm that

encloses all the other regions. From this we can for instance get the maximum possible mass fraction in size class 2, namely 0.43.

5.5.4 The variation of specific power with breakage kinetics

Figure 5.14 depicts the behavior of the fitting parameters k_1^{∞}, k_2 and b_{21} in Equations 5.2b and 5.3b. The breakage rate parameters of the material in the first and second size classes depend significantly on the specific power and can be described by a quadratic relationship.

The values of k_1 and k_2 however are nearly the same and are probably not significantly different. We can also see that the breakage distribution parameter does not vary much with specific power. The important result is that all of these parameters depend only on the specific power instead of the detailed kinematic and loading conditions. This was one of the major assumptions that we made in doing our attainable region analysis in Khumalo et al. (2006) and this has now been verified.
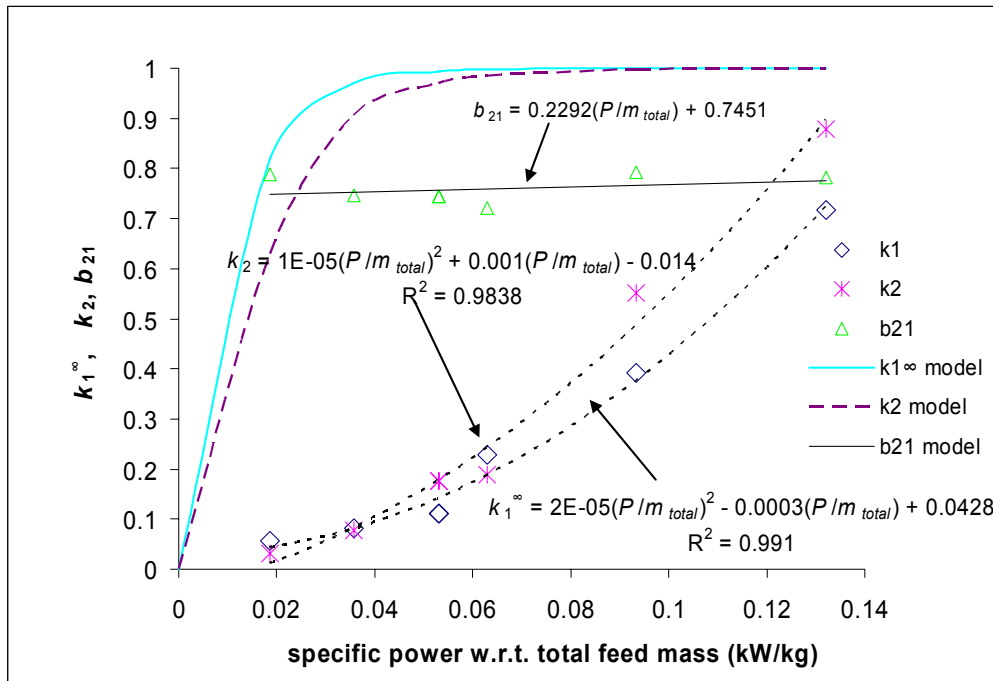
Figure 5.14: The plot of fitting parameters k_1, k_2 and b_{21} against specific power.

5.6 BATCH GRINDING EQUATION – SPECIFIC ENERGY DEPENDENCE

Herbst and Fuerstenau (1980) have argued that mills of different sizes achieve identical products for the same specific energy when fed with the same material. This has been confirmed from the analysis of our experimental results. One can therefore in principle write a population balance equation (Equation 5.10) that has specific energy dependence.

$$\frac{dm_i(\overline{E})}{dE} = -k^{\overline{E}}{}_i m_i(\overline{E}) + \sum_{j=1}^{i-1} k^{\overline{E}}{}_j b_{ij} m_j(\overline{E})$$

(5.10)

137

5.6.1 Comparison of the literature models to the ones developed here

The theoretical AR^c in Khumalo et al. (2006) was constructed using some correlations from the literature for the probability of breakage and the breakage distribution parameters. These were calculated from Equations 5.11 and 5.12, respectively. We emphasized in that paper that these equations were not absolute but they served a purpose to show that the AR ideas could be used in comminution for process synthesis.

Equation 5.11 shows that according to Tavares and King (1998) the probability of breakage, also referred to as the breakage rate parameter, is described by a log-normal distribution as a function of specific energy.

Table 5.3: Parameters used for the construction of the AR^C in Khumalo et al. (2006)

	Size class 1			Size class 2		
	$E_{m,50}$ (exp.) (kJ/kg)	$E_{m,50}$ (lit.) (kJ/kg)	σ_E	$E_{m,50}$ (exp.) (kJ/kg)	$E_{m,50}$ (lit.) (kJ/kg)	σ_E
t→0	0.07	0.010	0.4412			
t→∞	0.92	0.010	0.6083	0.92	0.015	0.6051
	T_{10} (exp.)	T_{10} (lit.)				
t→0	0.6589	0.4118				

Table 5.3 shows the fitting parameters for Equation 5.11 when the k_1^∞ and k_2 values in Table 5.1, are used. Substituting the values in Table 5.3 into Equation 5.11 and plotting against specific power results in the solid and dashed bold lines in Figure 5.14 for the breakage rates k_1^∞ and k_2 respectively. The fit is not good, and it is not the intention of our work to fit these accurately. The discrepancy may be due to the fact that these literature models are based on single particle breakage not batch grinding as in our experiments.

$$k_i^{\overline{E}} = 0.5\left[1 + erf\left(\frac{\ln(\overline{E}) - \ln(\overline{E}_{m50,i})}{\sqrt{2}\sigma_{\overline{E}}}\right)\right] \tag{5.11}$$

Equation 5.12 is another literature relationship for the breakage distribution parameter (King, 2001). We determine the value of T_{10} by fitting Equation 5.12 to the values of b_{21} determined from Equation 5.4, and compared them with those from literature. The values are probably comparable because Equation 5.12 was determined through similar experiments to ours.

$$b_{ij} = 1 - (1 - T_{10,i})^{\left(\frac{9}{i-1}\right)^{\alpha}} \tag{5.12}$$

where $T_{10,i}$ is defined as the fraction of the progeny smaller than $1/10^{th}$ of that size class, i, and α is a fitting value.

5.7 SUMMARY

We have shown that our experimental results for the laboratory ball mill run at different ball loadings and different mill speeds can be correlated in terms of the specific energy within the mill. This was the fundamental result that was needed to validate our attainable region approach in the paper by Khumalo et al. (2006).

We have further shown that a breakage system of silica sand and quartz particles in a smooth laboratory ball mill can have breakage rate parameters which change with time. However based on our results we have postulated that continuous systems have constant breakage rates at steady state because of the cushioning effect of daughter particles. We have also shown that the population balance model gives a good fit with the experimental results.

As the breakage rates now depend only on the specific energy input instead of the kinematic and loading conditions, the candidate attainable region can now be constructed from the knowledge of the specific energy. Equipment selection can then be made to match the specific energy required to achieve a specified objective function. At this point in time the results apply to ball mill-type equipment. However since particle breakage should be only as a result of energy input in all equipment, there is a need to demonstrate that the comminution rate in a wider set of equipment is determined only by the specific energy output of the device. This would simplify substantially the modeling and optimization of comminution circuits.

The representation of a whole particle size distribution as a point in space of mass fractions in different size class gives more information than the traditional representation. This is because we can now follow trajectories in our space. The points can be connected and they can be products from different process units. The candidate attainable region method can thus be used to solve both the process synthesis and optimization problems. The process synthesis problem is solved by interpreting as equipment, the path of that process vector which achieves the optimum objective function. The optimum path also provides the operating conditions as a function of the state of the system and one can use the mill rotational speed and the volume percent ball filling to follow this path, which solves the optimization problem.

We can see from the experimental results that the experimental attainable region is convex and is successfully modeled using the first order population balance model. Convex means that the region cannot be extended further by any mixing process. Therefore the breakage process on its own is sufficient to achieve the objective of maximizing the mass fraction in size class 2 for the fundamental processes of breakage and mixing.

5.8 REFERENCES

Austin, L.G.; Klimpel, R.R.; Luckie, P.T. (1984). Process engineering of size reduction: ball milling. pp. 181-247.

Beeck, R. (1970). Zement-Kalk-Gips. Vol. 23, pp. 413-416.

Glasser, D.; Hildebrandt, D. (1987). A geometric approach to steady flow reactors: the attainable region and optimization in concentration space. American Chemical Society, 26, 1803-1810.

Herbst, J. A.; Fuerstenau, D. W. (1973). Trans. SME/AIME, 254, 343-347.

Herbst, J. A.; Fuerstenau, D. W. (1980). Scale-up procedure for continuous grinding mill design using population balance models. International Journal of Mineral Processing, 7, 1-31.

Horn, F. (1964). Attainable and non-attainable regions in chemical reaction technique. 3rd European Symposium on "Chemical Reaction Engineering". Pergamon Press Ltd. Great Britain.

Khumalo, N.; Glasser, D.; Hildebrandt, D.; Hausberger, B.; Kauchali, S. (2006). The application of the attainable region analysis to comminution. Chemical Engineering Science, 61, 5969-5980.

King, R. P. (2001). Modeling & Simulation of Mineral Processing Systems. Butterworth-Heinemann: Great Britain. 144-151.

Mitrani, I. (1998). Probabilistic modeling; University Press: Cambridge, pp. 156-168.

Reid, K. J. (1965). A solution to the batch grinding equation. Chemical Engineering Science, 20, 953-963.

Schonert, K. (1988). Fundamentals of particle breakage. Course Notes, Section F6, Division of Continuing Engineering Education, University of the Witwatersrand, Johannesburg.

Tavares, L. M.; King, R. P. (1998). Single-particle fracture under impact loading. Int. J. Miner. Process. 54, 1-28.

Verma, T.; Rajamani, R. K. (1995). Environment-dependent breakage rates in ball mill. Powder Technology, 84, 127-137.

5.9 LIST OF SYMBOLS

AR	attainable region
AR^c	candidate attainable region
exp.	experimental
E	specific energy (kJ/tonne)
frac.	fraction
i	size class interval
$k^{\overline{E}}{}_1$	specific energy dependent rate of breakage out of size class 1
k_1	time dependent rate of breakage out of size class 1
k_2	time dependent rate of breakage out of size class 2
rpm	rotations per minute
%	volume percent ball filling

CHAPTER 6

Improving comminution efficiency using classification: An attainable region approach[§]

Khumalo N.*, Glasser D., Hildebrandt D., Hausberger B.

School of Chemical and Metallurgical Engineering
University of the Witwatersrand
Private Bag 3
Wits, 2050
Johannesburg, South Africa
February 2, 2007
Tel: +27(011)7177584
Fax: +27(011)7177557
Email: zwekhums@hotmail.com

ABSTRACT

The AR for the fundamental processes of breakage and mixing was constructed in an earlier paper (Khumalo et al, 2006). This work presents the AR constructed when the process of classification is combined with the processes of breakage and mixing. The process of classification extends the AR. An additional variable of energy consumption is introduced, increasing the dimensionality of the geometric construction from 2-D to 3-D. The AR shows that there is a linear relationship between consecutive particle size distributions with grinding time. However total energy consumption results in concavities when plotted against mass fraction in the median size class.

This work demonstrates the degree to which there is an advantage of including the additional fundamental process of classification to particle breakage. The attainable region (AR) of a three particle size distribution can

---

[§] This chapter has been submitted for publication in Chemical Engineering Science Journal

easily be represented graphically. Process targets can be inferred from these graphs. The classification process has the effect of reducing total energy consumption to reach an objective particle size. This has cost implications since energy is often the predominant operating cost in size reduction systems. This work also shows that the benefits of classification are a function of the grinding extent for a system which consists of mono-sized feed particles. This suggests that classification should be introduced after some grinding at some point which is easily identified by analysing the AR construction.

Keywords: comminution, classification, attainable region (*AR*), population balance model, specific energy

6.1 INTRODUCTION

Comminution is both an energy intensive process and a large user of energy, which means that any marginal improvement in the efficiency of the milling circuit will be of immense economic benefit to the cement, ceramics, pharmaceutical, paper and minerals industries (Datta and Rajamani, 2002). Because the energy input to most comminution systems is far greater than that predicted from single particle breakage models, there is likely to be room for significant improvement.

Reid (1965) developed the discrete-sized population balance model for batch or plug flow grinding. Previous work has shown that the breakage distribution function does not depend on the grinding environment and can be normalised with size (Broadbent and Callcott, 1956; Herbst and Fuerstanau, 1980; Herbst et al., 1981). In our previous work in a laboratory ball mill (Khumalo et al., pending publication) the breakage function has been shown to depend on the specific energy input. The breakage function is analogous to the breakage probability developed for single and particle populations (Baumgardt et al., 1975; Dan et al., 1990; King et al., 1993a).

In this paper classification is the other fundamental process we will consider in addition to breakage and mixing. We have shown in an earlier paper (Khumalo et al., 2006) that mixing does not extend the AR because of the first order breakage kinetics with respect to the mass of particles in that discrete size class. Therefore the only fundamental processes discussed from here onwards are breakage and classification. Classification is achieved by either the forces of fluid dynamics or physical particle size screening. Ideally selectivity should be unity for perfect classifiers with all the material below a certain size being classified to the fines stream and the material above being

classified to the coarse stream. However this is not possible in practise. Industrial classifiers have a fractional selectivity number for a discrete size class i. Tromp curves are used to plot the selectivity numbers vs. size.

The attainable region (AR) analysis first proposed by Horn (1964) is a tool that describes the set of all possible outcomes that can be achieved by a set of fundamental processes operating on a given system and complying with the constraints on that system. Once all the possible outcomes have been determined for a system, it is possible to obtain an optimal design of the process in terms of the objective function e.g. energy consumption or particle size distribution. An example of this for reactor design lies in the development of the differential side stream reactor (DSSR) which is an idealized differential reactor structure that can be approximated by well accepted industrial units such as the cold shot cooled reactor (Glasser et al., 1994).

The approach used here constructs the candidate attainable region for the fundamental processes of breakage and classification for comminution, from which optimal control policies can be interpreted. The desired objective functions examined in this work are to maximise the amount of mass in some middle size class 2 and reduce the energy consumption to obtain some desired distribution.

6.1.1 Mass fraction distribution space

In Khumalo et al. (2006) we introduced the concept of representing particle size distributions as points in space. The mass fraction distribution vector *m* for three geometric size classes for any stream in the comminution system is shown in Equation 6.1.

$$\boldsymbol{m} = [m_1, m_2, m_3] \tag{6.1}$$

However because of an overall mass balance only two of the m_i are independent and so one can work in two dimensional space.

More size classes can be involved but three size classes are chosen for illustrative purposes. The mass in each size class as a fraction of the total mass in that stream is represented as m_i with i being the number of that size class. In this work the feed is assumed mono-sized and is classified as size class 1 and the next lower geometric size as class 2 with size class 3 being the smallest. Each stream particle size distribution vector is plotted in the x and y axis in 2-dimensions as single points as in Figure 6.1, which is a graph extracted from our previous experimental work (Khumalo et al., pending publication).
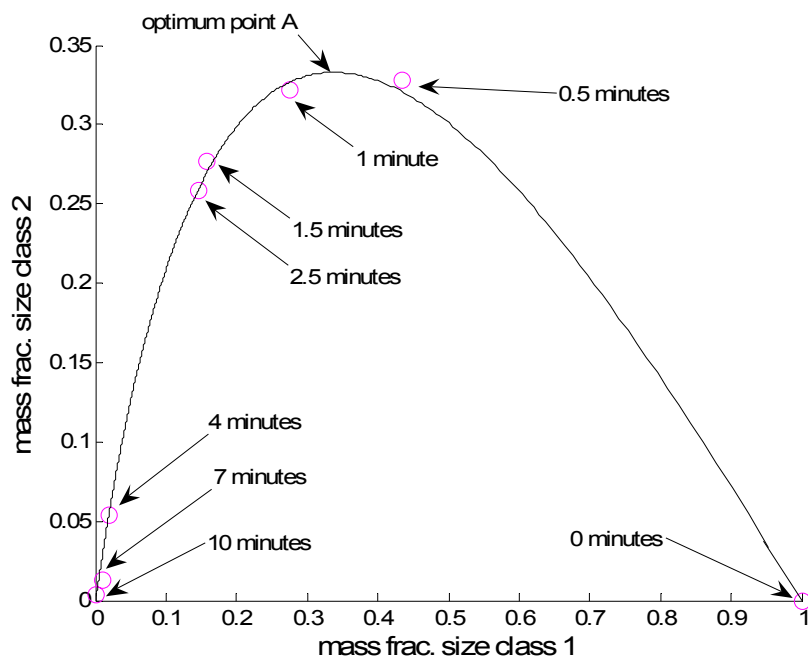
Figure 6.1: 2-dimensional mass fraction distributions represented as single points which constitute the path

The vector points can be connected together because subsequent product distributions depend on the past distributions through the present distribution, since comminution processes are Markov processes (Mitrani, 1998). This offers an opportunity to connect all the mass fraction distribution vectors into a path in geometric space as in Figure 6.1. The curve represents the output from the model that was developed.

6.1.2 The classification process

Classification is the splitting of product streams from a breakage process into two or more streams (Austin et al., 1984). The classification of particles is based on the physical property of the particle size relative to that of the relevant product, be it tailings or middlings or coarse material. These recovered streams can be recycled or retained as product according to the desired objective. It has been noted that repeated grinding stages result in excessive fines production due to over-grinding. There is likely to be an optimum point at which the separation process should be introduced to avoid over-grinding therefore optimizing energy consumption. The classification process also gives the opportunity for mixing streams of similar distributions so as to get the most efficient use of energy since different particle sizes have different mean specific fracture energies according to Equation 6.4. Introducing inter-stage separation can be used to maximise:

iii) The amount of material that meets the design specification.
iv) The energy efficiency by reducing the extent of over-grinding material beyond the design specification.

Various types of classifiers are used and they generally fall into two categories. There are those that separate by fluid dynamics and those that involve screening. Separation is currently used industrially in closed circuit processes and the purpose of our research is to quantify theoretically the reduced energy consumption and the maximised objective. This will provide a target against which to measure the efficiency of actual processes currently employing classification.

6.2 NECESSARY STEPS TO BUILD THE AR

The attainable region (AR) analysis can be used as a process synthesis tool. The AR describes the set of all possible outcomes that can be achieved by a set of fundamental processes operating on a given system and complying with the constraints of that system (Glasser and Hildebrandt, 1987). The procedure employed for building the AR in comminution for the fundamental processes of breakage and mixing is described in Khumalo et al. (2006). The only things that have changed are mentioned below.

6.2.1 The comminution system

The new comminution system consists of classification as an additional fundamental process. Figure 6.2 illustrates a comminution circuit sufficient for our purposes. The model handles three geometric size classes and classification results in size class 1 being recycled as feed and the product may go downstream for further classification to size classes 2 and 3.
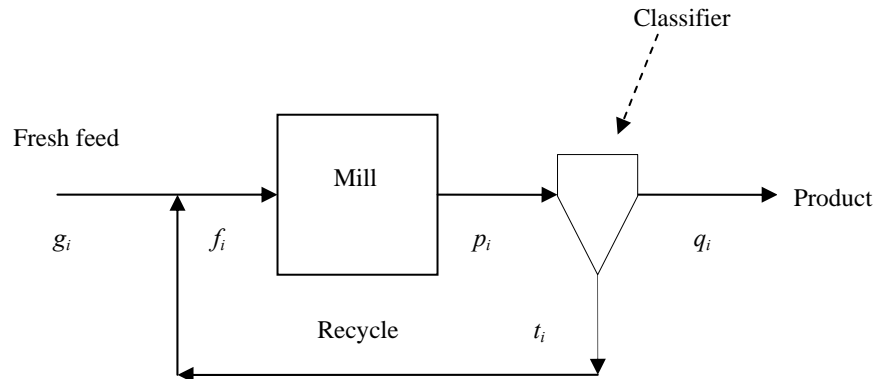
Figure 6.2: The illustration of closed circuit grinding incorporating grinding and classification processes.

The symbols in Figure 6.2 refer to the vector stream mass flow rate distribution in each size class, and their sum is the total stream flow rate. Because we regard the classification as perfect the recycle has the same composition (size class 1) as the feed simplifying the analysis. The mill feed f_i is related to the makeup feed g_i according to a mass balance of the grinding circuit in Figure 6.2 by;

$$f_i(1+C) = s_i p_i(1+C) + g_i \qquad (6.2)$$

C is the circulation ratio defined by the relative mass flow rates of the coarse or recycle stream Σt_i to the product stream Σq_i, $C = \Sigma t_i / \Sigma q_i$. The circulating load is often defined as $\Sigma f_i / \Sigma q_i = 1 + C$ (Austin et al., 1984).

6.2.2 Identification of the process variables

There is an additional variable of total energy (E_T) consumption to be taken into account when using some objective functions. This is the total energy irrespective of the mass broken. For a fixed time period at steady state it is possible to determine the total energy consumption for a continuous process.

6.2.3 The characteristic vector

The characteristic vector c now consists of the additional variable of total energy consumption making the AR construction a 3-D problem. For example Equation 6.3 is the characteristic vector when the objective function takes into account the energy required to reach a certain objective.

$$c = [E_T, m_1, m_2] \tag{6.3}$$

6.2.4 The classification vector

The classification vector is defined as z. It is the fraction of the size class i in the feed to the classifier that reports to the coarse stream which could be the recycle stream as well. Assuming ideal classification, z is a constant row vector of zeros except for the size class to be separated out which is one, i.e. for three size classes and for an objective to separate out size class 1, z=[1 0 0]. In this model we have assumed that the energy required for classification is negligible compared to that for grinding. One could do the analysis for non-perfect classification but this would complicate the analysis without really changing the qualitative behaviour.

6.3 THE AR APPROACH TO COMMINUTION CIRCUITS

From this section forward we apply the ideas of the attainable region to optimise the grinding circuit of Figure 6.2 in terms of maximising the mass in size class 2 and reducing the total energy consumption in order to reach a specific objective. The advantage of the AR approach for process synthesis is

153

that it investigates the optimal circuit operation instead of just single unit operations. It has been argued in reaction engineering that there is no point in optimising the reactor performance individually at the expense of all unit operations in the flow-sheet.

According to the characteristic vector, Equation 6.3, the AR for the system of Figure 6.2 must be examined in 3-D. However due to the breakage kinetics being first order and assuming ideal classification, we do not expect any concavities in the output mass fraction distribution profiles. The curve in Figure 6.1 is convex according to our definition and the process of mixing cannot extend it. By a concavity we mean if there was a hollow part on the curve of Figure 6.1, then a mixing line tangent to the ends of the hollow part would extend the region. However there could be concavities when there is interaction between the two different variables of total energy and mass fraction distribution. Initially we do an analysis of the 2-D projections.

6.3.1 Objective function: Maximum production of mass in size class 2

Whole product size distributions can now be represented as points in space. An algorithm was set up in Matlab® to calculate the evolution of the mass fraction distribution for the system shown in Figure 6.2. The specific power, $\overline{P}$, is kept constant while the grinding time t is increased.

$$k_i\left(\overline{P}t\right) = 0.5\left[1 + erf\left(\frac{\ln\left(\overline{P}t\right) - \ln\left(\dfrac{E_{m50,i}}{t}\right)}{\sqrt{2}\sigma_E}\right)\right] \qquad (6.4)$$

The constants found in Equation 6.4 are σ_E and E_{m50} which are the geometric variance and the median specific fracture energy, respectively. The breakage rate function k_i used in previous work has been modified to be a function of specific power instead of specific energy and this is shown in Equation 6.4. The reason for this modification is that specific energy is an appropriate variable for instantaneous breakage of single particles in drop weight tests. However for batch grinding the variable of interest becomes the specific power because the system shown in Figure 6.2 is a continuous operation. The rest of the model is as described in Khumalo et al. (2006).

The characteristic vector for maximising the mass fraction in size class 2 is given by Equation 6.5. One of the necessary conditions for building the AR is to include the feed point and the variable of interest which in this particular case is size class 2. We note that in this case the characteristic vector is:

$$\mathbf{c} = [m_1, m_2] \tag{6.5}$$

The fundamental processes considered are breakage and classification and the accumulation of the mass in size class 2 from the feed size class 1 is tracked in 2-dimensional space. In this case the AR problem is only a 2-D problem as the specific power is merely a parameter in the system equations as in Equation 6.4. As the fundamental equation is linear, the curves generated will all be convex. Figure 6.3 shows the product distributions of the two systems for:

i)   breakage with classification and,
ii)   breakage only without classification.

Figure 6.3 shows that the maximum mass in size class 2 is obtained by using the two fundamental processes of breakage and classification for 0.2 J/g specific energy input. The particle fracture specific energy has been described as the least amount of specific energy required to cause breakage (Tavares, 1998). 0.2 J/g is the estimated particle fracture energy from the statistical model of Tavares et al. (1998) for the feed particle size considered in this work. Less than this specific energy input will result in no breakage. The maximum mass fraction in size class 2 is 0.749 for the system of breakage and classification, whereas it is 0.5078 for the system of breakage alone. This is a 48% increase in the mass fraction reporting to size class 2, assuming perfect separation. The result of Figure 6.3 not only tells us the maximum possible mass fraction in size class 2, but also provides the optimum operating conditions. This justifies the claim that the process of classification extends the region of possible mass fraction products and this is shown through the use of simple geometric ideas such as in Figure 6.3.
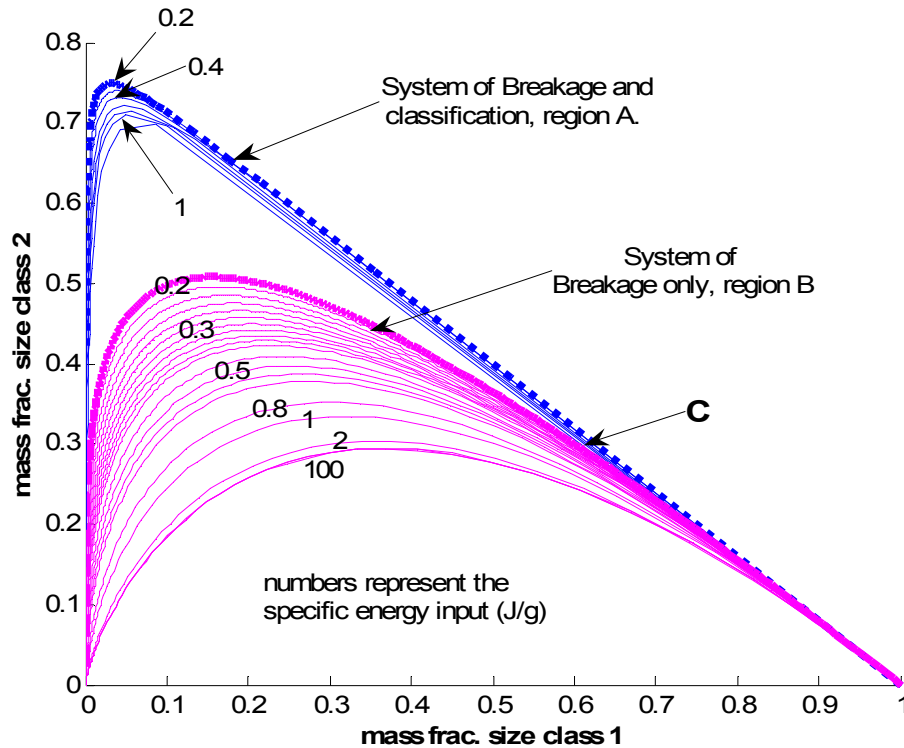
Figure 6.3: Illustration of the systems of breakage with and without classification for increasing specific energy input.

6.3.2 Impact of classification on energy consumption

Section 6.3.1 has looked at what is the possible maximum mass fraction in size class 2. However we still would like to compare the total energy consumption of the two systems of breakage with and without classification. This involves defining the total energy consumption and the mass fraction in size class 2 as our variables of interest. Redefining our characteristic vector as Equation 6.6, i.e. this represents a system where we endeavour to reduce the total energy consumption in the system to get to a value of material in size class 2. This is a 2-D projection of the full 3-D plot. The variation of the mass in size class 2 with energy results in a useful 2-D plot for process synthesis and optimisation.

$$c = [E_T, m_2] \hspace{4cm} (6.6)$$

Figure 6.4 is a representation of the change in mass fraction of the material in size class 2 with total energy consumption for a specific energy input of 1 J/g. As can be seen from the graph with and without classification both systems effectively consume the same energy for a given mass fraction of size class 2 at long grind times. The system for breakage only has a maximum in the amount of size class 2 being produced but its maximum value is lower than that of the system for breakage with classification. Not only do we get information about the possible maximum mass in size class 2 produced but we also get equipment design information on the size of the grinding equipment. Incorporating total energy consumption into the characteristic equation thus yields useful results.
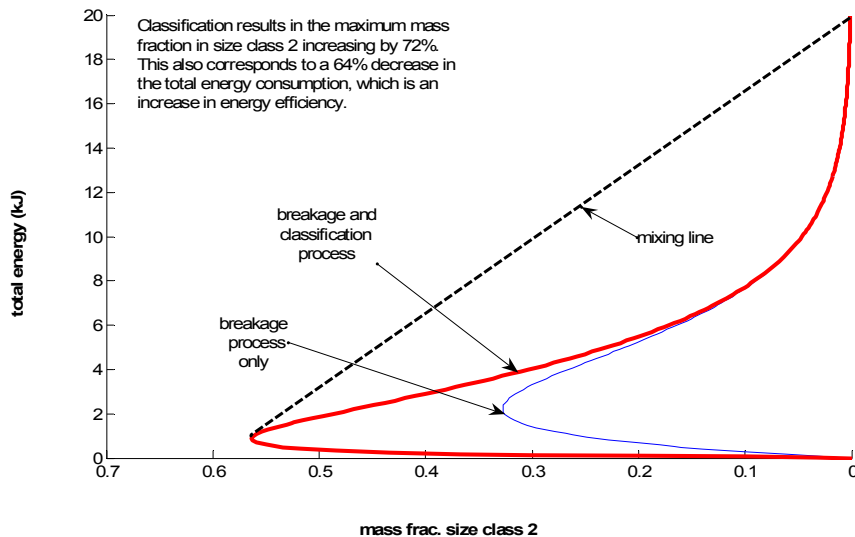
Figure 6.4: Illustration of the processes of breakage only and breakage with classification at a specific energy input of 1 J/g.

The maximum mass fraction is achieved by the system with breakage and classification at a lower total energy consumption than that without classification as can be seen from Figure 6.4. The maximum mass fraction in size class 2 is achieved at a total energy consumption of 0.848 kJ for the system of breakage and classification compared to 2.2515 kJ for the system of breakage alone. This is a 62% decrease in total energy consumption as well as the 48% increase in material in size class 2. We know that industrial circuits incorporate classification; here we are offering a definite tool against which to synthesize and optimise the process. Noting that by doing this optimally, there are significant improvements to be made.

The plots in Figure 6.4 have concavities and therefore are non-convex. This shows that the relationship between the mass in size class 2 and energy is non linear. Introducing a mixing line as shown in Figure 6.4 does extend the region. However this extension results in increased energy consumption when the objective is to minimise energy consumption.

This approach leads to increased process efficiency and gives a target against which to measure actual circuits. This procedure shows how to optimise the circuit for the least energy consumption. Classification reduces the extents of over grinding and particle shielding resulting in a more energy efficient system with increased mass in size class 2.

6.3.3 Maximising the production of size class 2 for all possible specific energy inputs

In Section 6.3.1 and 6.3.2 we have shown significant improvements in maximising size class 2 and minimising total energy consumption for the system of breakage and classification compared to the one for breakage

alone. Only a single value of specific energy of 1 J/g was used in the above analysis. This section considers all the possible outputs when increasing values of specific energy are considered.

We can also use Figure 6.3, as we have contour plots for equal specific energy, to see how the maximum value of mass fraction changes with specific energy with and without classification.

Remember that Figure 6.3 is a result of the system described in Figure 6.2 where breakage takes place and the material below the feed size class is classified out. The feed material is continuously broken and classified and recycled. The system of breakage and classification produces a region A of possible mass fraction distributions. Classification favours the production of sharp mass fraction distributions which are mostly favoured for instance by the pharmaceutical industry. This is a result of the system having an optimum breakage residence time for a particular specific energy input. The residence time can be interpreted from the profile achieving a given objective function. Higher specific energy inputs will have shorter residence times to reach the maximum value of size class 2.

The system of breakage without classification produces region B in Figure 6.3 for the various specific energy inputs. Clearly we see that region A is an extension of region B. This plot clearly shows that the additional process of classification extends the 2-D AR region. Initially the boundary of the path followed by both regions from the feed point are nearly the same up to about point C, but we can then see the benefit of including classification after point C in terms of extending the AR with respect to mass fraction in size class 2. This initial grinding without classification can be used to obtain the mean residence time of the mill and so enables us to decide on the mill size.

6.3.4 Improving energy efficiency in producing size class 2

Also of interest in particle size reduction processes is the energy cost. Reducing the total energy consumption is one of the major areas of study in comminution. The candidate AR constructed using fundamental processes for a system could be used as the base from which the performance of a system is rated. When classification is incorporated for an objective function to produce size class 2 at minimal energy, Equation 6.6 is the required characteristic vector.
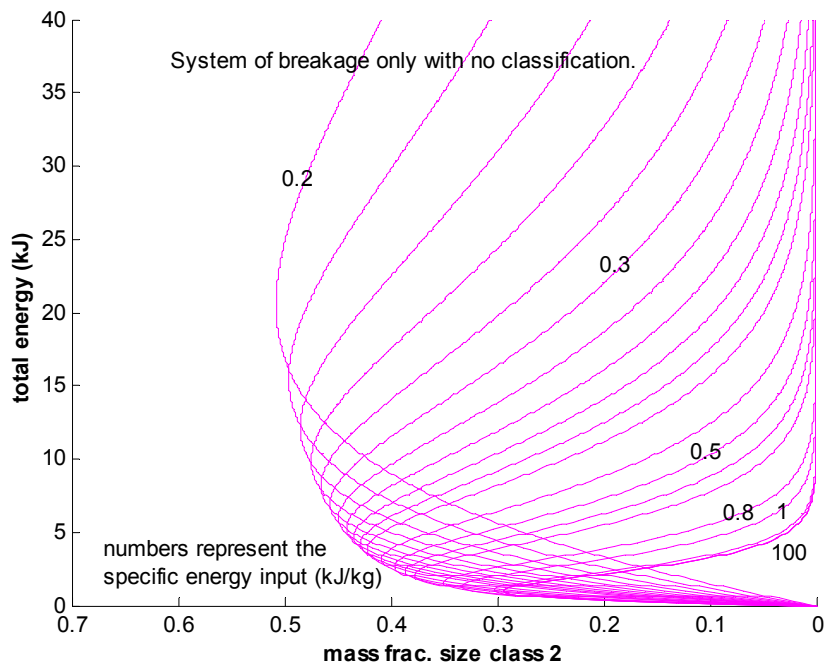
Figure 6.5: Energy consumption for the system of breakage without classification.

The fractional breakage rate function, k_i, is a function of specific power. The use of different specific power values results in the mass fraction distribution profiles shown in Figures 6.5 and 6.6. A Matlab® algorithm was used to

produce the different profiles for constant specific power as in Figures 6.5 and 6.6.These plots show how the total energy consumption varies for different specific power inputs.

Both Figure 6.5 and Figure 6.6 show clearly that the curves have concavities. However this point has been explained in Section 6.3.2. Extending the region by a mixing line will not extend the region in terms of maximising the mass in size class 2. The mixing line involves using more energy to get a certain amount in size class 2. We can see that when maximising the mass in size class 2 the minimum energy consumption is found at the turning point. Up to the turning point there are no concavities and so mixing is not required.

Figure 6.5 and Figure 6.6 both clearly show that the total energy consumption for initial breakage decreases as the specific energy input increases. However the maximum mass in size class 2 decreases as the specific energy increases. The total energy consumption for achieving a maximum mass fraction in size class 2 is achieved in both cases using a specific energy of 0.2 J/g and is;

    i)   20.3 kJ for the system of breakage without classification and the corresponding maximum mass fraction in size class 2 is 0.5078,

    ii)   2.9 kJ for the system of breakage with classification and the corresponding maximum mass fraction in size class 2 is 0.749.
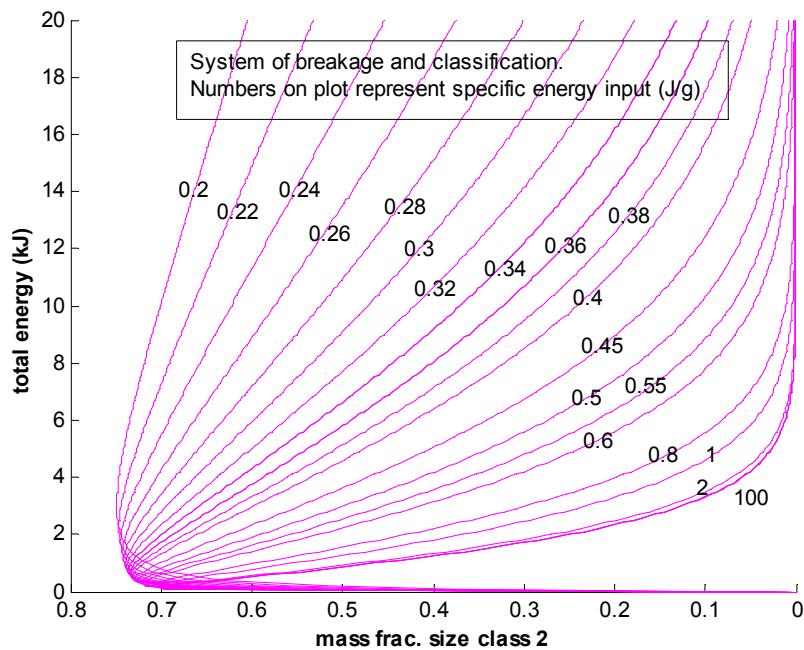
Figure 6.6: Energy consumption for the system of breakage with classification.

The additional process of classification reduces the total energy consumption by 700% while giving more of the desired material and this information is easily extracted from the graphical plot. The system of breakage with no classification produces a smaller maximum mass fraction in size class 2, and yet it consumes more energy than the system of breakage with classification. Thus by using the system of breakage with classification we increase the production of the maximum mass in size class 2 while decreasing the total energy consumption.

Previously for the system of breakage only, we showed that lower levels of specific energy maximise the production of mass in size class 2. For the system with breakage and classification processes, we can clearly see from Figure 6.5 that increasing the specific energy from 0.2 to 1 J/g decreases the maximum mass in size class 2. Higher levels of specific energy result in a

decrease in the maximum mass reporting to size class 2. These results are in line with those of Tavares and King (1998) who have reported the minimum impact energy input which would result in the fracture of single particles of different sizes. Tavares and King's work has been used in this thesis to show that different sized particles have different fracture energies. The energies have been modeled according to some power law. Therefore it is possible to determine the necessary energy input level to achieve.

We note that for both Figure 6.5 and Figure 6.6, we can draw an envelop along the lowest points of each curve up to the maximum in size class 2. This envelops represents a path to get to a specific value of size class 2 using the lowest total energy. We also note that we can get to the maximum point of size class 2 via two paths, the first by following the envelop and the second by using a specific energy input of 0.2 J/g.

By following the envelop we are following a grinding policy where the specific energy input is changing with time. Thus we can use this graph to get a grinding policy to reduce the total energy consumption to get to a specific mass fraction of size class 2.

We do not claim that this policy is the best as it is possible that we could even do better by changing the policy in a different manner. We could only ascertain this by looking at the full 3-D AR. This will be done in a subsequent paper, which work will be part of the recommended future work.

6.3.5 The Attainable Region

A complete attainable region analysis requires us to describe the set of all possible outputs for our system. The total system of interest includes the

mass fraction in three size classes and the total energy consumption. We have three size classes and the total energy input. So there are four variables of interest i.e. m_1, m_2, m_3 and *total energy*. The mass fraction in size class 3 is however found by mass balance, reducing the dimensionality of the problem to 3-D space. Equation 6.3 becomes the characteristic vector.

An initial candidate of attainable mass fraction distributions has been constructed by considering all the input specific energy values from 0.2 to 100 J/g. We note this is not necessarily the full AR as to do this we would have to consider changing specific energy policies and this has not been done in this paper.

Figure 6.7 is a plot of all the possible distributions for different specific energy values for the system with breakage and classification. Figure 6.8 is a plot for the system of breakage without classification while considering all the input specific energy values from 0.2 to 100 J/g.
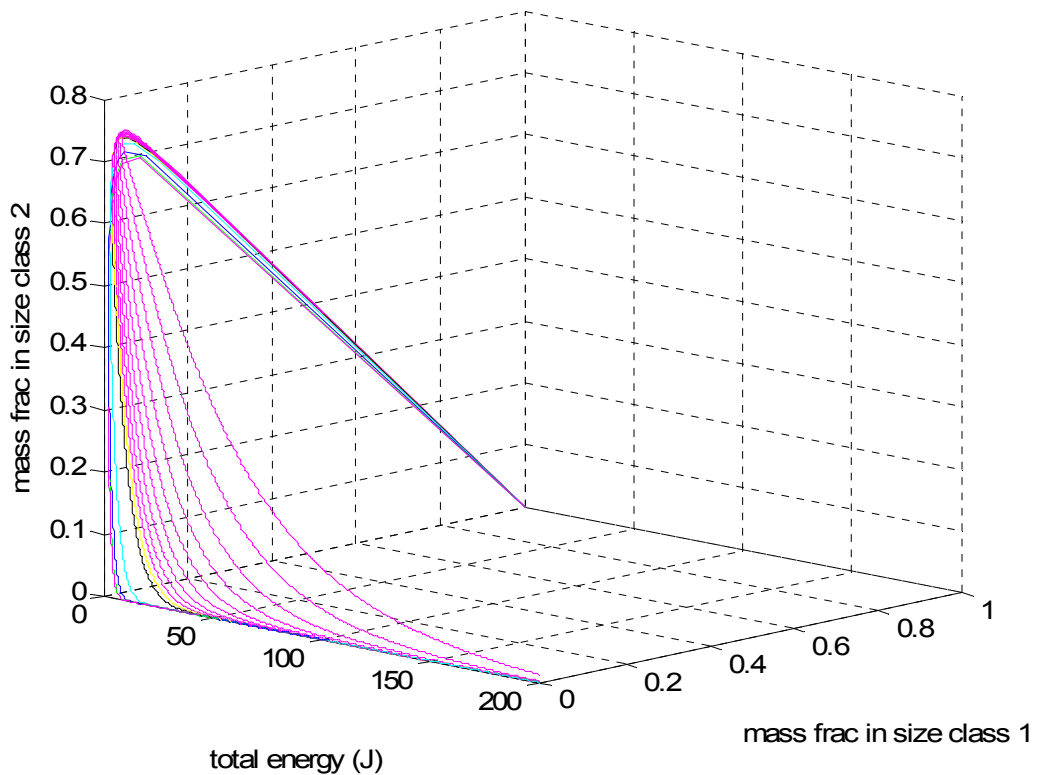
Figure 6.7: Plot of all possible outputs for the system of breakage and classification processes with specific energy varying from 0.2-100 J/g.

The major differences between the two plots have been discussed in sections 6.3.3 and 6.3.4 through the analysis of the 2-D projections.

We have managed to demonstrate how important the process of separation is in:

i)   increasing the amount of material into a particular size class,

ii)   improving the energy efficiency of size reduction systems by reducing the total energy consumption.
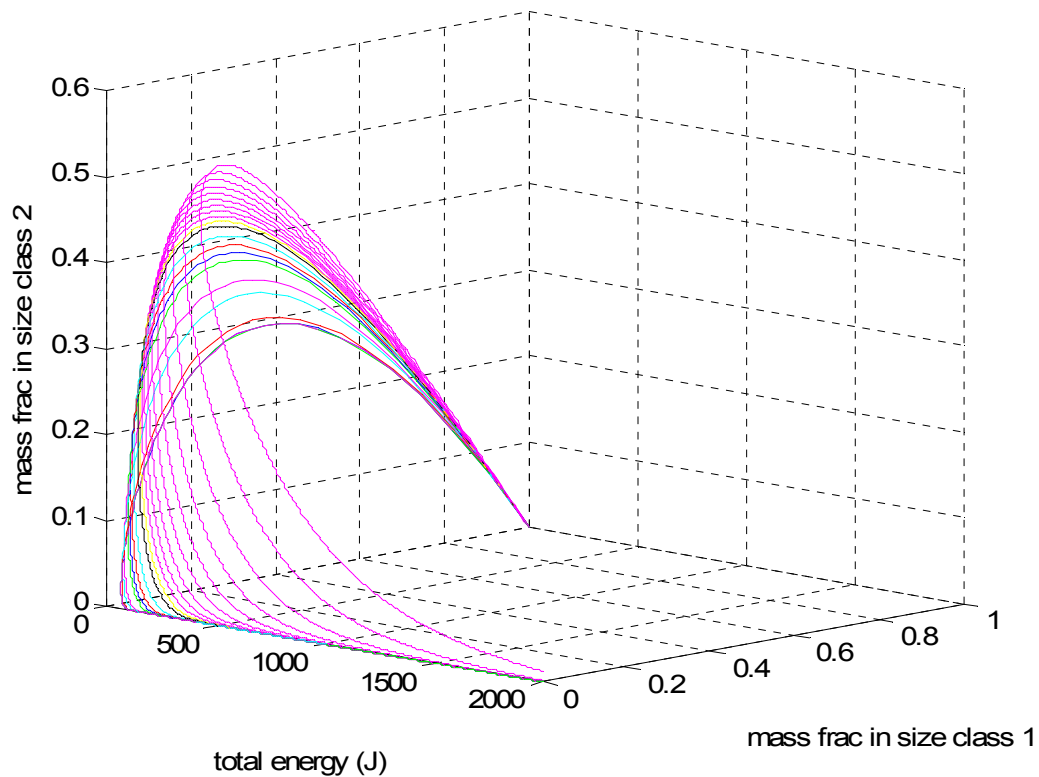
Figure 6.8: Plot of all possible outputs for the system of breakage only with specific energy varying from 0.2-100 J/g.

6.3.6 Objective function: Maximum production of material in size class 3

So far we have looked at how to maximise the production of the median size class 2, with benefits of lower total energy consumption due to classification. The desire of pharmaceutical industries is usually to have sharp particle size distributions. We have seen how classification aids in this. However there are some industries especially gold mining whose objective function is to make the particle size distributions as fine as possible, although there is a lower limit. We therefore consider a scenario with an objective function to produce as much as possible of the material in size class 3 possibly taking into account the energy consumption.

An investigation is carried out using the system of Figure 6.2 with breakage and classification as the fundamental processes. The AR approach requires a definition of the characteristic vector, Equation 6.7, which takes into account the feed point and the variable of interest which is size class 3, in this particular case.

$$\mathbf{c} = [m_1, m_3] \tag{6.7}$$
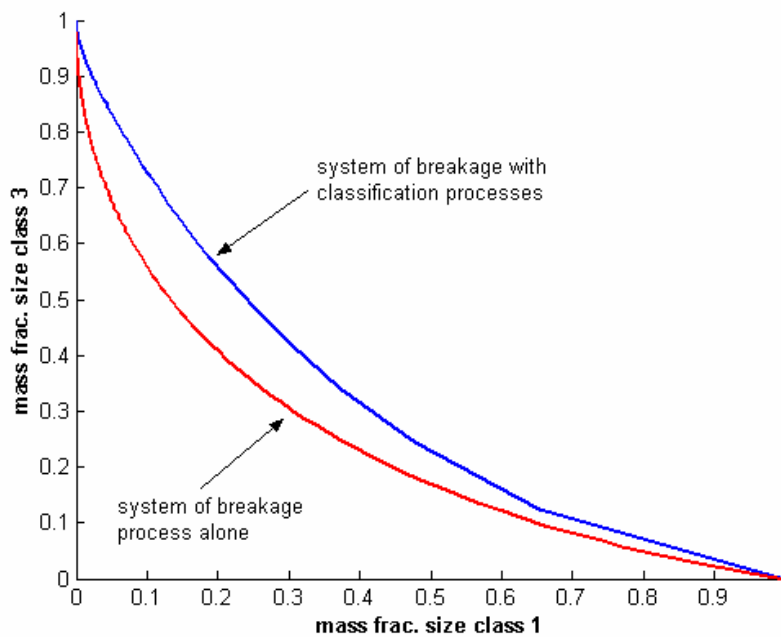
Figure 6.9: Product mass fraction profiles for the two systems of breakage with and without classification at a specific energy input of 0.5 J/g.

The evolution of the mass in size class 3 from the feed size class 1 is tracked in 2-dimensional space. Figure 6.9 shows the product mass fraction distributions of the two systems of:

iii)   breakage with classification and,
iv)   breakage without classification.

The important point to note is that ultimately both processes achieve the same amount of material into size class 3. All the feed is converted to size class 3. Besides this there is not much useful information to be drawn from Figure 6.10, therefore we introduce another variable which is energy consumption to show the difference between the two systems of breakage with and without classification.

6.3.7 Impact of classification on energy consumption in producing size class 3

Redefining our characteristic vector as Equation 6.8, i.e. this represents a situation where we endeavour to reduce the total energy consumption in the system while specifying the formation of material in size class 3.

$$\boldsymbol{c} = [E_T, m_3] \tag{6.8}$$
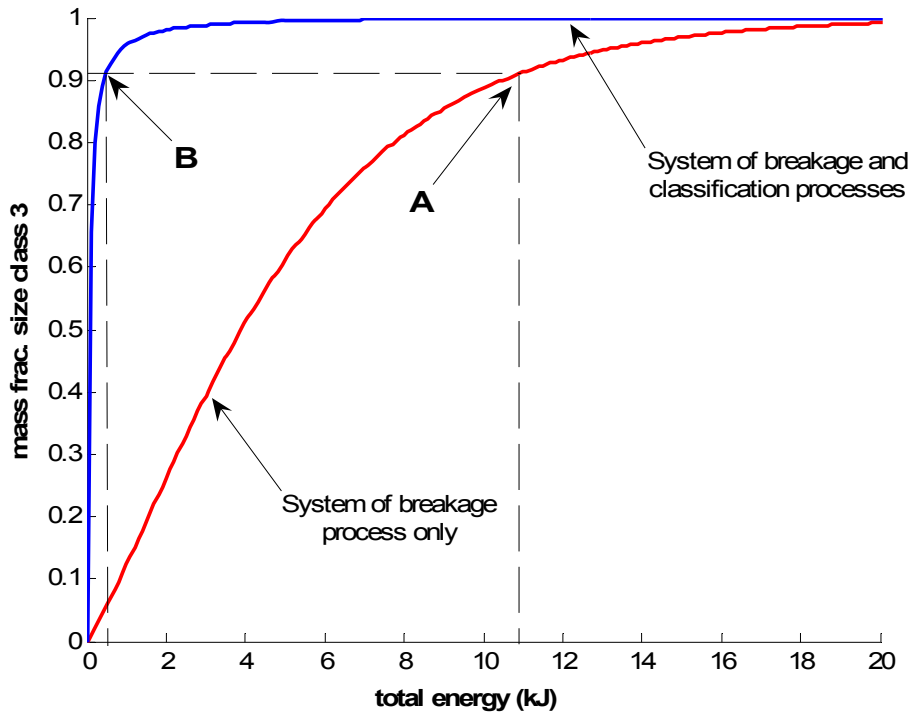
Figure 6.10: Total energy consumption for the production of material in size class 3 for the two systems of breakage with and without classification at a specific energy input of 0.5 J/g.

Figure 6.10 is a representation of the change in mass fraction of the material in size class 3 with total energy consumption for a specific energy input of 0.5 J/g. As noted before, ultimately both systems produce the same amount of mass in size class 3 as in Figure 6.9. However incorporating total energy consumption into the characteristic equation yields more instructive results. For an objective function to produce 92% of the material in size class 3, the total energy consumption for the system of breakage and classification processes is 0.6 kJ. The same objective function for the system of breakage only without classification consumes 11.4 kJ of energy. The additional fundamental process of classification results in a 95% energy saving. This high energy saving value may appear too theoretical but it offers target

170

opportunities. It is a result of theoretical experiments which assumes classification at each specific energy input, resulting in far more classification stages compared to the industrial practise of one or two classifiers. The specific energy reported is for one stage of breakage and then classification. The continuous system of Figure 3 is approximated by the implementation of a system of multiple grinding stages with inter-stage classification.

Classification reduces the extent of over-grinding and particle shielding resulting in an efficient system with increased production of the mass in size class 3. This kind of approach leads to increased process efficiency and gives a target against which to measure actual circuits.

6.4 DISCUSSION

The process of classification has been investigated and shown to extend the region of possible mass fractions. The classification process results in trajectories that extend the AR.

Given an objective function to maximise the production of mass in the median size range, size class 2, the process of classification gives two advantages over breakage without classification. Classification allows for size class 2 to be removed before further breakage. Classification avoids over-grinding and coarse particle shielding by the fine particles resulting in a more efficient process. This maximises the production of size class 2. The second point is that this leads to lower energy consumption. Constant specific energy in all grinding units result in a 48% increase in the mass reporting to size class 2 for the system of breakage with classification as compared to that of breakage only.

The candidate 2-D attainable regions for the two systems of breakage with classification and breakage without classification have been constructed. The system with classification achieves a maximum of 0.749 mass fraction in size class 2 and an energy consumption of 2.9 kJ. The system without classification achieves a maximum of 0.5078 mass fraction in size class 2 and an energy consumption of 20.3 kJ. In the event the system of classification solves two objectives simultaneously. It produces an increased amount in size class 2 at lower total energy consumption.

For an objective to maximise the mass fraction in size class 3, the fines range, both systems have been shown to ultimately convert all the feed into size class 3, producing fines. The system with classification however reduces total energy consumption, for example by 95% when 92% mass fraction reports to size class 3 in both systems. Classification avoids over-grinding and coarse particle shielding by the fine particles resulting in a more efficient process.

The AR technique constructs the region of all possible outputs for given fundamental processes in comminution. The resulting candidate AR provides a measure against which actual process performance can be measured.

6.5 SUMMARY

The system that has been studied in this paper is a simplified one with respect to the number of size classes and the classification. This has been done with a view to being able to present the results graphically in order to help in respect of the interpretation. However the method that has been presented is perfectly general and so can readily be applied to more complex

situations. The calculations though more complex will not present a problem to competent engineers and scientists.

The results are however indicative of the large savings that are possible by having properly designed circuits. The method not only highlights the potential energy savings but also allows one to find the equipment conditions that will allow these savings to be realised. The methods can be used for both system synthesis as well for analysing existing operations.

In particular one can readily see that use of energy intensity control in a milling circuit could prove to be an extremely valuable tool in their design and operation. Furthermore it is also shown that while the use of classification causes significant improvements in the circuit it is also important to insert the classification into the system at the appropriate place after the required amount of grinding. All of these aspects can be addressed using the AR analysis.

In higher dimensions one will not readily be able to analyse the results graphically as well as has been done in this paper. So in principle one can solve specific problems mathematically but obviously at the expense of losing some graphical insight. However instead of using mass fraction distribution in specific size classes as our variable, one can use the moments of the particle size distributions. Often by using only the first two moments (the median and the variance) as our variables one can still keep the dimensionality used in this paper but solve problems with many more particle sizes or even ones with continuous distributions. Such an approach in looking at ARs' in polymerisation has already been done (Smith and Malone, 1997).

6.6 REFERENCES

Austin, L.G.; Klimpel, R.R.; Luckie, P.T. (1984). Process engineering of size reduction: ball milling. pp. 234-247.

Baumgardt, S.; Buss, B.; May, P.; Schubert, H. (1975). On the comparison of results in single grain crushing under different kinds of load. Proc. 11th Int. Miner. Process. Congr., Cagliari, 3-32.

Broadbent, S.R. & Callcott, T.G. (1956). A matrix analysis of processes involving particle assembly. Philos. Trans. R. Soc. London, Ser. A 249, pp. 99-123.

Dan, C.C.; Schubert, H. (1990). Breakage probability, progeny size distribution and energy utilization of comminution by impact. Aufbereit.-Tech., **31**, 241-247.

Datta, A. & Rajamani, R.K. (2002). A direct approach of modelling batch grinding in ball mills using population balance principles and impact energy distribution. Int. J. Miner. Processs., **64**, pp. 181-200.

Glasser, D.; Hildebrandt, D. (1987). A geometric approach to steady flow reactors: the attainable region and optimization in concentration space. American Chemical Society, **26**, 1803-1810.

Glasser, D.; Hildebrandt, D.; Godorr, S. (1994) The attainable region for segregated, maximum mixed, and other reactor models. Ind. Eng. Chem. Res., **33**, 1136-1144.

Herbst, J.A. & Fuerstenau, D.W. (1980). Scale-up procedures for continuous grinding mill design using population balance models. Int. J. miner. Process., **7**, pp. 1-31.

Herbst, J.A., Siddique, M., Rajamani, K., Sanchez, E. (1981). Population balance approach to ball mill scale-up: bench and pilot scale investigations. Trans. SME/AIME, **272**, pp.1945-1954.

Horn, F. (1964). Attainable and non-attainable regions in chemical reaction technique. 3rd European Symposium on "Chemical Reaction Engineering". Pergamon Press Ltd. Great Britain.

Luckie, P.T.& Austin, L.G. (1972). A review introduction to the Solution of the Grinding Equations by digital computation. Minerals Science and Engineering, **4**, pp. 24-51.

Khumalo, N.; Glasser, D.; Hildebrandt, D.; Hausberger, B.; Kauchali, S. (2006). The application of the attainable region analysis to comminution. Chemical Engineering Science, **61**, 5969-5980.

Khumalo, N.; Glasser, D.; Hildebrandt, D.; Hausberger, B. (pending publication). An experimental validation of a Specific Energy Based Approach for Comminution. Chemical Engineering Science Journal.

King, R.P.; Bourgeois, F. (1993a). Measurement of fracture energy during single-particle breakage. Miner. Eng., **6**, 353-367.

King, R.P. (2001). Modeling & Simulation of Mineral Processing Systems; Butterworth-Heinemann: Great Britain. 144-151.

Mitrani, I. (1998). Probabilistic modeling; University Press: Cambridge, pp. 156-168.

Reid, K. J. (1965). Chemical Engineering Science, **20**, 953-963.

Smith, R.L.; Malone, M.F. (1997). Attainable regions for polymerization reaction systems. Ind. Eng. Chem. Res., **36**, 4, 1076 – 1084.

Tavares, L.M.; King, R. P. (1998). Single-particle fracture under impact loading. Int. J. Miner. Process., **54**, 1-28.

Tavares, L.M. (1999). Energy absorbed in breakage of single particles in drop weight testing. Minerals Engineering. **12**, 43-50.

6.7 LIST OF SYMBOLS

AR	attainable region
PSD	particle size distribution
DSSR	differential side stream reactor
2-D	2 dimensional
3-D	3 dimensional

7 CONCLUSIONS

In summary, the aim of this thesis was to answer the process synthesis and optimisation of the comminution circuit. The attainable region analysis was chosen as a process synthesis tool because of its success in chemical reaction engineering. It has been shown in chemical reaction engineering that the optimal combination of fundamental processes generate the boundary of the candidate attainable region. This boundary is then interpreted as equipment and process conditions for a given objective function.

Complete product particle size distributions were defined as points in the Euclidian space. Each discreet size interval of a particle size distribution was taken as a unique species which is analogous to the concentration of a reacting species. The particle size distribution is traditionally described by many discreet size intervals. However the characteristic vector is comprised of the feed point and the objective function, and this helps to reduce the dimensionality of the problem.

Three fundamental processes were defined as taking place in a comminution circuit. They are breakage, mixing and classification. Using breakage as the fundamental process only, the product particle size distributions were determined using the specific energy dependent population balance model. As mentioned earlier the product particle size distributions were geometrically presented as points in space which afforded us the opportunity to connect them, resulting in a dynamic system. This is a deviation from the traditional practice of representing particle size distributions as cumulative plots, as these cannot be inter-linked. These points of particle size distributions are vectors in space and they described a convex trajectory, showing that the fundamental process of mixing would not extend the boundary of the candidate attainable region any further.

One of the necessary conditions for building the candidate attainable region is that it should be convex. A convex region provides a single optimum. Different levels of specific energy input resulted in different convex trajectories. The optimum for the objective function is easily read off the turning point of these convex trajectories. This answers the optimisation problem of the level of specific energy to be used in a given equipment to achieve a certain objective function which could be maximising the mass of material reporting to a specified discreet size interval.

Lower levels of specific energy input result in the outermost boundary of the candidate attainable region. The mixing process can be used to achieve the rest of the particle size distributions in bounded region. Also breakage at higher specific energy levels can be used to achieve the distributions in the bounded region. We have shown that grinding units in series help to maximise a desired particle size distribution whereas parallel arrangements of units only increases production by duplicating the production of the units in series.

Experimental validation of the candidate attainable region for the fundamental process of breakage was carried out in a laboratory ball mill using silica and quartz particles. Breakage products are shown to be a function of specific energy input only. Some workers have shown the relationship to be linear and we have shown the relationship to be some polynomial but the dependence is still maintained. The linear dependence is due to the assumption of independent breakage kinetics of particles of all sizes. We show that the presence of other sized particles affects the breakage kinetics maybe due to cushioning, resulting in a non-linear system. Dynamic modelling is essential to take into account of this non-linear breakage kinetics.

The breakage rate is shown to be a function of time but asymptotes to a constant value for increased grind times. Designers should be aware of this non-linearity especially when the feed is mono-sized. The trajectories of the breakage products from the laboratory ball mill are convex and they depend on the specific power to the mill. The lower specific power results in more material reporting to the middle discreet size class intervals, as in the theoretical simulations. These convex boundaries solve the optimisation problem.

Finally the fundamental process of classification is considered together with breakage and mixing. Classification extends the candidate attainable region for the objective function to maximise the amount of material in the middle discreet size classes. It avoids over-grinding of material already meeting the product specifications. Classification results in substantial energy savings in the regions of 100% when compared to breakage without separation for achieving the same product specifications.

The attainable region analysis has been successfully applied in comminution solving the process synthesis and optimisation of the comminution circuit. The resulting geometric structures are easy to interpret and it can be used not only at design stage but also as a target for existing processes. Therefore we safely conclude that the attainable regions analysis is an appropriate conceptual design tool since it takes into account the fundamental processes and their constraints without being equipment specific first.

8 RECOMMENDATIONS

The mineral processing circuit consists of various processing units with different fundamental processes taking place and its objective is to produce minerals at the minimum cost. This means that the combination of these fundamental processes must be optimum for the circuit to be efficient. The attainable regions analysis offers an opportunity to optimally combine all these fundamental processes. Individually optimising units, as is currently done, does not necessarily result in an efficient system.

The application of the attainable regions approach for process synthesis in comminution is still in its infancy yet there are a lot of opportunities as an extension of this work. The concept can be extended to the maximisation of the final product as the objective function. This implies the inclusion of downstream processes such as leaching, flotation and smelting as future work.

Future work should also focus on setting up a comminution pilot plant to include grinding and classification equipment. The setup should be integrated with process controllers and indicators for measurement of variables like power draw, torque, rotational speed and particle size distribution. Test runs should be carried out for all the major variables in a factorial experiment. We have shown in our theoretical simulations that the use of different energy policies result in an attainable region that is optimum in terms of time. This needs experimental investigation; therefore it is paramount to design the experimental setup to be able to achieve this. The experimental results will enable detailed integrated process modeling.

Once the process is modeled satisfactorily, then the next step will be to develop comminution software for process synthesis and optimisation. This

will enable the end user to provide feed data and the objective function to the template and the software would automatically simulate the comminution circuit and provide the optimum control policies.

The pilot plant modeling and simulation results should enable industry to improve the design and operation of comminution circuits, based on the targets. More energy efficient comminution circuits will result for the mining industry. This will significantly reduce the electrical loads on national grids enhancing profitability of the relevant industries. The comminution software to be produced could be patented and/or commercialized.

Appendix A: Matlab program – Dynamic programming for the fundamental process of breakage for the specific energy dependent population balance model

```matlab
k4=0.0434;
k5=3.48;%0.7326
k6=1.61;
sigma=0.4407;
k7=0.388;                              %  model  parameters
k8=0.0176;
s=0.75;
ks=1;
nn=4;
b=0:2;
bb=3;                                  % number of size classes equal to 3
E1=1;                                  %specific energy input J/g

for w=1:length(b)
  d1(w)=1/((sqrt(2)^2)^b(w));          % number of size classes
  E50(w)=k4*(1+(k5/d1(w)))^k6;         % median specific fracture specific energy
  for i=1:length(E1)
    S1(w,i)=0.5*(1 + erf(((log(E1(i))-log(k4*(1+k5/d1(w))^k6))/sqrt(2*sigma)))); % selection function/breakage rate
    T10(w,i)=k7*(1-exp(-((k8*E1(i))./E50(w))));                                  %breakage distribution function
  end
end

for j=1:length(S1(1,:))
  S(:,:,j)=diag(S1(:,j));              %selection function vector changed into a diagonal matrix
end

a(1,:)=d1(1,:);%:-0.25:0
for i=2:length(d1(1,:))
  a1(i,:)=d1(1,i:end);%:d1(i);
  a(i,:)=[d1(i)*ones(1,(length(a(1,:))-length(a1(i,:)))) d1(1,i:end)];
  clear a1;
end
a = a';     % uncommented
for i=1:length(a(1,:))
  n(:,i)=(d1(i)./a(:,i));
end

for ii=1:length(n(1,:))
  for j=2:length(n)
```

```
        for k=1:length(T10(1,:))
            B1(1,ii,k)=1;
%           B1(1,1,k)=1;
%           B1(2,3,k)=0;
            B1(j,ii,k)=1-((1-T10(ii,k))^((9/(n(j,ii)-1))^s));   % breakage distribution function at any other size less than
                                                                1/n of  the parent size
        end
    end
end




for i=1:length(B1(:,1))
    for j=2:length(B1(1,:))
        g1(j,i)=B1(j-1,i)-B1(j,i);                       %breakage distribution function lower triangular matrix
    end
end
g(1,:)=B1(bb,:);
g1=[g1(2:end,:);g(1,:)];

B=B1*S*(inv(B1));
for i=1:length(B(1,:))
    Bsum(i)=sum(B(:,i));

    for j=1:length(B(:,1))
        BB(j,i)=B(j,i)./Bsum(i);
    end
end

I=eye(bb);        % identity matrix
zz=(d1<0==0)';  % separation vector

for i=1:length(E1)
    pp(:,1,i)=[1;zeros(bb-1,1)];                      % feed mass fraction size distribution
end

mm=1:100;   % number of grinding stages

for j=1:length(mm)
    for ii=1:length(E1)
        f(:,j,ii)=zz.*pp(:,j,ii);%+g(:,j,ii)*(pp(:,1,ii));       % feed mass fraction in each stage
        pp(:,j+1,ii)=(I+S(:,:,ii)*g1(:,:,ii)-S(:,:,ii))*f(:,j,ii);   % product mass fraction from each stage
        ff(:,j,ii)=sum(f(:,j,ii));
    end
end
```

```
for i=1:length(pp(1,:))
    ppsum(i)=sum(pp(:,i));
    for j=1:length(pp(:,1))
        pp(j,i)=pp(j,i)./ppsum(i);
    end
end


ll=1:length(mm);
for j=1:length(ll)
        for i=1:length(E1)
            EEE(j,i)=E1(:,i);          % calculation of specific energy to each unit
        end
end


EEE=EEE';
for i=1:length(E1)
    EE(i,:)=EEE(i,:).*ff(:,:,i);      % calculation of total energy used in each successive unit
End


for j=1:length(E1)
    for j=2:length(mm)
        E(:,1)=EE(:,1);
        E(:,j)=E(:,j-1)+EE(:,j);      %total energy available
    end
end
E=[linspace(0,0,length(E1))' E];   % cumulative energy input
EEE=[E1' EEE];


id=(linspace(1,1,length(mm)+1));   %process identifier: 2=breakage+separation


for i=1:length(E1)
    dataset1(:,:,i)=[pp(:,:,i);E(i,:); [0 mm]; id(1,:); EEE(i,:)]; %breakage only dataset
end
merge=dataset1';
mm=[0 mm];


figure(2);
hold on;
plot(merge(:,1), merge(:,2), 'c')        % geometrical plot in 2-dimensional space
xlabel('mass frac in size class 1')
ylabel('mass frac in size class 2')
```

185

Appendix B: Experimental Data

B1. Quartz particles: Ball loading – 30%

Mill rotational speed – 37 rpm

time (minutes)	2.5	5	10	15	20	25	40
size (µm)	exp1-1	exp1-2	exp1-3	exp1-4	exp1-5	exp1-6	exp1-7
4000	278.97	243.04	204.33	142.53	108.56	83.27	39.24
2000	66.02	85.36	91.36	106.97	98.98	84.25	47.99
1000	7.59	11.73	16.34	20.76	21.92	21.1	12.69
600	2.51	3.82	5.79	7.79	8.88	9.33	6.03
300	2.2	3.42	7	9.37	11.89	14.19	2.12
0	7.19	17.64	40.22	77.63	114.75	152.87	247.64
total mass (g)	365.01	365.01	365.04	365.05	364.98	365.01	365.04

B2. Silica sand: Ball loading – 0%

Mill rotational speed – 37 rpm

size (µm)	4000	2000	1000	600	300	0	total mass (g)
Mass (g)	330.55	29.64	1.89	0.93	0.67	0.69	365.07

B3. Silica sand: Ball loading – 10%

Mill rotational speed – 37 rpm

time (minutes)	40	30	25	20	15	10	5	2.5
size	exp2-1	exp2-2	exp2-3	exp2-4	exp2-5	exp2-6	exp2-7	exp2-8
4000	13.46	24.19	29.67	38.84	65.06	85.91	135.13	188.48
2000	41.5	62.7	75.48	94.51	111.41	126.68	130.75	120.62
1000	62.36	64.84	66.09	67.39	62.44	58.25	46.4	29.65
600	57.9	53.27	51.3	48.53	40.58	33.79	21.69	11.33
300	76.85	67.23	60.24	51.64	39.27	28.74	15.58	7.56
0	112.31	92.21	81.51	63.69	45.73	31.02	15.13	7.07
total mass (g)	365.09	365.18	365.05	365.01	364.93	364.99	365.08	365.1

B4. Silica sand: Ball loading – 20%

Mill rotational speed – 37 rpm

time (minutes)	40	30	25	20	15	10	7.5	5	3.5	2.5	1
size (µm)	exp3-1	exp3-2	exp3-3	exp3-4	exp3-5	exp3-6	exp3-7	exp3-8	exp3-9	exp3-10	exp3-11
4000	4.25	7.63	14.71	20.09	31.86	53.46	107.15	90.46	107.15	146.9	213.55
2000	5.54	11.77	20.42	32.53	52.74	87.42	127.51	124.03	127.51	122.17	103.53
1000	1.94	5.26	8.81	20.62	42.03	52.85	52.08	52.8	52.08	40.64	24.09
600	2.13	7.43	15.83	33.32	45.13	42.15	26.19	31	26.19	19.96	9.13
300	19.56	56.95	72.7	81.95	70.95	51.41	23.69	29.43	23.69	16.22	7.12
0	333.28	276.79	232.81	176.83	122.27	77.57	27.06	36.75	27.06	18.14	6.58
total mass (g)	364.97	365.07	365.06	365.15	365.15	365.09	363.68	364.97	365.08	364.94	365.06

B5. Silica sand: Ball loading – 30%

Mill rotational speed – 37 rpm

time (minutes)	40	30	20	15	10	7.5	5	2.5
size (µm)	exp4-1	exp4-2	exp4-3	exp4-4	exp4-5	exp4-6	exp4-7	exp4-8
4000	0	0.68	6.4	18.73	46.1	72.85	88.91	153.78
2000	0.22	1.79	14.98	44.65	81.99	90.51	116.81	109.33
1000	0.27	1.41	10.9	26.45	39.77	43.21	44.54	37.4
600	0.27	1.82	14.7	26.95	31.23	30.33	27.55	19.37
300	2.36	17.99	57.72	63.18	49.48	42.18	31.63	18.7
0	364.05	342.43	260.84	185.03	115.54	85.13	54.48	25.5
total mass (g)	365.16	365.2	365.13	365	365.15	364.9	365.07	365.02

B6. Silica sand: Ball loading – 20%

Mill rotational speed – 92 rpm

time (minutes)	10	7	4	2.5	1.5	1	0.5
size (µm)	exp5-1	exp5-2	exp5-3	exp5-4	exp5-5	exp5-6	exp5-7
4000	0.17	3.41	6.9	53.45	57.28	100.16	158.31
2000	1.25	4.64	19.71	93.61	99.96	116.66	119.56
1000	1.5	6.95	34.34	63.93	67.83	58.62	39.48
600	4.35	23.88	56.5	43.39	42.58	30.5	17.33
300	56.26	97.16	96.38	47.31	43.06	27.47	14.66
0	301.16	227.43	150.53	61.13	50.7	29.39	14.65
total mass (g)	364.99	365.17	365.06	365.01	365.07	365.06	365.06

B7. Silica sand: Ball loading – 20%

Mill rotational speed – 65 rpm

time (minutes)	15	10	7	4	2	1
size (µm)	exp6-1	exp6-2	exp5-3	exp6-4	exp6-5	exp6-6
4000	0.89	8.04	18.01	43.65	82.59	127.9
2000	2.48	12.05	34.83	74.62	111.36	130.96
1000	1.48	10.84	33.99	58.99	59.34	46.17
600	3.37	26.3	46.57	47.17	34.36	21.01
300	45.01	90.91	83.52	56.78	34.16	18.15
0	311.67	216.02	147.04	81.28	41.12	19.18
total mass (g)	365.16	365.11	365.07	364.99	365.09	364.99

B8. Silica sand: Ball loading – 20%

Mill rotational speed – 13 rpm

time (minutes)	58	35	30	20	10	5
size (µm)	exp7-1	exp7-2	exp7-3	exp7-4	exp7-5	exp7-6
4000	13.28	38.11	51.1	80.08	142.58	196.71
2000	69.23	124	139.61	153.94	144.42	120.35
1000	93.21	79.09	69.49	57.1	37.61	24.88
600	52.77	38.29	32.75	24.88	15	9.06
300	55.53	36.54	31.29	22.13	11.65	6.79
0	79.88	47.92	39.51	25.93	12.83	6.48
total mass (g)	365.05	365.1	364.99	365.16	365.06	365.07